Downloaded from orbit.dtu.dk on: Apr 25, 2024

DTU Library

Model Based Beamforming and Bayesian Inversion Signal Processing Methods for Seismic Localization of Underground Source

Oh, Geok Lian; Agerkvist, Finn T.; Brunskog, Jonas; Sze Kim, Pang

Publication date:
2014

Document Version
Peer reviewed version

Link back to DTU Orbit

Citation (APA):
Oh, G. L., Agerkvist, F. T., Brunskog, J., & Sze Kim, P. (2014). *Model Based Beamforming and Bayesian Inversion Signal Processing Methods for Seismic Localization of Underground Source*. Technical University of Denmark, Department of Electrical Engineering.

General rights
Copyright and moral rights for the publications made accessible in the public portal are retained by the authors and/or other copyright owners and it is a condition of accessing publications that users recognise and abide by the legal requirements associated with these rights.

- Users may download and print one copy of any publication from the public portal for the purpose of private study or research.
- You may not further distribute the material or use it for any profit-making activity or commercial gain
- You may freely distribute the URL identifying the publication in the public portal

If you believe that this document breaches copyright please contact us providing details, and we will remove access to the work immediately and investigate your claim.

Technical University of Denmark

Geok Lian, Oh

Model Based Beamforming and Bayesian Inversion Signal Processing Methods for Seismic Localization of Underground Source

PhD thesis, June 2014

DTU Electrical Engineering
Department of Electrical Engineering

www.elektro.dtu.dk

Department of Electrical Engineering

Acoustic Technology

Technical University of Denmark

Ørsteds Plads

Building 348

DK-2800 Kgs. Lyngby

Denmark

Tel: (+45) 45 25 38 00

PREFACE

This thesis is submitted to the Technical University of Denmark (DTU) as partial fulfilment of the requirements for the degree of Doctor of Philosophy (Ph. D.) in Electronics and Communication. The work presented in the thesis was completed between March 15, 2011 and June 14, 2014 at Acoustic Technology, Department of Electrical Engineering, DTU, under the supervision of Associate Professor Finn Jacobsen at DTU (main supervisor) for two years, and Associate Professor Jonas Brunskorg at DTU (main supervisor) who took over after Finn Jacobsen passed away. The thesis is also co-supervised by Associate Professor Finn T. Angerkvist at DTU and Dr Pang Sze Kim at DSO National Laboratories. The project was co-funded by DSO National Laboratories (Singapore) and DTU Elektro.

This PhD dissertation follows a monograph format, as recommended by the DTU PhD guidelines.

Chapter 1 (Introduction) defines the motivation of the project with main goal to examine the use of the recorded seismic signals, the combination of physical models, seismic inversion and seismic beamforming signal processing algorithms to detect the underground inhomogeneities such as underground facilities. The chapter provides a general introduction to the active seismic methodology related to detection of underground facilities, and gives a comparison of the proposed methodology developed in the PhD study against the literature findings.

Chapter 2 (Background), provides the general background relevant to the study, discussing the seismic wavefield theory, the beamforming and Bayesian inversion signal processing methodologies, and the measurement setup of the seismic signals for the underground tunnel localization problem.

Chapter 3 to Chapter 5 contain the main contributions of the PhD work. The work described in Chapter 3 has been accepted for publication by the Journal of Acoustical Society of America and been scheduled for publication in the first issue that appear three months from 6 June 2014. In addition, part of the work in Chapter 3 has been published in Proceedings of Meetings on Acoustics, Volume 19, Number 1. The work described in Chapter 4 and 5 are submitted as well.

Chapter 3 (Investigation of model based beamforming and Bayesian inversion signal processing methods for seismic localization of underground sources), consider the problem of determining the location of an underground tunnel using seismic interrogation signals. The ground where the tunnel is located is assumed to be a horizontally stratified medium, where complete knowledge of material elastic parameters is available from separate geophysical measurements. The chapter proposed combination of two physical models (acoustic approximation ray tracing model and the finite difference time domain (FDTD) 3D elastic wave model to represent the received seismic signal), and two localization algorithms (beamforming and Bayesian inversion methods), leading to four methodologies for solving the location of the underground tunnel. The proposed four methodologies are demonstrated and compared using seismic signals recorded by geophones set up on the ground surface generated by a surface seismic excitation, and tested with the field data. The results show that inversion for localization is most advantageous

when the forward model completely describe all the elastic wave components as is the case of the FDTD 3D elastic model.

Chapter 4 (Joint seismic inversion and localization comparing Simulated Annealing and Metropolis Hasting), extends the findings in Chapter 3 to apply the combination of elastic wavefield model and Bayesian inversion to solve a joint Bayesian inversion problem to determine the tunnel position in the ground and also the material elastic parameters of a horizontally stratified medium. The chapter proposes a reduced modelling scheme to reduce the dimension of the unknown material elastic parameter vector so as to improve the stability and convergence of the inversion process. Two Monte Carlo algorithms, Monte Carlo Metropolis Hasting and Simulated Annealing, are implemented. The performance of algorithms are illustrated through a simulation example and compared.

Chapter 5 (Seismic inversion applied to underground tunnel localization problem) extends the investigation of the joint Bayesian Inversion algorithm developed in Chapter 4 to solve a real-world problem to detect and localize the presence of an underground tunnel from measurements made by an array of seismic sensors deployed on the ground surface. The results reflect that the point MAP estimate provides a more accurate representation for the location parameters exhibiting multi-modal distribution behaviour as observed in the field data.

Finally the thesis ends with conclusions and suggestions for further research (Chapter 6).

SUMMARY (ENGLISH)

This PhD study examines the use of seismic technology for the problem of detecting underground facilities, whereby a seismic source such as a sledgehammer is used to generate seismic waves through the ground, sensed by an array of seismic sensors on the ground surface, and recorded by the digital device. The concept is similar to the techniques used in exploration seismology, in which explosions (that occur at or below the surface) or vibration wave-fronts generated at the surface reflect and refract off structures at the ground depth, so as to generate the ground profile of the elastic material properties such as the elastic wave speeds and soil densities. One processing method is casting the estimation problem into an inverse problem to solve for the unknown material parameters. The forward model for the seismic signals used in the literatures include ray tracing methods that consider only the first arrivals of the reflected compressional P-waves from the subsurface structures, or 3D elastic wave models that model all the seismic wave components. The ray tracing forward model formulation is linear, whereas the full 3D elastic wave model leads to a nonlinear inversion problem.

In this PhD study, both the linear and nonlinear inverse problems are investigated, in order to solve the problem to locate the position of an underground tunnel. One practical limitation of geophysics inversion problem is the high dimension of the unknown parameter space, such as the elastic wave speeds, soil density values of the discretized ground medium, which leads to time-consuming

computations and instability behaviour of the inversion process. In addition, the geophysics inverse problem is generally ill-posed due to non-exact forward model that introduces errors. The Bayesian inversion method through the probability density function permits the incorporation of a priori information about the parameters, and also allow for incorporation of theoretical errors. This opens up the possibilities of application of inverse paradigm in the real-world geophysics inversion problems.

In this PhD study, the Bayesian inversion paradigm for the tunnel localization problem was investigated. A formulation of the mathematical framework of the inverse problem to solve the specific tunnel localization problem defined in the PhD study has been proposed. On this basis, two optimization algorithms, namely the Monte Carlo Metropolis Hasting and Simulated Annealing have been studied, and a new reduced modelling scheme to reduce the dimension of the ground material elastic parameter space has been proposed. Also, the linear ray tracing and nonlinear 3D elastic wave models have been examined using the Bayesian inversion algorithms and conventional source localization beamforming algorithms. Additionally, an experiment validation of the inversion framework is performed through conducting seismic measurements at an underground tunnel site using an array of geophones deployed on the ground surface and using a surface seismic source.

The examples show with the field data, inversion for localization is most advantageous when the forward model completely describe all the elastic wave components as is the case of the FDTD 3D elastic model. The simulation results of the inversion of the soil density values show that both the global optimization

method, i.e., Monte Carlo Metropolis Hasting algorithm and Simulated Annealing, are able to provide fairly good estimates which agree with the investigations in the literatures that focus only on geo-inversion of the elastic medium. The results of Monte Carlo Metropolis Hasting inversion to solve the source localization problem, i.e., invert for source depth and source range, display large fluctuations in the range and depth samples generated. However the point MAP estimates derived from 5000 runs of the Metropolis Hasting method are relatively close to the true values. The results of the Simulated Annealing using an initial guess as the MAP estimate calculated from a small number of runs of the Monte Carlo Metropolis Hasting algorithm (in the simulation, we use 50 runs), is able to improve the accuracy of the range and depth estimate of the source. The field results of the joint inversion of material elastic parameters and tunnel location show an agreement with the simulated results. The PDF curves of range and depth derived from Monte Carlo Metropolis Hasting samples shows multi-modal distribution behaviour, which made the mean estimate not a suitable parameter for processing the Monte Carlo samples. The MAP estimates derived from both the Monte Carlo Metropolis Hasting and Simulated Annealing methods however match well against the location of the underground tunnel. These results reflect that the point MAP estimate, in agreement with the simulation results, provides a more accurate representation for the location parameters exhibiting multi-modal distribution behaviour.

SUMMARY (DANISH)

Denne ph.d.-projekt undersøger brugen af seismiske teknologier til at detektere underjordiske anlæg, ved at bruge en seismisk kilde, såsom en forhammer, til at generere seismiske bølger gennem jorden, som opfanges af en et antal seismiske sensorer på jordoverfladen, og registreres digitalt. Metoden er meget lig de teknikker, der anvendes til seismologisk efterforskning, hvor eksplosioner eller vibrations bølge-fronter genereret på reflekteres og spredes af strukturer i jorden, dette giver mulighed for at bestemme jordens elastiske materialeegenskaber såsom elastiske bølge hastigheder og jordmassefylder. I en af disse metoder omformuleres problemet i et inverst problem at løse for det ukendte materiale parametre. Modeller for de seismiske signaler, der anvendes i litteraturen omfatter både strålegangsmetoder som kun betragter de første modtagelser af de reflekterede kompression P-bølger fra undergrunden, og 3D elastiske bølge modeller, der medtager alle komponenter i de seismiske bølger. Strålegangsmodelformuleringen er lineær, mens den fuld 3D elastiske bølgemodel fører til et ikke-lineært inverst problem. I dette ph.d.-studie undersøges begge aspekter, det lineære og ikke-lineære inverse problem at finde placeringen af en underjordisk tunnel. En praktisk begrænsning af geofysiske inversion problemer er den høje dimension af det ukendte parameterrum, såsom de elastiske bølgehastigheder, jorddensitetsværdier af det diskretiserede jordmedium, hvilket fører til tidskrævende beregninger og ustabilitet i inversionsprocessen. Desuden er inverse geofysiske problemer generelt dårligt stillet på grund af manglende nøjagtigheder i udbredelsesmodellen.

Bayesianske inversion metoder tillader inkorporering af a priori information om parametrene og deres sandsynlighedsfordelingsfunktion, og giver også mulighed for inkludere af teoretiske fejl. Dette gør det muligt at anvende inverse metoder på praktiske geofysiske problemer.

I dette ph.d.-studie undersøges Bayesianske inversion metode til tunnel lokaliserings problemet. En matematisk formulering beregnet på at løse det specifikke tunnel lokalisering problem er defineret i ph.d.-studiet. På dette grundlag har to optimeringsalgoritmer, nemlig Monte Carlo Metropolis Hasting og 'Simuleret nedkøling' blevet undersøgt, og der foreslås et ny algoritme med et reduceret antal dimensioner af jordens elastiske materialeparametre. Desuden er de lineære strålegangs- og ulineær 3D elastiske bølgemodeller blevet undersøgt ved hjælp af Bayesian inversion algoritmer og konventionelle kilde lokalisering algoritmer, som beamforming. Derudover er en eksperimentel validering de inverse metoderne udført via af seismiske målinger på en underjordisk tunnel hvor et antal geofoner opsat på jordoverfladen og en seismisk kilde placeret på jordoverfalden.

Eksemplerne viser med feltdata inversion til lokalisering er mest fordelagtigt, når fremad model fuldstændigt beskrive alle de elastiske bølgekomponenter som det er tilfældet i FDTD 3D elastiske model. Simuleringen resultater af inversion af tæthedsværdier jord viser, at både den globale optimering metode, dvs Monte Carlo Metropolis Hasting algoritme og Simuleret nedkøling, er i stand til at give rimeligt gode skøn, som er enige med undersøgelserne i litteratur, der fokuserer kun på geo -inversion af elastisk medium. Resultaterne af Monte Carlo Metropolis Hasting inversion at løse kilden lokalisering problem, nemlig, vendes til kilden dybde og kilde rækkevidde, viser store udsving i omfanget og dybden prøver genereret, selvom

Point Kort estimater stammer fra 5000 løber af Metropolis Hasting metoden er relativt tæt på den sande values.The resultaterne af Simuleret nedkøling ved hjælp af et indledende gæt som MAP estimat beregnet ud fra et lille antal kørsler af Monte Carlo Metropolis Hasting algoritme (i simuleringen, bruger vi 50 kørsler), er i stand til at forbedre nøjagtigheden af omfanget og dybden estimat af kilden. Feltet resultaterne af den fælles inversion af væsentlige elastiske parametre og tunnel placering viser en aftale med de simulerede resultater. PDF kurver af rækkevidde og dybde stammer fra Monte Carlo Metropolis Hasting prøverne viser multimodal fordeling adfærd, hvilket gjorde den gennemsnitlige estimat ikke et egnet parameter til behandling af de Monte Carlo prøver. Kortet skøn udledt fra både Monte Carlo Metropolis Hasting og Simuleret nedkøling metoder dog passer godt mod placeringen af den underjordiske tunnel. Disse resultater afspejler, at det punkt MAP skøn efter aftale med simuleringen resultater, giver en mere nøjagtig gengivelse af de geografiske parametre udviser multimodal fordeling adfærd

ACKNOWLEDGEMENTS

Completion of this doctoral dissertation was made possible with the support of many people, and I will like to express my sincere gratitude to all of them.

First of all, I am extremely grateful to my advisor, Dr. Jonas Brunskorg, who took over the supervision of the Ph.D. after Finn Jacobsen passed away. I wish to thank him for his valuable guidance, scholarly inputs and advice I received throughout the research work. His guidance was crucial to the realization of this thesis. I will like to express my most sincere thanks to Jonas for his unconditional support during the last phase of the PhD research, particularly for all his time to proof-read the journal paper submission and the dissertation chapters.

Although he passed away before the completion of this thesis, I will also like to convey my special thanks to Finn Jacobsen. He was the one who offered me the opportunity to do my Ph.D in the Acoustic Technology group. He was a great supervisor and a great scientist and his untimely death left a void in all of his PhD. Students and the whole Acoustic Technology group.

I will also like to express my thanks to my co-advisor, Dr. Finn Agerkvist, for taking time to proof-read my dissertation chapters. In addition, big thanks to Nadia Jane Larsen for taking times to correct for the grammatical errors in the thesis.

I wish to give my acknowledgements to my company, DSO National Laboratories (Singapore), for the support of this doctoral study. I also wish to thank my CEO Mr Quek Gim Pew, my division director Mr Chan Hian Lim and my program director Mr Adrian Yap for their support to offer me the opportunity to pursue my doctorate. Big thanks to give also to my colleague Mr Pang Sze Kim for agreeing to take on the task to be my co-supervisor in Singapore. I also want to thank my colleagues at my laboratory DSO for their assistance and participations in the geophysical measurements conducted in Singapore.

I want to thank also the rest at Acoustic Technology department for the great time I have in Denmark. I will like to thank my good friend Kim Wah for her support, particularly for the numerous Skype sessions during the times spent in Copenhagen.

I would like to thank my mother and sister who have encouraged and helped me at every stage of my personal and academic life.

Finally I will like to dedicate this dissertation to the memory of my father and Finn Jacobsen.

CONTENTS

CHAPTER 1

INTRODUCTION

This PhD study examines the use of seismic technology for the problem of detecting underground facilities. The main goal of the study is to examine the use of the recorded seismic signals, the combination of physical models, seismic inversion and seismic beamforming algorithms to detect the underground inhomogeneities such as underground facilities. In the thesis, the case of an underground tunnel is used as an example of an underground facility.

Detection of underground facilities is a difficult but important problem. Underground facilities are used to conceal unwanted activities that pose a threat to security. These unwanted underground activities include border tunnels used for smuggling drugs, weapons and people. There are several techniques that have been investigated, some of which include [1] imagery (visible, IR and SAR) techniques, vibration sensing of man-made sources in underground facilities, detection of chemical and biological signatures, detection of low-frequency electromagnetic emissions from man-made sources, seismic imaging (active and passive), gravimetry, low-frequency electromagnetic induction (resistivity imaging), etc. For the active seismic method investigated in this thesis, a seismic source such as a sledgehammer is used to generate seismic waves through the ground, sensed by an array of seismic sensors on the ground surface, and recorded by the digital device.

The concept is similar to the techniques used in exploration seismology, in which explosions (that occur at or below the surface) or vibration wavefronts generated at the surface reflect and refract off structures at the ground depth. In exploration seismology [2], the recorded signals are processed to generate the ground profile of the elastic material properties including the elastic wave speeds and soil densities.

The aim of the study is to investigate the methodologies, which include the beamforming and seismic inversion algorithms, for detection of the underground facilities. The main objective is to determine in the ground the position of the underground facilities. Two aspects of the problem have been examined as follows: The first aspect of the study looks into the investigation of both acoustic model and elastic model for representation of the seismic signals and combination of either beamforming algorithm or Bayesian inversion algorithm to solve for the position of the underground facilities. The term ‘acoustic model’ means that the seismic signal is estimated using approximation represent by the acoustic wave equation. The term ‘elastic model’ means that the seismic signal is estimated using the elastic Navier wave equation. These terminologies are often used in the field of geophysical signal processing. In the first attempt to implement the seismic inversion algorithm, it is assumed that the ground elastic material parameters are known from geophysical survey. Hence, in such cases, the inversion algorithm is intended to only determine the position of the underground facilities. On the other hand, the inversion algorithm also has the possibility to include estimation of the ground elastic material parameters. As it may be difficult at times to conduct a geophysical survey at the exact site where the underground facilities are located, the second aspect of this thesis investigates the inversion problem to jointly solve for the position and ground elastic material parameters.

The core part of the work is presented in Chapter 3 through 5 in this thesis. The work described in Chapter 3 has been accepted for publication by the Journal of Acoustical Society of America and been scheduled for publication in the first issue that appear three months from 6 June 2014. In addition, part of the work in Chapter 3 has been published in Proceedings of Meetings on Acoustics, Volume 19, Number 1. The work described in Chapter 4 and 5 are submitted as well. Each of the chapters in the thesis is self-contained with their own bibliography section.

1.1 Active Seismic Detection of Underground Facilities

There are good reasons why the active seismic method has become an essential technique for detecting underground facilities [3-7]. The main advantage of the method is that it can provide images of underground structures giving detailed information about the depth and dimension of the underground facilities. The images are typically obtained from the reflected waves, while the material elastic parameters of the soil above the underground facilities can be determined through analysis of the refracted waves and the reflected waves [1]. Figure 1-1 describes the propagation behaviour in the elastic ground medium. Typically the ground is assumed as a horizontally stratified elastic medium where both compressional P-wave and shear S-wave propagate. More details about the different types of seismic waves (compressional P-waves, shear S-waves and Rayleigh R-wave) that propagate in the elastic ground medium will be explained in Chapter 2. The seismic source on the ground surface generates seismic waves that propagate through the ground, which produce reflected & refracted waves at the soil layer interface, as well as from the underground facilities.

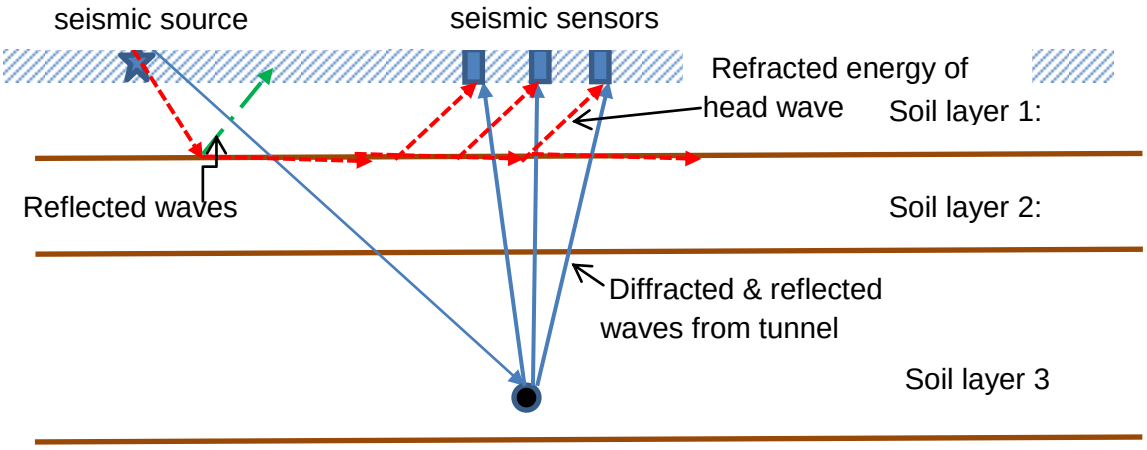

Figure 1-1 Diagram of the elastic waves in the ground.
Each soil layer is characterized by the elastic material properties that comprises of the elastic wave speeds and soil densities.

The seismic sensors deployed on the ground surface for measurement are typically geophones which are used for geophysical exploration. Figure 1-2 displays the setup of an array of *GS11D* vertical component geophones. These geophones measure only the vertical component of the particle velocity of the ground vibrations.

Geophones which measure the particle velocity of the ground vibration are based on an inertial mass suspended from a spring. They function much like a microphone and are constructed with a coil of wire surrounding a magnet. The magnet is fixed to the geophone case and the coil represents the proof mass. The natural frequency of the *GS11D* geophone used in the measurement is 4.5 Hz. In Figure 1-3, a picture of the *GS11D* geophone is displayed. The geophone is preferred over the accelerometer (which measures the physical quantity acceleration of the ground vibration) as it has better sensitivity in the low

frequency range (below 100 Hz) where the dominant seismic energy is lying. The frequency range of the GS11D geophones is from 4.5 Hz to 100 Hz.

Figure 1-2 Picture of an array of GS11D vertical component geophone array set up on the ground surface for the measurement

Figure 1-3 Picture of a GS11D vertical component geophone.

The underground facility of interest to detect in this thesis is a heritage tunnel located in Singapore, see Figure 1-4. The tunnel is $3\ \mathrm{m}$ in diameter and buried in depth approximately $6\ \mathrm{m}$ to $8\ \mathrm{m}$ deep. The geophones are deployed not far from the tunnel location at a distance about $8\ \mathrm{m}$ to $15\ \mathrm{m}$ on the ground surface. Geophysical surveys are conducted along LINE-1, LINE-2A and LINE-2B (see Figure 1-4). The geophone array is deployed on the surface in a linear configuration perpendicular to LINE-1 along the axis of the tunnel length (Line-G).

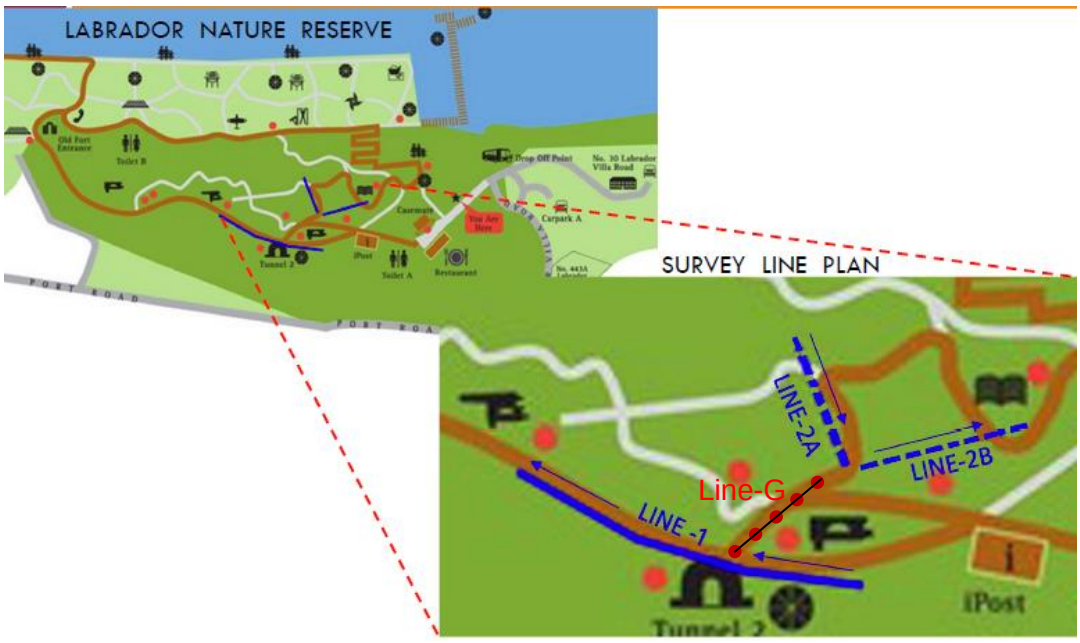

Figure 1-4. Picture of layout of a heritage tunnel located in Singapore

1.2 Comparison of the Proposed Methodology with Findings in the Literature

In the seismic reflection methods reported in the literatures [8-14], which rely on the seismic waves reflected from geological interfaces to detect presence of underground cavity, the general approach is to rely on the processing of the first arrivals of the reflected P-wave from the underground cavity. In geophysical exploration, the common approach [15-17] to estimating the elastic material parameters of the ground is also to pose the problem into a linear seismic inverse problem by assuming a smooth background model with perturbations for the subsurface. This assumption will allow one to solve the forward problem in the inversion processing using a combination of the Born or single scattering approximation and ray theoretical methods. The ray theoretical methods work by stating the ray geometries and paths, while the Born approximation describes the solution of the forward model as a sum of single reflected waves. Hence the ray and Born combination implies that the solution of the wave equation is defined by the sum of primary reflected waves from a set of selected reflectors in the ground model. More discussions of the ray method are presented in Chapter 2.

In recent years, there have been many efforts involved in solving the full wave inversion (FWI) problem. The full wave inversion problem exploits all components of the elastic waves propagating in the ground. Virieux & Operto [18] cited three challenges for efficient implementation of FWI as follows: (1) Building an accurate forward model to describe the complex elastic field recorded by the seismic sensors. (2) Defining a robust minimization criteria for the inversion processing so as to reduce the sensitivity of the inversion process to errors and noises, and also when

estimating a large dimension of parameters. (3) Improving the computational efficiency of the elastic FWI processing.

Pioneering successful applications for seismic efficiency imaging of the ground subsurface were restricted to processing the reflection data of the seismic body waves only. There remains a gap to incorporate the surface waves in the imaging process. In his paper [19], Rydén proposes a forward model to calculate the phase-velocity spectrum of the surface waves and applies fast simulated annealing algorithms to solve the inversion problem that minimize the difference between the measure phase-velocity spectrum and that calculated from a theoretical layer model. For efficient implementation of FWI that incorporate the inversion of both the seismic body and surface waves, one challenge that remains to be solved is to derive efficient optimization framework to ensure the convergence of the elastic mullti-parameter space to the true values, as the discretization of the ground medium contributes to a large unknown parameter dimension space.

In this thesis, we look into different physical models (acoustic ray tracing, 3D finite difference time difference (FDTD) elastic model), and different signal processing algorithm (frequency-wavenumber beamformer or time-delay beamformer, acoustic or full elastic wave-form Bayesian inversion Bayesian inversion) to solve the underground tunnel localization problem assuming that the ground elastic properties are known. An investigation of different combination of the physical models and signal processing methods are conducted and validated with field data. Our results show that the combination of the 3D FTDTD elastic model and full elastic waveform Bayesian inversion lead to the best performance for the source position estimation. The second part of the thesis then focuses on improvement of

the efficiency and accuracy of full elastic waveform inversion (FEWI) problem. The FEWI problem is now extended to jointly solve for the ground elastic parameter values and the position of the underground tunnel using observational data made with an array of geophones deployed on the ground surface. We develop a physical ground model for dimension reduction of the ground elastic parameter space so as to reduce ill-posedness arising from having to infer many parameters from a few observations. Two optimization algorithms, the Monte Carlo Metropolis Hasting and Simulated Annealing, are subsequently investigated for sampling the reduced parameter space to solve the Bayesian inversion problem. All the above-mentioned methodologies are evaluated first on synthetic data, and then further verified on field data collected at the heritage tunnel located in Singapore.

1.3 Summary of the Thesis

The main part of the thesis consists of three self-contained chapters, chapters 3 - 5. The main subject is related to detection of underground facilities using the active seismic technology. Both the acoustic and elastic models are used for representation of the recorded seismic signals, and then combinations with either the beamforming or Bayesian inversion algorithm are applied to determine in the ground subsurface the location of the underground facilities. For the Bayesian inversion to work effectively, a crucial aspect is the availability of a fairly accurate ground model for the forward model which solves the elastic wave equation. The Bayesian inversion algorithm is expanded to jointly estimate the tunnel location and the elastic material parameters. In the thesis, the algorithms developed are evaluated using the field data collected at the heritage tunnel site described.

The paper in Chapter 3, **Investigation of linear and nonlinear signal processing methods for seismic localization of underground tunnels,** presents the techniques to determine the location of an underground tunnel with seismic interrogation signals. Much of the work has involved either defining a P-wave acoustic model or a dispersive surface wave model to the received signal, and applying the time-delay processing technique and frequency-wavenumber (F-k) processing to determine the location of the underground tunnel. Considering the case of determining the location of an underground tunnel, this chapter proposed two physical models, the acoustic approximation ray tracing model and the FDTD 3D elastic wave model to represent the received seismic signal. Two localization algorithms, beamforming and Bayesian inversion, are developed for each physical model. The beam-forming algorithms implemented are the modified time-and-delay

beamformer and the F-K beamformer. Inversion is posed as an optimization problem to estimate the unknown position variable using the described physical forward models. The proposed four methodologies are demonstrated and compared using seismic signals recorded by geophones set up on the ground surface generated by a surface seismic excitation. The examples show with the field data, inversion for localization is most advantageous when the forward model completely describe all the elastic wave components as is the case of the FDTD 3D elastic model.

Chapter 4, **Joint seismic inversion and localization comparing Simulated Annealing and Metropolis Hasting**, presents two optimization methods (Simulated Annealing and the Metropolis Hasting algorithm) to solve the joint Bayesian inversion problem to estimate the material elastic parameters of a horizontally stratified medium, and the tunnel position in the ground. A reduced modelling scheme is proposed to reduce the size of the material elastic parameter vector in the estimation. The algorithms are then illustrated through a simulation example and compared. The results of the inversion of the soil density values show that both the global optimization method, i.e., Monte Carlo Metropolis Hasting algorithm and Simulated Annealing, are able to provide fairly good estimates which agree with the investigations in the literatures that focus only on geo-inversion of the elastic medium. As for the inversion result of the unknown source position, the range and depth samples generated by the Monte Carlo Metropolis Hasting inversion method display large fluctuations. But the point MAP estimates of the range and depth derived from 5000 runs of the Metropolis Hasting method are relatively close to the true range and depth of the source position. Simulated Annealing method which was implemented using an initial guess derived from the MAP value estimated from a small number of runs of the Monte Carlo Metropolis Hasting algorithm (in the

simulation, we use 50 runs), is able to improve the accuracy of the range and depth estimate of the source position.

Chapter 5, **Seismic inversion applied to underground tunnel localization problem**, extends the investigation of the joint Bayesian Inversion algorithm developed in Chapter 4 to solve a real-world problem to detect and localize the presence of an underground tunnel from measurements made by an array of seismic sensors deployed on the ground surface. The PDF curves of range and depth derived from Monte Carlo Metropolis Hasting samples shows multi-modal distribution behaviour, which made the mean estimate not a suitable parameter for processing the Monte Carlo samples. The MAP estimates derived from both the Monte Carlo Metropolis Hasting and Simulated Annealing methods however match well against the location of the underground tunnel, in agreement with the results of chapter 4 for the simulated data.

BIBLOGRAPHY

1. H. Arbarkanel, J. Cornwall, A. Despain, D. Eardley, R. Garwin, D. Hammer, R. Jeanloz, J. Katz, O. Rothaus, M. Ruderman, R. Schwitters, S. Treiman, J. Vesceky, ”Characterization of Underground Facilities,” *JASON, The MITRE Corporation, Virginia, JSR-97-155, 1999.*

2. N. Bleisten, J. K. Cohen, J. W. Stockwell, Jr., “Mathetmatics of multidimensional seismic imaging, migration and inversion,” *Springer-Verlag, New York, 2001*.

3. R. Miller, C. B. Park, J. Ivanov, D. W. Steeples, N. Ryden, R. F. Ballard, J. L. Llopis, T. S. Anderson, M. L. Moran, S. A. Ketcham, “Tunnel Detection Using

Seismic Methods," *in Proc. American Geophysical Union Meeting, Baltimore MD, 2007. NS21A-07.*

4. A. C. Gurbuz, J. H. McClellan, W. R. Scott, G. D. Larson, "Seismic tunnel imaging and detection," *IEEE International Conference on Image Processing, 3229-3232, 2006.*
5. Y. Ashida, "Seismic imaging ahead of a tunnel face with three component geophones," *International Journal of Rock Mechanics & Mining Sciences, **38(6)**, 823-831, 2001.*
6. S. L. Walters, R. D. Miller, Jianghai Xia, "Near surface tunnel detection using diffracted P-waves: a feasibility study," *Society of Exploration Geophysics (SEG) Annual Meeting, San Antonio, Texas 2007. SEG-2007-1128.*
7. S. Sloan, S. Peterie, J. Ivanov, R. Miller, and J, McKenna, "void detection using near-surface seismic methods," *Advances in Near-surface Seismology and Ground-penetrating Radar: 201-218, 2010.*
8. E. D. Guy, R. C. Nolen-Hocksema, J. Jeffery, J. J. Daniels, T. Lefchik, "High-resolution of SH-wave seismic reflection investigations near a coal mine-related roadway collapse features," *J. Appl. Geophys., **54(1-2)**, 51-70, 2003.*
9. D. Leparoux, A. Britri, G. Grandjean, "Underground cavities detection: a new method based on seismic Rayleigh waves," *EJEEG, **5**, 33-53, 2000.*
10. J. A. Baker, M. I. Shoemaker, M. Roark, N. Anderson, R. Hinds, "Reflection seismic mapping of caverns and collapsed caves, Cathage, Missouri" , *10^{th} EEGS Symposium on the Application of Geophysics to Engineering and Environment Problems, SAGEEP, Reno, 1997.*
11. B. A. Luke, D. A. Chase, "Detecting caves using seismic surface waves: a feasibility study," *The Engineering Geology and Hydrogeology of Karst Terrains,*

Proceeding of the 6th multi-disciplinary conference on sinkholes and the engineering and environment impacts of karst, Springfield, Missouri, Rotterdam, Netherlands: A. A. Balkema, 419-424, 1997.

12. B. Piwakowski, J. M. Waletet, D. Moreaux, “High resolution seismic prospection of old gypsum mines- evaluation of detection possibilities,” *Eur J. Environ. Eng. Geophys., **2**, 109-120, 1997.*
13. R. D. Miller, D. W. Steeples, “Detecting voids in a 0.6 m coal seam, 7 m deep, using seismic reflection,” *Geoexploration**, 28**, 109-119, 1991.*
14. J. C. Cook, “Seismic mapping of underground cavities using reflection amplitudes,” *Geophysics, **30(4)**, 527-538, 1965.*
15. A. Tarantola, “Inversion of seismic reflection data in the acoustic approximation,” *Geophysics, **49**, 1259-1266, 1984.*
16. Z. Koren, K. Mosegaard, E. Landa, P. Thore, A. Tarantola, “Monte Carlo estimation and resolution analysis of seismic background velocities,” *Journal of Geophysical Resarch, **96**, 20289-20299, 1991.*
17. S. Jin, R. Madariaga, J. Virieux, G. Lambare, “Two-dimensional asymptotic iterative elastic inversion,” *Geophysical Journal International, **108**, 575-588.*
18. J. Virieux, S. Operto, “An overview of full-waveform inversion in exploration geophysics,” *Geophysics, **74(6)**, 1-26, 2009.*
19. N. Ryden, C.B. Park, “Fast simulated annealing inversion of surface waves on pavement using phase-velocity spectra,” *Geophysics, **71(4)**, R49-R58, 2006.*
20. J. Martin, L. C. Wilcox, C. Burstedde, O. Ghattas, “A stochastic Newton MCMC method for large-scale statistical inverse problems with application to seismic inversion,” *Siam J. Sci. Comput., **34(3)**, A1460-1487,2012.*

CHAPTER 2

BACKGROUND

This chapter starts with a presentation of the basic equations of the theory of elasticity, which are required in the theory of the propagation of seismic wave. This is followed by a discussion of the methods (FDTD and ray tracing with the eikonal equation) used to generate synthetic seismograms and forward models in this thesis. The formulation of the seismic localization of a subsurface structure is next discussed in Section 2.3. In this thesis, we considered specifically the localization of an underground tunnel. The signal processing algorithms considered in this thesis to solve the localization problems are the beamforming and Bayesian (and other) inversion methods, which are elaborated in Section 2.4 & 2.5 respectively. Finally this chapter concludes with a discussion of the setup of the seismic experiments.

2.1 The seismic wave equation and representation of seismic signals

Seismic wave propagation in an elastic earth medium can be described by a differential vector equation that describes the direction and the quantity of energy transport at each location $\mathbf{x}$ in the medium as a function of time, see Aki and Richards [1]. In this chapter, $\mathbf{x}$ (x_1,x_2,x_3) is used in place of the normal (x,y,z).

The fundamental basis for the wave equation is the Newton's law of motion given as follows,

$$\rho(\mathbf{x})\frac{\partial^2 u_i}{\partial t^2} - \frac{\partial \sigma_{ij}}{\partial x_j} = f_i. \qquad \text{Equation (2-1)}$$

The displacement vector field $\mathbf{u}(\mathbf{x},t)$ at position $\mathbf{x}$ is described by a differential equation involving the stress tensor σ, an external force *f* provided by a point impulsive source, and density $\rho(\mathbf{x})$ of the ground. Each of the terms u_i, σ_{ij} and f_i is a function of position $\mathbf{x}$ and time.

Figure 2-1 introduces the components of the stress tensor σ. The meaning of the individual subscripts in the stress tensor components σ_{ij} is explained as follow. The first subscript, *i* , indicates that the plane element is perpendicular to the *i-th* axis. The second subscript, *j* , denotes the *j-th* component of the corresponding force. For example, σ_{21}, σ_{22} and σ_{23} are the components of the force acting on a surface element that is perpendicular to the axis x_2, see Figure 2-1.

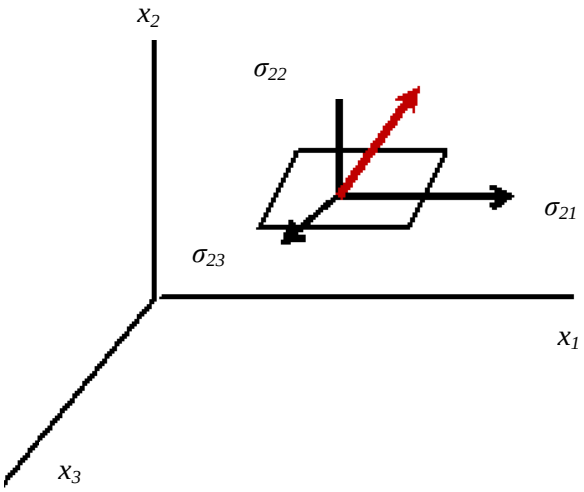

Figure 2-1 Introduction of the components of the stress tensor and the coordinate system

The stress tensor $\boldsymbol{\sigma}$ and the strain tensor $\boldsymbol{\varepsilon}$ satisfy a stress-strain relation known as the Hooke's law in a linear elastic medium, defined as follows,

$$\sigma_{ij} = c_{ijkl}\varepsilon_{kl} = \sum_{k=1}^{3}\sum_{l=1}^{3} c_{ijkl}\varepsilon_{kl}, \qquad \text{Equation (2-2)}$$

where c_{ijkl} is the fourth-order viscoelastic Hooke's tensor and the repeated latin indexes are summed according to Einstein's sum convention. The general elastic Hooke's tensor has $3^4 = 81$ components, but the number of independent elastic coefficients can be reduced to 21 for an arbitrary anisotropic medium [1].

The strain tensor ε_{ij} is defined by,

$$\varepsilon_{ij} = \frac{1}{2}\left(\frac{\partial u_i}{\partial x_j} + \frac{\partial u_j}{\partial x_i}\right),$$

For an isotropic, elastic medium (c_{ijkl} is invariant with respect to rotation) which has the same elastic properties in all directions, the elasticity is characterized by two elastic coefficients which can be represented by the Lamé parameters $\lambda(\mathbf{x})$ and $\mu(\mathbf{x})$.

The Hooke's law for an isotropic medium then takes the form as follows,

$$c_{ijkl} = \lambda\delta_{ij}\delta_{kl} + \mu\left(\delta_{ik}\delta_{jl} + \delta_{il}\delta_{jk}\right), \qquad \text{Equation (2-3)}$$

where δ_{ij} is the Kronecker delta. The coefficient $\mu(\mathbf{x})$ is the stress modulus that is the measure of the resistance of the material to stress but the coefficient $\lambda(\mathbf{x})$ has no immediate physical interpretation. In this case, a complete description of the material properties is given by $\{\lambda(\boldsymbol{x}), \mu(\boldsymbol{x}), \rho(\boldsymbol{x})\}$. Another equivalent parameterization, that is adopted in this study, is $\{v_p(\boldsymbol{x}), v_s(\boldsymbol{x}), \rho(\boldsymbol{x})\}$ where $v_p(\boldsymbol{x})$, $v_s(\boldsymbol{x})$ denote the wave

speeds of the P and S waves, and $\rho(\mathbf{x})$ denotes the soil density. The two set of parameters are related as follow,

$$v_p = \sqrt{\frac{\lambda + 2\mu}{\rho}},$$

$$v_p = \sqrt{\frac{\mu}{\rho}}.$$

Substitution of Equation (2-3) into Equation (2-2) gives the stress-displacement equation

$$\sigma_{ij} = \lambda(\delta_{ij}\partial_k u_k) + \mu(\partial_i u_j + \partial_j u_i). \qquad \text{Equation (2-4)}$$

where the notation $(\partial_i u_j) = \frac{\partial u_j}{\partial x_i}$ is used.

Combination of Equation (2-4) into the Newton's equation of motion Equation (2-1) gives the elastic wave equation for particle displacement (Navier equation),

$$(\lambda + \mu)\frac{\partial}{\partial x_1}\cdot\left(\frac{\partial u_1}{\partial x_1} + \frac{\partial u_2}{\partial x_2} + \frac{\partial u_3}{\partial x_3}\right) + \mu\nabla^2 u_1 + f_1 = \rho\frac{\partial^2 u_1}{\partial t^2},$$

$$(\lambda + \mu)\frac{\partial}{\partial x_2}\cdot\left(\frac{\partial u_1}{\partial x_1} + \frac{\partial u_2}{\partial x_2} + \frac{\partial u_3}{\partial x_3}\right) + \mu\nabla^2 u_2 + f_2 = \rho\frac{\partial^2 u_2}{\partial t^2},$$

$$(\lambda + \mu)\frac{\partial}{\partial x_3}\cdot\left(\frac{\partial u_1}{\partial x_1} + \frac{\partial u_2}{\partial x_2} + \frac{\partial u_3}{\partial x_3}\right) + \mu\nabla^2 u_3 + f_3 = \rho\frac{\partial^2 u_3}{\partial t^2}. \qquad \text{Equation (2-5)}$$

The Navier equation can be expressed in the vector form as follows

$$(\lambda + \mu)\nabla(\nabla\cdot\mathbf{u}) + \mu\nabla^2\mathbf{u} + \mathbf{f} = \rho\frac{\partial^2\mathbf{u}}{\partial t^2}, \qquad \text{Equation (2-6)}$$

where ∇ is the vector operator $(\partial/\partial x_1, \partial/\partial x_2, \partial/\partial x_3)$ and ∇^2 is the scalar operator $\frac{\partial^2}{\partial x_1^2} + \frac{\partial^2}{\partial x_2^2} + \frac{\partial^2}{\partial x_3^2}$. The Navier equation completely specifies all the seismic waves in an isotropic, purely elastic system. The system is linear as there is no higher order term in the displacement vector **u**, and ∇ and ∇^2 are linear operators. The Navier equation can be applied directly to solve for synthetic seismograms.

From the Navier equation, one can also derive two special forms of the equation of motion for a homogeneous isotropic medium, known as the wave equations. Here, the body force **f** is neglected. Applying the divergence operator to the Navier equation and we arrive at a scalar wave equation for the acoustic potential or volume dilatation $\nabla \cdot \mathbf{u} = \partial u_1 / \partial x_1 + \partial u_2 / \partial x_2 + \partial u_3 / \partial x_3$,

$$\frac{\partial^2 (\nabla \cdot \mathbf{u})}{\partial t^2} = \frac{1}{v_p^2} \nabla^2 (\nabla \cdot \mathbf{u}), \qquad \text{Equation (2-7)}$$

where $v_p(\mathbf{x})$ denotes the velocity of propagation of dilatation changes (longitudinal waves, compressional waves) such that $v_p = \sqrt{\frac{\lambda + 2\mu}{\rho}}$.

Applying the curl operator to Navier equation and we arrive at vector wave equation,

$$\nabla^2 (\nabla \times \mathbf{u}) = \frac{1}{v_s^2} \frac{\partial^2 (\nabla \times \mathbf{u})}{\partial t^2}, \qquad \text{Equation (2-8)}$$

where $v_s = \sqrt{\frac{\mu}{\rho}}$ is the velocity of the propagation of distortion changes (transverse waves, shear waves) .The operator is defined as follows,

$$\nabla \times \mathbf{u} = \left(\frac{\partial u_3}{\partial x_2} - \frac{\partial u_2}{\partial x_3} \right) \hat{x}_1 + \left(\frac{\partial u_1}{\partial x_3} - \frac{\partial u_3}{\partial x_1} \right) \hat{x}_2 + \left(\frac{\partial u_2}{\partial x_1} - \frac{\partial u_1}{\partial x_2} \right) \hat{x}_3 .$$ Equation (2-9)

It follows from Equations (2-8) and (2-9) that two types of elastic waves can propagate in a homogeneous elastic medium. These two types of elastic waves are namely the longitudinal compressional wave (P-wave) and the transverse shear waves (S-wave). The superposition of the P and S waves produces surface waves that also propagate in the elastic medium, see Aki and Richards [1]. There are two types of surface waves, namely the Rayleigh wave (R-wave) and Love wave (L-wave).

In a transversely isotropic Earth (e.g. the horizontally stratified elastic medium assumed in this study), the wave speed of Rayleigh wave is a function of the compressional, and vertically polarized shear wave speeds. The direction of the Rayleigh wave displacement is a combination of compressional and vertically polarized shear displacement. The wave speed of the Love wave in a transversely isotropic Earth depends primarily on the horizontally polarized shear wave speed. Moreover the displacement of the Love wave is parallel to the displacement associated with a horizontally polarized shear wave. In a transversely isotropic media, both types of surface waves exhibit a dispersion nature, i.e. their wave speeds depends on frequency. In this thesis, we are mainly concerned with the R-waves as the seismic source is a surface source generating mostly R-waves, and also the selected seismic sensors are vertical component geophones measuring the vertical ground vibrations, being related to the R-wave.

2.2 Methods for Computing Synthetic Seismograms

Finite difference (FD) [2-5], finite-element (FEM) [6-7], and ray-tracing [9-10] are among the main methods applied for the computation of seismic wavefields.

FD and FEM methods give complete solution of the wave equation, where accuracy of solution is related to the discretization of the elastic continuum by a discrete set of grid points or model elements to approximate the differentials in the Navier equation. In this thesis, we implemented the Finite Difference Time Domain (FDTD) method that employs finite differences as approximations to both the spatial and temporal partial derivatives that appear in the Navier equation. The other seismic wavefield generation method implemented in the thesis is asymptotic ray tracing methods based on high frequency asymptotic. Unlike FD and FEM, the calculation of ray-tracing methods is not performed directly in terms of the spatial coordinates of the ground medium. The wave-field is considered as an ensemble of rays in the high frequency approximation such that each ray is parameterized by a travel time and an amplitude function. As an example, the seismic wave-field is given as a sum of pre-specified events, such as, a sum of the primary reflected P-waves from a set of selected reflectors in the ground model.

2.2.1 Finite Difference Modelling

Consider the Cartesian representation of the elastic wave equation (refer to Equation (2-5) which is formulated in the 2D coordinate (x_1, x_2) as follow,

$$(\lambda + 2\mu)\frac{\partial^2 u_{x_1}}{\partial x_1^2} + (\lambda + \mu)\frac{\partial^2 u_{x_2}}{\partial x_1 \partial x_2} + \mu \frac{\partial^2 u_{x_1}}{\partial x_2^2} = \rho \frac{\partial^2 u_{x_1}}{\partial t^2}, \quad \text{Equation (2-10)}$$

and a similar equation for u_{x_2} displacement with an exchange of x_1 and x_2.

2.2.1.1 FDTD Equations

In the FDTD calculations, the partial differential operators in the elastic wave equations are expressed via 2nd order finite differential expansion in space and time respectively. In this thesis, we applied the 2D FDTD numerical algorithm from the CREWES numerical software [34]. The method keeps track only of the displacement of seismic wavefield and provides the output of the x_1 and x_2 displacements for each time step. The numerical algorithm applies the differential equation for the displacement u_{x_1} (Equation 2-10) directly for calculation at each time step. This is done through applying the finite difference representation to the components of Equation (2-10) and implementing a staggered grid (see Figure 2-2) for displacement representation in which the velocities and stresses are computed at different grid points, offset by half a grid length in both x_1 and x_2 illustrated by Figure 2-2. The error in this approximation is smaller because the sampling interval has been halved.

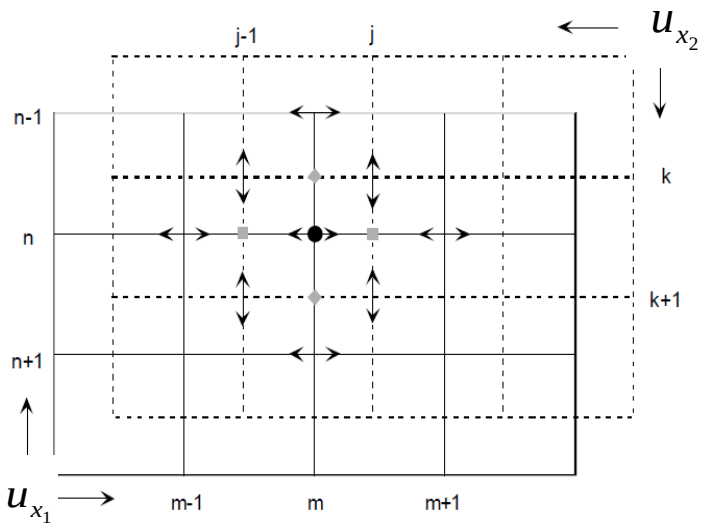

Figure 2-2 The staggered grid for displacement representation [34] . Similarly we can replace the same calculations for the x_2 displacement at the next time step with the components rotated 90 degrees.

2.2.1.2 Initial Conditions

The elastic ground medium is in equilibrium at time $t = 0$, i.e., stress and displacement are set to zero everywhere in the medium.

2.2.1.3 Boundary Conditions

The internal interfaces within the elastic ground medium are represented in terms of the changes of elastic wave speeds and density in a horizontally stratified medium assumed in this thesis. The explicit boundary conditions are imposed on the four edges of the finite-sized vertical grid where the FDTD calculations are performed. Different boundary conditions can be defined dependent on the problem to investigate. In the FDTD calculations performed in this thesis, the boundary conditions on the edges of the stratified soil layer model (excluding the source) are defined as followed; a free surface at $z=0$, a mirror surface at offset $x=0$, a transparent boundary at the right side, and a rigid bottom. The free surface boundary condition at $z=0$ simulates a real seismic experiment under flat topography and allow R-waves to be simulated. The mirror surface at offset $x=0$ act as if there is a continued geological model anti-symmetric about the zero x axis. The bottom is modelled as a rigid boundary and therefore a strong reflector. In our case where these reflections are not wanted, we introduce a large value for the depth of the final ground layer.

2.2.1.4 Source Excitation

The source is modelled with forcing input to the Navier wave equation using a Ricker[1] wavelet with a mean spectral energy density at *0.5 Hz*, and a spatial delta function.

2.2.2 Ray Theory and the Eikonal Equations

Ray theory is only strictly valid for medium where length scale variations of the Lamé parameters are much larger than the seismic wavelength. This is known as the high frequency assumption. At low frequencies, diffraction and scattering can be significant such that ray theory is generally not valid. In the implementation of the ray theory method, the seismic wave-field is considered as an ensemble of rays in the high frequency approximation such that each ray is parameterized by a travel time and an amplitude function. Thus solving the elastic wave equations, with substitution of the travelling wave expression for displacement $\mathbf{u}$ into the elastic wave equations, is reduced to solving for the travel times and amplitude functions. The travelling wave expression for displacement $\mathbf{u}$ is given as follows,

$$u(\mathbf{x_r}, t) = A(\mathbf{x_r}; \mathbf{x_s}) \exp\left[-i\omega\left(t + T(\mathbf{x_r}; \mathbf{x_s})\right)\right] \qquad \text{Equation (2-11)}$$

where $A(\mathbf{x_r}; \mathbf{x_s})$ denotes the wave amplitudes, and $T(\mathbf{x_r}; \mathbf{x_s})$ is a phase function which describes the arbitrary distribution in space of a surface of constant phase. The notations $\mathbf{x_r}$ and $\mathbf{x_s}$ denote the position vectors of the seismic receiver and the source respectively.

[1]Ricker wavelets are zero-phase wavelets with a central peak and two smaller side-lobes. A Ricker wavelet is uniquely defined in terms of its peak frequency given as $r(t) = \left(1 - 2\pi^2 f^2 t^2\right)\exp\left(-\pi^2 f^2 t^2\right)$. Ricker wavelet is commonly used by geophysicists to generate synthetic seismograms.

Consider the propagation of P-waves (refer to Equation (2-7)) given as

$$\frac{1}{v_p^2(\mathbf{x})}\frac{\partial^2\phi(\mathbf{x}_\mathbf{r},t)}{\partial t^2}-\nabla^2\phi(\mathbf{x}_\mathbf{r},t)=0, \qquad \text{Equation (2-12)}$$

where ϕ represents the scalar potential of a P-wave and $v_p(\mathbf{x})$ denotes the velocity of propagation of dilatation changes (compressional waves). Substitution of Equation (2-11) into (2-12) leads to the following,

$$\nabla^2 A-\omega^2 A|\nabla T|^2-i[2\omega\nabla A\cdot\nabla T]+\omega A\nabla^2 T=\frac{-A\omega^2}{v_p^2}, \text{ Equation (2-13)}$$

The Eikonal equation is derived from the real part by dividing through by $A\omega^2$ and taking the high frequency approximation yielding the expression as follow:

$$|\nabla T(\mathbf{x}_\mathbf{r};\mathbf{x}_\mathbf{s})|^2=\left(\frac{1}{v_p(\mathbf{x})}\right)^2, \qquad \text{Equation (2-14)}$$

Equation (2-14) models the kinematic propagation of the high frequency waves and solving it leads to estimation of the phase function $T(\mathbf{x}_\mathbf{r};\mathbf{x}_s)$ of the ray solution. The Transport equation is derived by dividing through by ω the imaginary part of Equation (2-13). The Transport equation is used for computation of the wave amplitude $A(\mathbf{x}_\mathbf{r};\mathbf{x}_\mathbf{s})$.Similar substitution into the S-wave vector potential described by Equation (2-8) leads to identical expressions for eikonal and transport equations.

2.3 Seismic Localization of Subsurface Structures

The principal task is to locate a subsurface structure in an elastic medium using the scatterings from a subsurface structure recorded by an array of seismic sensors on the ground surface. This thesis considers a tunnel as the subsurface structure of interest to locate in the problem.

The geometry of the problem is shown in Figure 2-3. The environment consists of an elastic bottom half-space with air in the upper half space. There is a tunnel present in the bottom half space as shown in Figure 2-3. The medium inside the tunnel is air. To represent the active scenario, there is a source on the surface that generates seismic waves that will travel through the elastic medium to interact with the tunnel. The seismic sensors to detect the seismic sensors are placed on the ground surface that perpendicular to the tunnel to represent a 2D problem. The source is a weight generating an impulse.

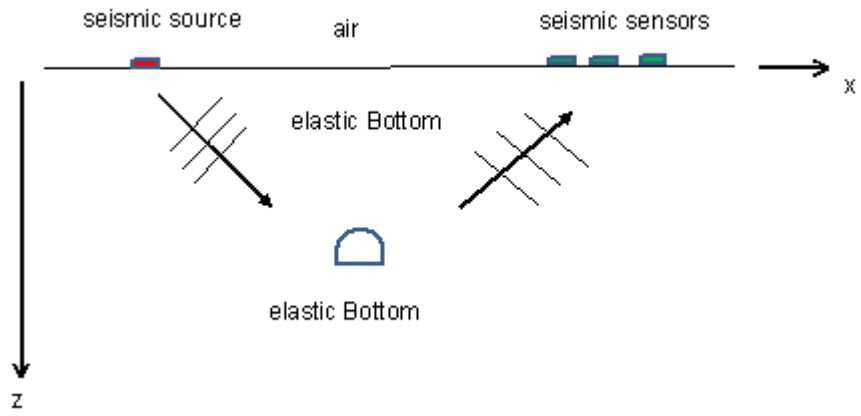

Figure 2-3 A general scenario representing the problem of seismic localization of subsurface structure

2.4 Seismic Beamforming Methods

2.4.1 Summary of work done in Seismic beamforming in the Literatures

The basic principle of beamforming techniques [11] for localization consists of first computing the relative time difference of arrivals to the signals recorded at the seismic array in order to correct for the non-coincidence arrival of the seismic waves at the different seismic sensors, and then averaging the energy of the seismic signals. The position of the seismic source is computed from the averaged beamformed output corresponding to the position where a peak in the beamformer power occurs. The time delays are defined by the physical model, which is described by a signal model represented by the elastic wave equation, and by the model parameters that include subsurface geology, position of seismic sensors & source.

In [12], the authors apply the sum-delay beamforming technique to noisy seismic refraction data. The time delays are calculated from the travel time curve for the different refraction segments corresponding to the each soil layer (see Figure 1-1). In [13], the sum-delay beamformer was first tested using synthetic seismic reflection data from shots in a borehole to a linear array on the ground surface, and the earthquake data recorded with a broadband three-component array. A three-component array is an array of three-component geophones that measure the seismic waves along the three orthogonal directions of the x, y, z axes.

In [14], Lacosse et al. applied a frequency domain beamformer, namely the frequency-wavenumber analysis (F-K) for analysing the wave speeds and frequency properties of seismic waves. The F-K beamformer performed a search on a dense wavenumber grid for each frequency for estimation of both the seismic source

location and the seismic wave speed corresponding to maximum F-K beamformer power. The F-K analysis is used mostly for analyzing the dispersive R-wave propagation in the elastic ground medium [15-16].

2.4.2 Sum-Delay Beamformer

The sum-delay beamformer is one of the simplest beamforming algorithm. It works by assuming that the signals recorded by the seismic array comprises of one type of elastic wave with wave speed v. The seismic sensor *j* records the time series $x_j(t)$ as

$$x_j(t) = s\left(t - \tau_j\right) + n_j(t), \qquad \text{Equation (2-15)}$$

where τ_j denotes the time for the elastic wave to propagate from the seismic source to the sensor, and $s\left(t - \tau_j\right)$ denotes the delayed seismic velocity signal. The notation $n_j(t)$ denotes the measurement noise.

Assume that the tunnel is located at (x_s, z_s), and we can write τ_j as,

$$\tau_j = \tau_0(x_s, z_s) + \tau_j(x_s, z_s),$$

where $\tau_0(x_s, z_s)$ denotes the time it takes for the elastic wave to travel from the seismic source to the tunnel location, and $\tau_j(x_s, z_s)$ denotes the time for the elastic scatterings from the tunnel to reach seismic sensor *j.*

In the sum-delay beamformer, a search space is considered where the tunnel is assumed to be located. For each assumed location of the tunnel at (x, z), the algorithm computes the times of arrival τ_j for all sensors in the array and perform time-shifting as follows,

$$\tilde{x}_j(t) = x_j(t + \tau_j). \qquad \text{Equation (2-16)}$$

The beamforming power of the time-shifted signals for the seismic array comprising of *M* sensors is then computed as follows,

$$P_{bf}(x,z) = \frac{1}{M}\sum_{j=1}^{M}\left\{\int\left(\tilde{x}_j(t)\right)^2 dt\right\}. \qquad \text{Equation (2-17)}$$

The location of the tunnel is subsequently derived from the location (x,z) where the peak in the beamforming power occurs.

2.4.3 Frequency-Wavenumber (F-K) Beamformer

A frequency-wavenumber (F-K) beamformer simultaneously calculates the beamformer power distributed among different slowness vector $\boldsymbol{s}$ for a fixed frequency of the seismic signal. The slowness vector is dependent on the azimuth angle θ (see Figure 2-4) and the wave speed v as follow,

$$\mathbf{s} = \begin{pmatrix} s_x \\ s_z \end{pmatrix} = \begin{pmatrix} \cos\theta / v \\ \sin\theta / v \end{pmatrix}, \qquad \text{Equation (2-18)}$$

The slowness vector $\boldsymbol{s}$ is also related to the wavenumber vector $\boldsymbol{k}$ as follow,

$$\mathbf{k} = \omega \cdot \mathbf{s} = \begin{pmatrix} k_x \\ k_z \end{pmatrix} = \frac{\omega}{v}\begin{pmatrix} \cos\theta \\ \sin\theta \end{pmatrix} \qquad \text{Equation (2-19)}$$

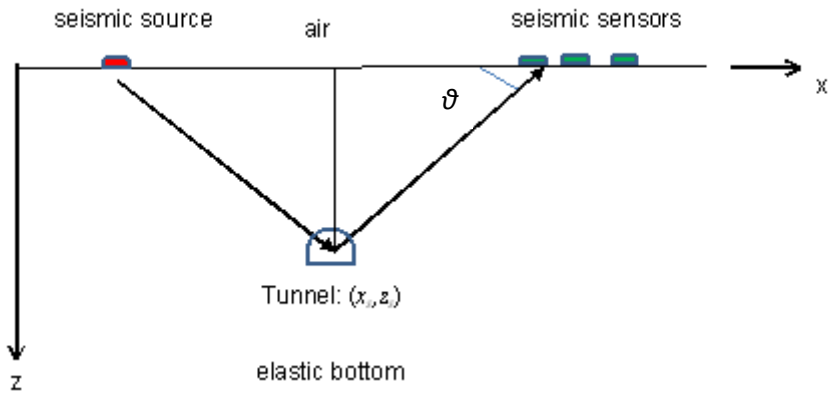

Figure 2-4 A general scenario representing the F-K beamforming problem

The first step of the F-K beamformer is a filtering process to transform the signals to a narrowband signal. Let f_o denotes the center frequency of the filtered signal. The F-K beamforming computes the time shifts for all plausible combinations of wave speed v and azimuth angle θ for the seismic array, and then summed up the time-shifted seismic array signal to find the best (v,θ) parameter combination that gives the highest amplitude of the summed signals. From this, the position of the tunnel can be estimated.

2.5 Seismic Inversion

Generally stated, inverse problems are concerned with determining causes for a desired or observed effect (Engl, Hankel and Neuber [17]). The opposite problem is finding the effect of a cause, also known as the forward modelling problem.

2.5.1 Summary of work done in Seismic Inversion in the Literatures

The scenario of a typical seismic inversion problem [18] is described as follow. A seismic source at known location excites the ground surface producing a seismic

wave that travels through the soil, interacting with the subsurface, and the waves reflected from the subsurface are recorded by an array of seismic sensors on the ground surface. The calculation of the synthetic seismic data for a known ground model is called the seismic forward modelling problem, while seismic inversion is concerned with finding material elastic properties of the ground model from the recorded data.

The seismic inversion problem of finding the elastic material properties (P, S wave speeds and soil densities) of the ground is a large scale optimization problem involving a large set of parameters depending on the discretization of the ground.

Most of the recent real-data case studies of seismic full wave inversion have been performed at acoustic isotropic approximation, considering only the P-wave velocities as the model parameter [19-26] to reduce the dimension of the unknowns so as to make the inversion better posed.

A limited number of full waveform inversion of all the elastic parameters have been proposed. Tarantola [27] recommends inversion first for P-wave speeds, second for S-wave speeds, and finally for density. This strategy is generally suitable if the footprint of the S-wave velocity structure on the seismic wavefield is small. In their paper [28], Brossier et al conclude that joint inversion for the P and S wave speeds is necessary for inversion of land data involving both body waves and surface waves. The presence of the high amplitude surface waves require inversion of the S wave speeds with the P wave speeds. Another recent application of elastic full wave inversion to a gas field is presented in [29]. The authors invert the Lamé parameters and image the Poisson’s ratio anomalies associated with presence of gas.

2.5.2 Formulation of the Inversion Problem for Tunnel Localization

In our study, we are interested to infer from the seismic measurements both the material elastic properties and information about presence of the tunnel such as its location.

Hence we formulate the seismic inversion problem as follow. To determine from the seismic observational data measured by an array of seismic sensors on the ground surface an unknown parameter vector $\mathbf{m(x)}$, $\mathbf{m(x)} = \{v_p(\mathbf{x}), v_s(\mathbf{x}), \rho(\mathbf{x}), (x_s, z_s)\}$ and $\mathbf{m(x)} \in \Re^N$

The ground is modelled as a horizontally stratified medium comprising of K soil layers. The model parameter dimension can be calculated as $N = 3K + 2$. In this study, we adopt a five layer soil structure which leads to a search space of dimension $N = 17$ that is also considered as a large scale optimization problem in the inversion process. In Chapter 5 of this dissertation, we have proposed a reduced modelling scheme with a ground model to reduce the search dimension for the ground elastic parameters.

2.5.3 Forward Modelling

The forward model is the calculation of the synthetic seismogram comprising of the scatterings (reflections, diffraction waves) from the tunnel, given that the seismic source signature and the ground model are known. The tunnel investigated in the study is of diameter $3\ \mathrm{m}$ with height $3\ \mathrm{m}$. It is made of concrete and filled with air cavity. Researchers using seismic techniques for cavity detection apply the presence of three phenomena for evidence of a cavity: free oscillations or resonance of the cavity walls, anomalous amplitude attenuations, and delay of arrival times [30-33].

The cavity with the thick concrete walls can be assumed to act as a point source that will cause the seismic waves impinge on it be reflected, and the scatterings are then recorded by the sensors deployed on the ground surface.

We introduced the forward model to model the scatterings (reflections & diffractions) from the complex tunnel structure as follow. Assume that a source is located at the tunnel location (x_s, z_s) and the ground is described by a horizontally stratified medium. Apply the 2D FDTD method to solve the Navier equation to generate the elastic particle displacement measured by an array of seismic sensors placed on the ground surface.

2.5.4 Classical Inversion

The discretized seismic data recorded by an array of M seismic sensors on the ground surface is given by,

$$\mathbf{d}_{obs} = g(\mathbf{m}) + \mathbf{n}, \qquad \text{Equation (2-20)}$$

where g is a nonlinear forward modelling operator and $\mathbf{n}$ is the error term. The error terms models the random ambient noise and the system errors. There is no explicit expression for the forward modelling operator in this case. However it can be implemented numerically by solving the Navier wave equation using the FDTD method (see Section 2.2.1).

The deterministic inverse problem is interested to estimate $\mathbf{m}$ from $\mathbf{d}_{obs}$ by minimizing the misfit between the forward model predictions $g(\mathbf{m})$ and the observed data $\mathbf{d}_{obs}$ in the $\mathbf{W}$-norm.

$$E = \frac{1}{2}\left\| g(\mathbf{m}) - \mathbf{d}_{obs} \right\|_{\mathbf{W}}^{2}$$
$$\mathbf{m}^{*} = arg\min_{\mathbf{m}} \left(\frac{1}{2}\left(g(\mathbf{m}) - \mathbf{d}_{obs}\right)\mathbf{W}^{-1}\left(g(\mathbf{m}) - \mathbf{d}_{obs}\right) \right) \qquad \text{Equation (2-21)}$$

where $\mathbf{W} \in \Re^{M} \times \Re^{M}$ is a matrix. For most deterministic inversion algorithms, the matrix $\mathbf{W}$ is generally defined as the identity matrix. Equation (2-21) is subsequently solved by interative local search methods such as steepest descent, conjugated gradients, Gauss-Newton or the Levenberg-Marquard methods [36]. However a problem with these local search techniques is that the search could be trapped in local optima due to the non-convex nature of the objective function defined by Equation (2-21). Possible ways around this problem is to apply global search strategy such as simulated annealing [37], and genetic algorithms [38]. Both the local and global optimization methods only provide a point estimate of the solution and do not provide uncertainty analysis for the solutions obtained. Whereas, the Bayesian inversion algorithm which allows incorporation of the probabilistic models for the signal and noise will provide both the point MAP estimate and the posterior statistical information such as the mean and variance.

The deterministic inverse objective function defined by Equation (2-21) is often compared and related to the maximum likelihood function. If the error terms **n** is assumed to be zero-mean Gaussian with covariance $\mathbf{C}_{\text{noise}}$, the maximum likelihood solution is defined by minimizing the following expression,

$$E(\mathbf{m}) = \frac{1}{2}\left(g(\mathbf{m}) - \mathbf{d}_{obs}\right)\mathbf{C}_{noise}^{-1}\left(g(\mathbf{m}) - \mathbf{d}_{obs}\right), \qquad \text{Equation (2-22)}$$

which is identical to the weighted least squares expression described Equation (2-21) where the weighting matrix $\mathbf{W}$ is given by the inverse of the noise covariance matrix.

2.5.5 Bayesian Inversion

Inverse problems are usually ill-posed where many different choices of model parameters may be consistent with the data. One reason for the non-uniqueness is the uncertainty in both the measurements and the model. The classicial inversion algorithms described in the previous section only estimate the "best" parameter values that fit the data. However we are interested in not just getting the point estimate of the best-fit parameters but also to obtain a complete statistical description of the model parameter values. The Bayesian method is able to do so by formulating the inverse problem as a statistical inference framework, incorporating uncertainties in the measurements & forward model, and prior information on the model parameters. The solution of the Bayesian inversion method is the posterior joint probability density function of the parameters that contains the uncertainty level or degree of confidence of the estimated parameter values.

The Bayes theorem expresses the posterior probability density of the model parameters given the data $\mathbf{d}_{obs}$ as the conditional probability given as,

$$\pi_{\text{posterior}}(\mathbf{m}) = \pi(\mathbf{m}|\mathbf{d}_{\text{obs}}) = \frac{\pi_{\text{prior}}(\mathbf{m})\pi(\mathbf{d}_{\text{obs}}|\mathbf{m})}{\pi(\mathbf{d}_{\text{obs}})} . \qquad \text{Equation (2-23)}$$

$\pi_{\text{prior}}(\mathbf{m})$ is the prior probability density function for the model parameter $\mathbf{m}$ which expresses the probability distribution of the model parameter before the data is observed. The probability density function $\pi(\mathbf{d}_{\text{obs}}|\mathbf{m})$ defines a function of $\mathbf{m}$ known as

the likelihood function. $\pi(\mathbf{d}_{\text{obs}})$ is the marginal density for the data $\mathbf{d}_{\text{obs}}$ and is written as follow,

$$\pi(\mathbf{d}_{\text{obs}}) = \int \pi_{\text{prior}}(m)\,\pi(\mathbf{d}_{\text{obs}}\,|\mathbf{m})d\mathbf{m}. \qquad \text{Equation (2-24)}$$

As $\pi(\mathbf{d}_{\text{obs}})$ does not depend on the unknown $\mathbf{m}$, it can be considered as a normalizing constant. Henceforth we can write Equation (2-24) into another form as follows,

$$\pi_{\text{posterior}}(\mathbf{m}) \propto \pi_{\text{prior}}(m)\,\pi(\mathbf{d}_{\text{obs}}\,|\mathbf{m}), \qquad \text{Equation (2-25)}$$

where the symbol $\propto$ indicates proportionality. The complete solution for $\mathbf{m}$ is hence represented by the posterior distribution which also includes the uncertainty. The posterior solution for $\mathbf{m}$ includes the posterior mean and the maximum posterior (MAP), while the uncertainty is described by the posterior covariance matrix.

The conditional mean estimate is defined as

$$\mathbf{m}_{CM} = E\{\mathbf{m}\,|\,\mathbf{d}_{obs}\} = \int \mathbf{m}\pi(\mathbf{m}\,|\mathbf{d}_{\text{obs}}(x,z,t))d\mathbf{m}, \qquad \text{Equation (2-26)}$$

where E is the expectation operator (which in Monte Carlo simulations can be realized as the arithmetic mean).

The maximum posterior (MAP) solution which provides the point estimate for $\mathbf{m}$ is defined as follows,

$$\mathbf{m}^{*} = arg\,\max_{\mathbf{m}}\{\pi(\mathbf{m}\,|\mathbf{d}_{\text{obs}}(x,z,t))\}. \qquad \text{Equation (2-27)}$$

The uncertainty of the model is described by the posterior covariance matrix calculated as follows,

$$\mathbf{C}_{\mathbf{m}} = \mathrm{E}\left\{(\mathbf{m}-\mathbf{m}_{CM})(\mathbf{m}-\mathbf{m}_{CM})^{T}\right\} = \int (\mathbf{m}-\mathbf{m}_{CM})(\mathbf{m}-\mathbf{m}_{CM})^{T}\pi(\mathbf{m}\,|\,\mathbf{d}_{\mathrm{obs}}(x,z,t))d\mathbf{m}$$

Equation (2-28)

The variances of the solution model given by the diagonal components of the covariance matrix provide a means for evaluating the quality of the solution to the inverse problem.

2.5.6 Markov Chain Monte Carlo (MCMC)

For a high dimension $\mathbf{m}$ often encountered in seismic inversion problem, it is very time consuming to compute the posterior distribution for all possible combinations of $\mathbf{m}$. The MCMC method provides a numerical algorithm to generate samples from the posterior distribution by simulating a Markov chain[2]. The general idea of MCMC is to use the previous sample values to randomly generate the next sample value, generating a Markov chain (here the transition probabilities between sample values are only a function of the most recent previous value). In our example, the variables are the unknown parameter vector $\mathbf{m}$. By generating successive values of the model variables $\mathbf{m}_j$, $\mathbf{m}_{j+1}$, $\mathbf{m}_{j+2}$…, using MCMC sampling method, it can be shown that the distribution of $\mathbf{m}_j$'s when *j* is large is close to the posterior distribution. We may therefore say that for sufficiently large *j*, the random model variable $\mathbf{m}_j$'s is approximately the variable we are seeking.

[2] A Markov chain is a discrete-time stochastic process X_1, X_2, …, taking values in an arbitrary state space that has the Markov property and stationary transition probabilities:

- the conditional distribution of X_n given $X_1,\ldots X_{n-1}$ is the same as the conditional probability of X_n given X_{n-1} only, and
- the conditional distribution of X_n given X_{n-1} does not depend on *n*.

In this study, we implement the Metropolis Hasting algorithm which was proposed by Metropolis et al [39], and later generalized by Hastings [40]. Each step of the Metropolis algorithm is made up of two interacting random steps. The first step was a Monte Carlo simulation step to generate the model parameter set. The second step was accepting or rejecting the model parameter set proposed by the Monte Carlo simulation step, using an acceptance probability derived from the data noise distribution and the forward model.

Figure 2-5 describes the Metropolis Hasting sampling scheme while the pseudo-code of the Metropolis Hasting algorithm can be written as follow,

- At each step, vary one component of the parameter vector $\mathbf{m}_R$ generated from prior distribution $\mathrm{q}(\mathbf{m}_R)$
- Compute $\mathbf{d}_{\mathbf{m}}$ using the forward model.
- Compute the acceptance probability $P_{acc} = \frac{\pi_{posterior}(\mathbf{m}^{(pro)})}{\pi_{posterior}(\mathbf{m}^{(cur)})}$, $\mathbf{m}^{(pro)}$ is the proposed variable, and $\mathbf{m}^{(cur)}$ is the current variable value. The parameters are changed at each step by random selection from a uniform probability density function.
- Accept the changes to $\mathbf{m}^{(pro)}$ if $\min\{P_{acc},1\} > \mathrm{rand}$;

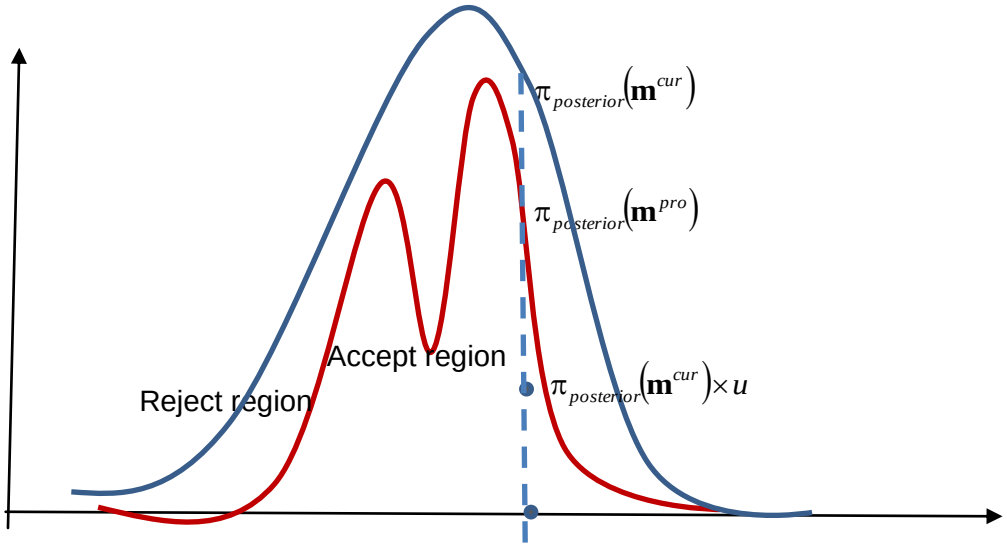

Figure 2-5 Metropolis Hasting sampling scheme:
Sample a candidate $\mathbf{m}^{(pro)}$ *and a variable* u *from uniform distribution.*
Accept the candidate sample if $\left(\pi_{posterior}\left(\mathbf{m}^{(cur)}\right)\times u\right) < \pi_{posterior}\left(\mathbf{m}^{(pro)}\right)$,
otherwise reject it.
The red pdf curve is the converged posterior pdf curve after multiple iterations of the Monte Carlo Metropolis Hasting sampling, while the blue pdf curve is the initial posterior pdf curve.

2.5.7 Simulated Annealing

Simulated annealing is a probabilistic approach proposed in Kirkpatrick, Gelett and Vecchi (1983) and Cerny (1985) for finding the global minimum of a cost function that may possess several local minima. It originates from a physical process whereby a solid is slowly cooled so that when eventually its structure is “frozen”, this happens at a minimum energy configuration. The cooling process is controlled by the temperature T such that the molecules are allowed to move freely at high temperatures and restricting their motion at low temperatures.

The steps to implement the simulated annealing are described as follow [43].

- Consider decreasing series of temperatures $T(t)$
- For each temperature, iterate these steps:

- Propose an update $\mathbf{m}_R^{(j+1)}$ of the unknown parameter and evaluate the optimization function $F(\mathbf{m}_R^{(j+1)})$
- Accept updates that improve solution
- Accept some updates that don't improve solution. Acceptance probability depends on "temperature" parameter and is defined as follow, $\exp\left[-\frac{1}{T(t)}\left(F(\mathbf{m}_R^{(j+1)}) - F(\mathbf{m}_R^{(j)})\right)\right]$
- As T goes to zero, the values simulated from this distribution becomes more concentrated around a narrow neighbor-hood of F.

2.6 Seismic Tunnel Experiments

The principal objective of the experiment is the detection of unknown tunnels by seismic experiments involving active sources on the ground surface and geophone arrays.

The experiment was performed as follows. The experiment was carried in Labrador park in Singapore to detect a heritage tunnel (see Figure 1-4). A geophone array is deployed along *LINE 1* (see Figure 2-6), crossing the tunnel at *90* degrees. Figure 2-6 describes the topological information of the tunnel site.

A geophysical survey for determining the compressional P-wave speed profile was carried out along *LINE-01, LINE-2A and LINE-2B* respectively. The seismic refraction method [44] widely used in engineering application is applied in the geophysical survey. The method measures the time it takes for a compressional sound wave generated by a sound source to travel down through the layers of the earth and back up to the geophones placed on the ground surface. From the time-

distance information, the compressional P-wave speed variations and depths to individual layers are calculated and modelled. The P-wave profile measured along *LINE-01* which is the closest to the tunnel is applied for the inversion processing in the later chapters. The compressional wave profile for *LINE-01* is displayed in Figure 2-10 where it can be seen that the compressional wave travels faster with increasing soil depth.

The seismic source is provided by a weight drop. A cylinder with a hemispherical end cap weighing 18 kg is designed to drop from a 1 m height to generate the seismic impact forcing on the ground surface. The support structure functions as a guide to ensure that the weight will not tumble when it lands on the ground surface. In addition, soft rubber pads are added on the metal plate at the base of the support structure so as to ensure that the weight will generate one main broadband seismic impulse function (see Figure 2-11) with minimum spurious re-bounce signals. The seismic sensors used for the experiment are the geophones (see Figure 2-12) which measures particle velocity of ground motion. In the experiment, two vertical component *GS11D* geophones are deployed which are capable of recording seismic vibration along the vertical component in the 4.5 to $100\ \mathrm{Hz}$ range. The geophone resonant or natural frequency which determine the low-frequency limit of the reliable seismic measurement is $4.5\ \mathrm{Hz}$ The geophones are connected to the *Brüel & Kjær* 32-bit, 4-channel digital recorder to digitize the measured seismic signals where the sampling frequency is fixed at $4096\ \mathrm{Hz}$.

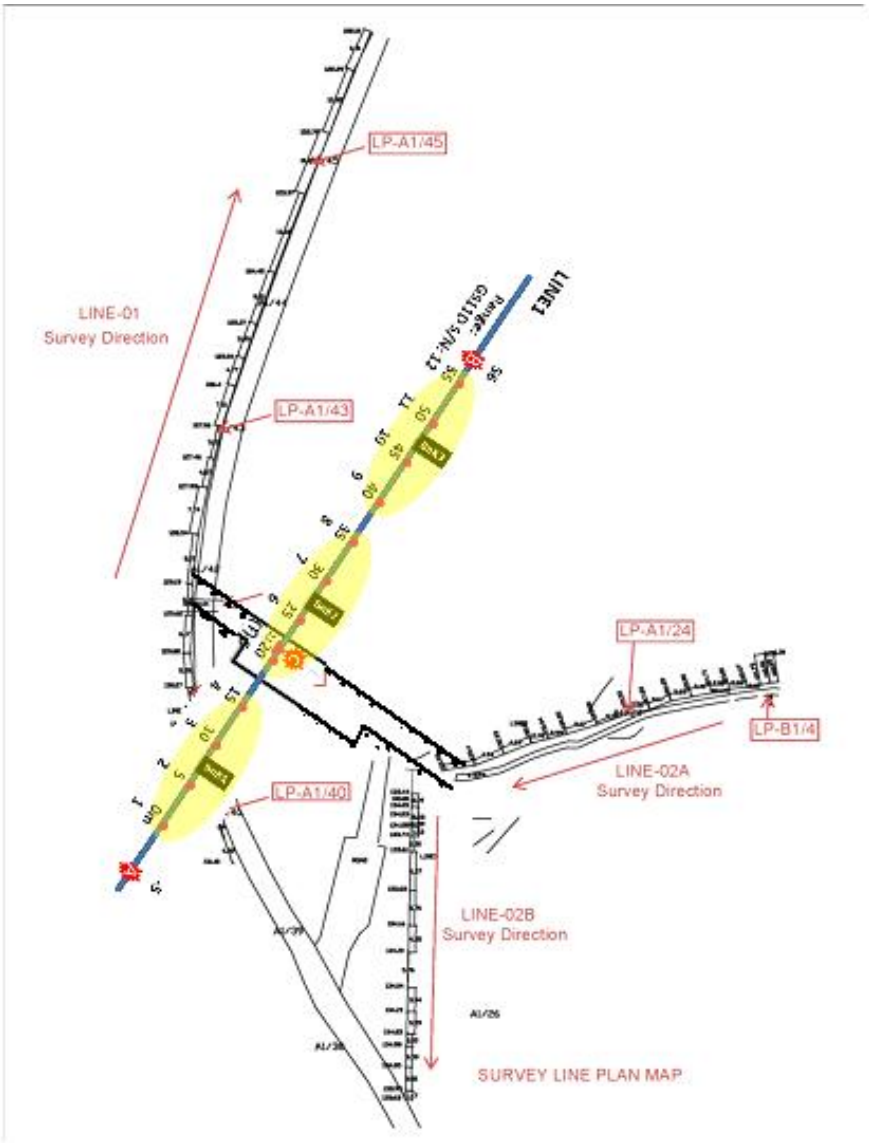

Figure 2-6 Location map of the geophone (LINE 1) relative to the tunnel and the survey lines.

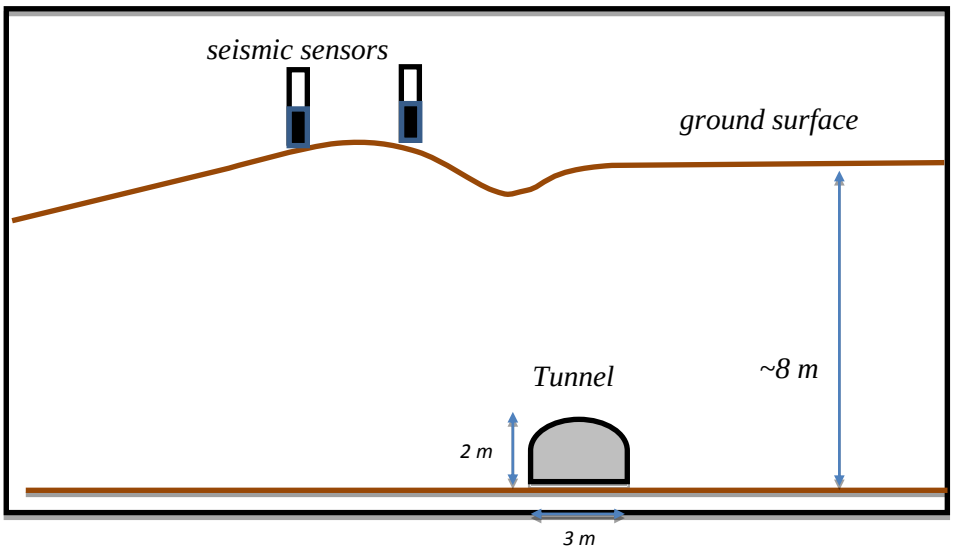

Figure 2-7 Estimated topographical information of tunnel trial site

Figure 2-8 Seismic source (weight drop) used in the geophysical survey

Figure 2-9 Setup of survey line 1 for the geophysical measurement

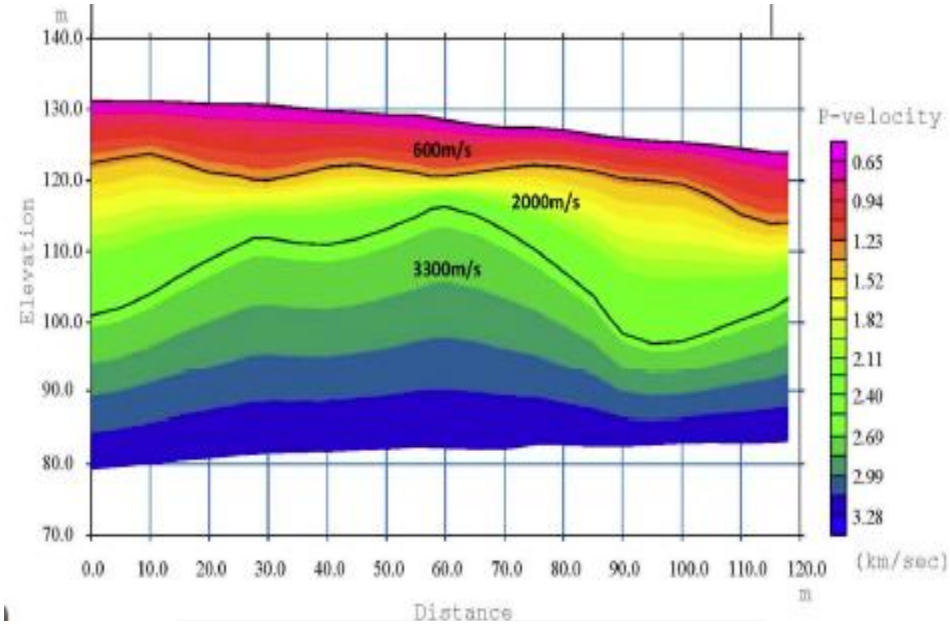

Figure 2-10 Compressional wave speed profile along LINE-01 located near tunnel

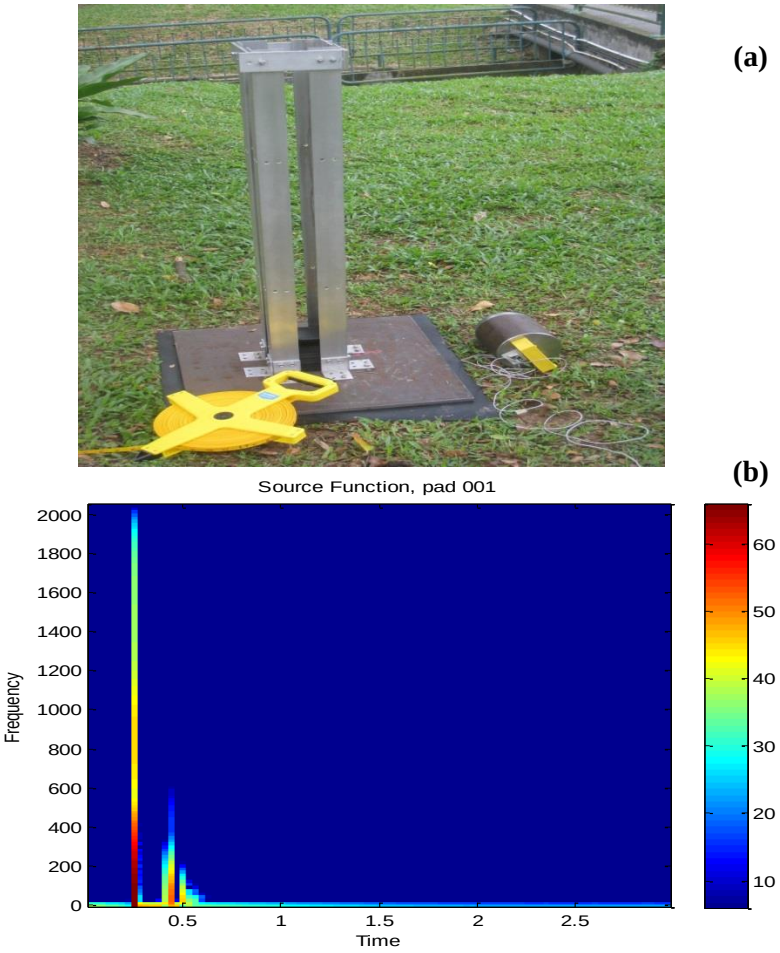

Figure 2-11 Seismic source, weight drop,
(b) Spectrogram of the measured source function from weight drop.
The signal is measured by an accelerometer mounted on the 18kg weight drop.

(a) (b)

Figure 2-12 Seismic sensors and the acquisition system.
(a) Vertical GS11D geophones, (b) Brüel & Kjær digital recorder

BIBLOGRAPHY

1. K. Aki, P. G. Richards, “Quantitative Seismology, Second Edition,” *(University Science Books, Sausalito, California, 2002).*
2. J. Virieux, “*SH*-wave propagation in heterogeneous media: Velocity-stress finite-difference method,” *Geophysics, **49**, 1933-1942, 1984.*
3. J. Virieux, “*P* – *SV* wave propagation in heterogeneous media: Velocity-stress finite difference method,” *Geophysics, **51**, 889-901, 1986.*
4. A. R. Levander, “Fourth-order finite-difference *P* – *SV* seismograms,” *Geophysics, **53**, 1425-1436, 1988.*
5. J. Carione, D. Kosloff, R. Kosloff, “Viscoacoustic wave propagation simulation in the earth,” *Geophysics, **53**, 769-777, 1988.*
6. J. Lysmer, L. A. Drake, “A finite element method for seismology,” *in B. Aider, B. S. Fernback, and B. A. Bolt, Eds., Methods in computational physics 11, Seismology: Academic Press.*
7. K. J. Marfurt, “Seismic modeling: A frequency-domain finite element approach,” *54th Ann. Internat. Mtg., Soc. Expl. Geophtsics., Expanded Abstracts, 1984.*
8. V. Červenŷ, I. Molotkov, II. Psencik, “Ray methods in seismology,” *Uiniverzita Karlova, 1977.*
9. V. Červenŷ, “The application of ray tracing to the numerical modeling of seismic wavefields in complex structures,” *in G. Dohr, Ed., Seismic Shear Waves, Part A: Theory.*
10. J. Virieux, G. Lambaré, “Theory and observations – body waves: ray methods and finite frequency effects,” *in B. Romanovitz & A. Diewonski (eds), Treatise of Geophysics, Volume 1: Seismology and structure of the Earth, Elsevier.*

11. S. Rost, C. Thomas, “Array seismology: Methods and Applications,” *Review of Geophysics, **40(3)**, 2-1 to 2-27, 2002.*

12. A. J. Ogah, A. D. Chinedu, “The beam-forming technique for enhancement of noisy seismic refraction data,” *International Journal of Geoscience, **3**, 866-871, 2012.*

13. W. Mao, D. Gubbina, “Simultaneous determination of time delays and stacking weights in seismic array beamforming,” *Geophysics, **60(2)**, 491-502, 1995*.

14. R. T. Lacoss, E. J. Kelly, M. N. Toksov, “Estimation of seismic noise structure using arrays,” *Geophysics, **34**, 21-38, 1969.*

15. S. R. Cinras, J. J. G-Merino, P. Alfaro, J. R-Herranz, “Optimizing the number of stations in array measurements: Experimental outcomes for different array geometries and the f-k method,” *Journal of Applied Geophysics, **102**, 96-133, 2014.*

16. S. Foti, R. Lancellotta, L. Sambuelli, L. V. Socco, “Notes on *fk* analysis of surface waves,” *ANNALI DI GEOFISICA, **43(6)**, 1199-1209, 2000.*

17. H. W. Engl, M. Hanke, A. Neubauer, “Regularization of Inverse Problems,” *(Kluwer Academic Publisher, Netherlands, 2000), Chap.1.*

18. N. Bleistein, J. K. Cohen, J. W. Stockwell, Jr., “Mathematics of multidimensional seismic imaging, migration and inversion,” *(Springer-Verlag, New York, 2001).*

19. J. X. Dessa, G. Pascal, “Combined traveltime and frequency domain seismic waveform inversion: A case study on multi-offset ultrasonic data,” *Geophysical Journal International, **154**, 117-113, 2003.*

20. C. Ravaut, S. Operto, L. Improta, J. Virieux, A. Herrero, P. Dell’ Aversana, “Multi-scale imaging of complex structures from multi-fold wide-aperture seismic data by

frequency-domain full-wavefield inversions: Application to a thrust belt," *Geophysical Journal International, **159**, 1032-1056, 2004.*

21. C. Chironi, J. V. Morgan, M. R. Warner, "Imaging of intrabasalt and subbasalt structure with full wavefield seismic tomography," *Journal of Geophysical Research, **11**, B05313, doi:10.1029/2004JB003593, 2006.*
22. F. Gao, A. R. Levander, R. G. Pratt, C. A. Zelt, G. L. Fradelizio, "Waveform tomography at a groundwater contamination site: Surface reflection data," *Geophysics, **72(5)**, G45-G55, 2006.*
23. F. Gao, A. R. Levander, R. G. Pratt, C. A. Zelt, G. L. Fradelizio, "Waveform tomography at a groundwater contamination site: VSP-surface data set," *Geophysics, **71(1)**, H1-H11, 2006.*
24. F. Bleibinhaus, J. A. Hole, T. Ryberg, G. S. Fuis, "Structure of the California Coast Ranges and San Andreas fault at SAFOD from seismic waveform inversion and reflection imaging," *Journal of Geophysical Research, doi: 10.1029/2006JB004611, 2007.*
25. K. Ellefsen, "A comparison phase inversion and traveltime tomography for processing of near-surface refraction traveltimes," *Geophysics, **74**, WCB11-WCB24, 2009.*
26. C. Shin, Y. H. Cha, "Waveform inversion in the Laplace-Fourier domain," *Geophysical Journal International, **173**, 922-931, 2009.*
27. A. Tarantola, "A strategy for nonlinear inversion of seismic reflection data," *Geophysics, **51**, 1893-1903.*
28. R. Brossier, S. Operto, J. Virieux, "Seismic imaging of complex structures by 2D elastic frequency-domain full wave inversion," *Geophysics, **74(6)**, WCC105-WCC118, 2009.*

29. Y. Shi, W. Zhao, H. Cao, “Nonlinear process control of wave equation inversion and its application in the detection of gas,” *Geophysics, **71(4)**, R9-R18,2007.*

30. J. C. Cook, “Seismic mapping of underground cavities using reflection amplitudes,” *Geophysics, **30(4)**, 527-538, 1965.*

31. W. Fisher, “Detection of abandoned underground coal mines by geophysical methods,” *USEPA Water Pollution Control Res. Ser., Project 14010EHN, 94 pages.*

32. J. S. Watkins, R.H. Dodson, K. Watson, “Seismic detection of near-surface cavities,” *U. S. Geological Survey, Professional Paper 599-A, 12 pages.*

33. R. Miller, C. B. Park, J. Ivanov, D. W. Steeples, N. Ryden, R. F. Ballard, J. L. Llopis, T. S. Anderson, M. L. Moran, S. A. Ketcham, “Tunnel Detection Using Seismic Methods,” *in Proc. American Geophysical Union Meeting, Baltimore MD, 2007. NS21A-07.*

34. P. M. Manning, G. F. Margrave, “Elastic wave finite difference modeling as a practical exploration tool,” *CREWES Research Report, Vol. **10**, 18-1 to 18-16, 1998.*

35. P. M. Sheary, “Introduction to Seismology, Second Edition,” *(Cambridge University Press, New York, 2009).*

36. L. R. Lines, S. Treitel, “Tutorial: A review of least-squares inversion and its application to geophysical problems,” *Geophys. Prosp., **32**, 159-186, 1984.*

37. S. C. Kirkpatrick, D. Gelatt, M. O. Vecchi, “Optimization by simulated annealing,” *Science, **220**, 671-780,1983.*

38. D. E. Goldberg, “Genetic algorithms in search, optimization and machine learning,” *Addison-Wesley, 1989.*

39. N. Metropolis, A. W. Rosenbluth, M. N. Rosenbluth, A. H. Teller, E. Teller, "Equation of state calculations by fast computing machines," *J. Che. Phys., **1**, 1087-1092, 1953.*

40. W. K. Hastings, "Monte Carlo sampling methods using Markov chains and their applications," *Biometrika, **57**, 97-109, 1970.*

41. S. Kirkpatrick, C. D. Gelett, M. P. Vecchi, "Optimization by simulated annealing," *Science, **220**, 621-630, 1983.*

42. V. Cerny, "A thermodynamic approach to the travelling salesman problem: An efficient simulation," *J. Optim. Theory Appl., **45**, 41-51, 1985.*

43. B. Dimitris, J. Tsitsiklis, "Simulated Annealing," *Statistical Science, **8(1)**, 10-15, 1983.*

44. M. B. Dobrin, "Introduction to Geophysical Prospecting," *McGraw-Hill Book Company, Inc., New York, Second Edition, 1960.*

CHAPTER 3

INVESTIGATION OF MODEL BASED BEAMFORMING AND BAYESIAN INVERSION SIGNAL PROCESSING METHODS FOR SEISMIC LOCALIZATION OF UNDERGROUND SOURCES

There are various detection technologies available that can be used to detect the presence of, e.g., underground tunnels through detection of anomalies in the physical properties of the subsurface ground layer. These techniques involve measurement of properties of the subsurface that include seismic wave, electrical resistivity, and gravitational field. We shall consider the seismic methods in this present paper.

Seismic methods comprise of active and passive seismic detection methodologies. The active method works in the same way as seismic survey commonly used in oil and gas exploration industry. A seismic source such as a sledgehammer is used to generate seismic waves through the ground, sensed by an array of seismic sensors on the ground surface, and recorded by the digital device. The recorded seismic signals are subsequently processed to provide ground soil velocity properties and/or other soil properties. This method is also used to detect the underground inhomogeneity such as tunnels. Passive seismic sources, such as those from nature or from the underground facilities can also be exploited for seismic

survey. The passive method looks at the detection of seismic activities present in the underground facilities e.g. tunnel digging, footsteps and generators.

In this chapter paper, we focus on the active seismic detection method [1-9] that exploits mechanical properties of underground structure and subsurface soil layer. To detect subsurface structures, a source at known location excites the ground surface producing a seismic wave that travels through the soil to interact with the underground objects. The elastic waves propagating back to the ground surface are recorded by a geophone array. The recorded seismic signals are further processed for location estimation of the underground tunnel in the soil.

There are three types of elastic waves propagating in the ground, namely the two types of body waves, namely compressional wave (P-wave) and shear wave (S-wave), and the surface wave (R-wave). To solve the source estimation problem in the elastic medium, one way is to simplify the elastic wavefield model by concentrating only on one class of the elastic waves. Refs. 1-4 assumed a diffraction model and define a ray model for the diffracted P-wave for calculation of its arrival time at the seismic sensors on the ground surface. This method works well for propagation of high frequency reflected P-wave to the ground surface. In Refs. 5-9, the authors concentrate on detecting and processing the dispersive surface waves traveling in the layered ground medium. The surface wave model is a simplification of the elastic wave-field propagating in a layered medium that works based on the assumption that the surface waves carry most energy. Frequency domain technique is used for processing the seismic signals as wave speeds of surface waves vary with frequency. The seismic data are first filtered in the wavenumber domain so that the filtered wave contains only the reflected waves from the underground structure.

The source location is then obtained by further windowing in the time around the arrival times of the reflected signal and performing averaging on the multichannel seismic recordings.

In the Refs.1-9, the authors apply a P-wave acoustic model or a dispersive surface wave model to the received signal, and apply the time-delay processing technique and frequency-wavenumber processing to determine the location of the underground tunnel, depending on their underlying assumption imposed on the seismic signal recorded on the ground surface. In this paper, we define two physical models for describing the seismic signals as follow, *Physical Model I:* Acoustic approximation and ray tracing; *Physical Model II*: Finite Difference Time Domain (FDTD) 3D elastic wave model, and apply two post processing techniques of Beamforming and Bayesian Inversion, to solve the underground tunnel estimation problem. Two variants each from the two categories of post processing techniques dependent on the two described physical models will be developed and implemented, giving in total four comparisons. The main objective for this paper is to integrate the wave-field modeling with the appropriate estimation algorithm to compare their performance in order to assess the different limitations of the physical model used.

Model I, the acoustic ray tracing [10] applies a high frequency approximation (i.e. assume that the length scale changes of the ground medium is large as compared to the seismic signal wavelength) such that ray theory holds. Under the high frequency approximation, the P and S waves can be treated separately. We assume negligible S-waves, and use ray theory to track the acoustic wave-front of the P wave. Model II, the FDTD, makes no such simplification on the elastic wave-field modeling,

considering all the body waves (P & S waves) and the surface waves. We apply finite difference modeling as it allows the modeling of surface waves for which ray tracing cannot be used. Both physical model I [11-18] and physical model II [19-27] have been used extensively by researchers as well as describing seismic measurements and applied to inversion problems in seismic problems primarily to recover elastic structures of the ground, such as sound speeds and density.

As indicated above, for both the physical models described, we will apply two different groups of signal processing methods.

The first group of methods falls under the category of beamforming algorithms. It works by computing the travel times of the seismic waves from the sources to the receivers' positions, and then applying beam-forming algorithms to perform spatially filtering to generate images containing the source locations. The computation of the travel times is dependent on the physical models assumed. For Model I, we apply the finite difference (FD) eikonal equation solver to the time-domain signal directly for estimation of the travel times. For Model II, we filter the time-domain signal in the wavenumber domain before applying the FD Eikonal equation solver.

The second group of methods is the inversion methodology [28] where the unknown model parameters are defined as the locations of the underground structures. We apply the Bayesian [29] inversion methodologies developed for both the linearized and nonlinear inverse scattering for source location estimation through incorporating physical models I & II. One advantage of the Bayesian method over the beamforming method is the quantification of uncertainty of the seismic data collected. Geophysical measurements are often strongly affected by noise and measurement uncertainty, and the subsurface elastic model that is derived from

geophysical survey measurements may also be highly uncertain. Bayesian setting allows one to incorporate prior information about any models with the information in the measured data. The outcome of Bayesian inversion is the posterior distribution which provides most probable solution based on the corresponding uncertainty.

The outline of the chapter is described as follows. Section 3.1 present the methodologies that include the physical models, algorithms and the seismic measurement setup of underground tunnel location problems. Section 3.2 contains the results of applying the algorithms to data collected in the field for the scenario with an underground tunnel, and noise clutter. Section 3.3 presents the discussions of the four proposed location methodologies, including findings found in the literature. Finally we conclude the findings in Section 3.4.

3.1 Methodology

Contrary to conventional techniques that assume a physical elastic wave-field model of either surface waves or P-waves, we propose two other physical models indicated above and explained in more details below. Model I is acoustic ray tracing assuming that the reflected waves from the underground source are primarily composed of P-waves. Model II is the FDTD solution of the elastic wave equation that models both the body (P & S waves) and the surface R waves. For both physical models, we solve the localization problem using the beamforming and Bayesian inversion methods. For Model I, we apply the Delay-and-Sum (DAS) beamforming method, and the 2D acoustic full waveform Bayesian inversion technique. And for Model II, we propose the frequency-wavenumber (F-K) beamformer, and the 2D elastic full waveform Bayesian inversion technique.

3.1.1 Physical Models

In this section, we present the detailed description of the two physical models.

First we assume that the ground is made up of horizontally stratified layers, and the elastic parameters of ground are known from measurements of a geophysical survey. Define $u(\mathbf{x}_\mathbf{r},t)$ as the seismic signal recorded on the ground surface at position $\mathbf{x}_\mathbf{r}$ due to a point impulsive force defined as $f(\mathbf{x}_\mathbf{s},t_0)=\delta(\mathbf{x}-\mathbf{x}_\mathbf{s})\delta(t-t_0)$ where $\mathbf{x}_\mathbf{r},\mathbf{x}_\mathbf{s}\in\Re^2$. Here we consider the 2D problem, for example corresponding to an underground tunnel at location $\mathbf{x}_\mathbf{s}$.

3.1.1.1 Model I: Acoustic Approximations & Ray Theory

For model I, only acoustic P-waves are considered. For a fixed source position, the signal measured at a receiver position, $u(\mathbf{x}_\mathbf{r},t)$, satisfies the inhomogeneous wave equation [11],

$$\frac{1}{v(\mathbf{x})}\frac{\partial^2 u(\mathbf{x}_\mathbf{r},t)}{\partial t^2}-\nabla^2 u(\mathbf{x}_\mathbf{r},t)=f(\mathbf{x}_\mathbf{s},t_0). \qquad \text{Equation (3-1)}$$

The wave speed profile $v(\mathbf{x})$ of the subsurface is assumed as known and smooth, and the density variations are neglected. Further considering first order scatterings only, we can rewrite the received signal as follows [11],

$$u(\mathbf{x}_\mathbf{r},t)=A(\mathbf{x}_\mathbf{r};\mathbf{x}_\mathbf{s})exp\left[-i\omega\left(t+\tau(\mathbf{x}_\mathbf{r};\mathbf{x}_\mathbf{s})\right)\right], \qquad \text{Equation (3-2)}$$

where $\tau(\mathbf{x}_\mathbf{r};\mathbf{x}_\mathbf{s})$ defines travel-time from source at position $\mathbf{x}_\mathbf{s}$ to the receiver at position $\mathbf{x}_\mathbf{r}$, and $A(\mathbf{x}_\mathbf{r};\mathbf{x}_\mathbf{s})$ denotes the amplitude function.

The travel-time can be estimated by solving the Eikonal equation defined below as follows,

$$|\nabla \tau(\mathbf{x_r};\mathbf{x_s})|^2 = \left(\frac{1}{v(\mathbf{x})}\right)^2 \qquad \text{Equation (3-3)}$$

The algorithm searches for first arrival travel-times, i.e., it assumes that there should be one ray connecting each source position $\mathbf{x_s}$ to each receiver position $\mathbf{x_r}$ (geometric optics assumption). In this paper, we apply the FD Eikonal equation solver downloaded from the CREWES numerical software [32].

3.1.1.2 Model II: FDTD 3D Elastic Wave Model

The propagation of seismic waves in Earth is modeled with the elastic wave equation [33]

$$\rho(\mathbf{x})\frac{\partial^2 u_i}{\partial t^2} - \frac{\partial \sigma_{ij}}{\partial x_j} = f_i, \qquad \text{Equation (3-4)}$$

which describes the displacement field u at coordinate *i* (assumed to range from *1* to *3* for the *3D x, y,* and *z* directions), to the density $\rho(\mathbf{x})$ of the ground, the stress tensor $\boldsymbol{\sigma}$, and an external force *f* provided by a point impulsive source. Each of the terms u_i, σ_{ij} and f_i is a function of position $\mathbf{x}$ and time.

The stress tensor $\boldsymbol{\sigma}$ and the strain tensor $\boldsymbol{\varepsilon}$ satisfy a stress-strain relation defined as follows,

$$\sigma_{ij} = c_{ijkl}\varepsilon_{kl} = \sum_{k=1}^{3}\sum_{l=1}^{3} c_{ijkl}\varepsilon_{kl},$$

where c_{ijkl} is the fourth-order viscoelastic Hooke's tensor, and ε_{ij} is the strain tensor defined by,

$$\varepsilon_{ij} = \frac{1}{2}\left(\frac{\partial u_i}{\partial x_j} + \frac{\partial u_j}{\partial x_i} \right).$$

For an isotropic, elastic medium (c_{ijkl} is invariant with respect to rotation), the elasticity is determined by only two elastic parameters such that the Hooke's tensor can be written in terms of the Lamé parameters $\lambda(\mathbf{x})$ and $\mu(\mathbf{x})$ as follows,

$$c_{ijkl} = \lambda\delta_{ij}\delta_{kl} + \mu\left(\delta_{ik}\delta_{jl} + \delta_{il}\delta_{jk}\right). \qquad \text{Equation (3-5)}$$

δ_{ij} is the Kronecker symbol. The readers can refer to Ref. 31 for detailed derivations.

A complete description of the ground material properties for an isotropic elastic medium is thus given by $\{\lambda(\mathbf{x}), \mu(\mathbf{x}), \rho(\mathbf{x})\}$. Another parameterization that is adopted in this paper is given by $\{v_p(\mathbf{x}), v_s(\mathbf{x}), \rho(\mathbf{x})\}$ where $v_p(\mathbf{x})$ and $v_s(\mathbf{x})$ denote the wave speeds of the P and S waves. The two sets of parameters are related as follows,

$$v_p = \sqrt{\frac{\lambda + 2\mu}{\rho}} \qquad \text{Equation (3-6)}$$

$$v_s = \sqrt{\frac{\mu}{\rho}} \qquad \text{Equation (3-7)}$$

Equation (4-4) can be formulated in 2D Cartesian coordinates as

$$(\lambda + 2\mu)\frac{\partial^2 u_i}{\partial x_i^2} + (\lambda + \mu)\frac{\partial^2 u_j}{\partial x_i \partial x_j} + \mu\frac{\partial^2 u_j}{\partial x_j^2} = \rho\frac{\partial^2 u_i}{\partial t^2}$$

$$(\lambda+2\mu)\frac{\partial^2 u_j}{\partial x_j^2}+(\lambda+\mu)\frac{\partial^2 u_i}{\partial x_i \partial x_j}+\mu\frac{\partial^2 u_i}{\partial x_i^2}=\rho\frac{\partial^2 u_j}{\partial t^2} \qquad \text{Equation (3-8)}$$

For solving the time dependent elastic wave partial differential equations, we apply FD modeling [35, 36]. For all the simulations in this paper, we apply the FDTD modeling for elastic waves solver from the CREWES numerical software [35]. The FD model consists of a spatial grid where at each node, various propagation parameters are specified for the ground material represented. In the paper, we adopt a horizontally stratified ground model, and the grid layout is simplified to comprising k number of layers with propagation parameters (P and S wave speeds, soil density) specified at each layer. The boundary conditions for the simulations are applied as followed, a free surface at z=0, a mirror surface at offset x=0, a transparent boundary at the right side, and a rigid bottom.

3.1.2 Signal Processing Methods of Seismic Source Localization

There is a big variety of methods for performing source localization. This section presents four cases that combine physical model I & II with the beamforming algorithm or the Bayesian inversion method to solve the problem of estimation of the location of the underground tunnel from seismic measurements recorded on the ground surface.

3.1.2.1 Physical Model I & Delay-and-Sum Beamformer

The delay-and-sum beamformer [37] is the simplest and most widely used technique for localization. Under physical model I, the received seismic signals are reflected P-waves which will arrive at the array of seismic sensors on the ground at different travel times depending on the location of the underground tunnel. Delay-and-sum beamformer thus works by first time-aligning the received seismic signals

across all possible locations of the underground tunnel, summing the aligned signals to generate a 2D beamforming image. The location of the underground tunnel is derived by seeking out the peaks in the beamforming image.

Delay-and-sum beamformer has limitation such as it can only be applied to signal with constant propagation speed. In the simulation, the ground is modeled as a *3*-layer structure with constant wave speed defined for each soil layer. The time delays are then computed by solving the Eikonal equation (4-3).

3.1.2.2 Physical Model II & Frequency-Wavenumber (F-K) Beamforming

Physical model II assumes a complete description of the recorded seismic signals described by the P-wave speed, S-wave speed, and soil density. F-K beamforming method [37] is applied as it allows the separation of the different seismic body waves (P, S waves) propagating at different wave speeds, and with a dispersive R wave.

Frequency-wavenumber (F-K) beamformer simultaneously calculates the beamformer power distributed among different slowness vector $\mathbf{s}$ for a fixed frequency of the seismic signal. The slowness vector is dependent on the azimuth angle θ and the wave speed v as follows,

$$\mathbf{s} = \begin{pmatrix} \cos\theta / \mathrm{v} \\ \sin\theta / \mathrm{v} \end{pmatrix}, \qquad \text{Equation (3-9)}$$

The slowness vector $\mathbf{s}$ is also related to the wavenumber vector $\mathbf{k}$ as follows,

$$\mathbf{k} = \omega \cdot \mathbf{s} = \begin{pmatrix} k_x \\ k_y \end{pmatrix} = \frac{\omega}{v} \begin{pmatrix} \cos\theta \\ \sin\theta \end{pmatrix} \qquad \text{Equation (3-10)}$$

In the F-K beamforming processing, by fixing the frequency of the seismic signal, a grid search is performed for all plausible combinations of wave speed v and azimuth angle θ in order to find the best (v,θ) parameter combination that gives the highest amplitude of the summed signal across the seismic signal recorded. As the measured signal may contain waves with different wave speeds, this method requires careful segmentation of the data to avoid ambiguous phase identification problems.

3.1.2.3 Physical Model I & 2D Acoustic Full Wave-form Bayesian Inversion

In this section, we shall consider the full waveform inversion with the acoustic wave-field model and the Bayesian inversion methodology. In full wave-form inversion [38-39], full wave equation modelling is performed at each iteration to solve the inverse optimization problem. For the case of physical model I, the acoustic wave-equation is solved for the forward modeling. To derive the location of the tunnel, Bayesian inversion [40-46] is used.

3.1.2.3.1 Forward Model

The forward model here solves the 2D wave equation. The inverse problem is solved on the spatial domain $\Omega = [0, L_x]\text{x}[0, L_z]$, where $x \in [0, L_x]$ represents the range on the ground, and $z \in [0, L_z]$ represents the depth beneath the surface. The surface source is modeled with a right-hand side forcing input to the wave equation (8) using a Ricker wavelet with a mean spectral energy density at *0.5 Hz*, and a spatial delta function at the surface $z = 0$. The ground subsurface model is modeled as a horizontally stratified medium, wherein each soil layer has its own elastic values. In this paper we shall assume complete knowledge of the seismic properties of the ground subsurface that can be extracted from geophysical physical survey

conducted before the experiment. For the case of a physical model I, the ground elastic parameter is the acoustic compressional P wave speed of the soil layers.

3.1.2.3.2 Bayesian Inversion Methodology

In the Bayesian inversion [38-41] framework, the solution of the inverse problem involves a set of observational seismic data u_{obs}, a forward model, setting up the parameterization and prior for the model parameters, and finally computing the posterior likelihood function PDF $\pi_{\text{posterior}}(\mathbf{m})$ as a function of unknown model parameters $\mathbf{m}$. In this paper, $\mathbf{m} = (x_s, z_s)$ where (x_s, z_s) denotes the location vector of the tunnel.

The forward model $g(\mathbf{m})$ to map the parameters $\mathbf{m}$ to the data measurement u_{obs} is given as follows,

$$u_{obs}(x,z,t) = g(\mathbf{m}) + n(t), \qquad \text{Equation (3-11)}$$

where *n(t)* is a noise signal (comprising sensor and/or background noise). If we assume that *n* is an additive Gaussian noise model with probability distribution of zero mean and covariance matrix $\mathbf{C}_{\text{noise}}$, then the probability density function (PDF) for $u_{obs}(x,z,t)$ becomes a normal distribution defined as follows,

$$P[u_{obs}(x,z,t)\,|\,\mathbf{m}] = \mathrm{N}[u_{obs}(x,z,t); g(\mathbf{m}), \mathbf{C}_{\text{noise}}]. \qquad \text{Equation (3-12)}$$

The solution of the Bayesian inversion methodology is the posterior joint probability density of the parameters. Applying Bayes Theorem, the posterior joint probability density of the parameters, $\pi_{\text{posterior}}(\mathbf{m})$ can be written as follows,

$$\pi_{\text{posterior}}(\mathbf{m}) = \pi(\mathbf{m}\,|\,u_{\text{obs}}(x,z,t)) \propto \pi_{\text{prior}}(m)\,\pi(u_{\text{obs}}(x,z,t)\,|\,\mathbf{m}), \qquad \text{Equation (3-13)}$$

where $\pi_{\text{prior}}(\mathbf{m})$ is the prior distribution, and $\pi\left(u_{\text{obs}}(x,z,t)|\mathbf{m}\right)$ denotes the likelihood function.

The likelihood function $\pi\left(u_{\text{obs}}(x,z,t)|\mathbf{m}\right)$ provides a probabilistic measure of how well the measured data u_{obs} matched the data defined by the forward model. Applying Equation (3-12), the likelihood function takes the form as follows,

$$\pi\left(u_{\text{obs}}(x,z,t)|\mathbf{m}\right) = exp\left\{-\frac{1}{2}(u_{\mathbf{m}}(x,z,t)-u_{\text{obs}}(x,z,t))^{T}\,\mathbf{C}_{\text{noise}}^{-1}\left(u_{\mathbf{m}}(x,z,t)-u_{\text{obs}}(x,z,t)\right)\right\},$$

Equation (3-14)

where $u_{\mathbf{m}}(x,z,t) = \mathrm{g}(\mathbf{m})$ denotes the data generated by the forward model with the unknown model parameter $\mathbf{m}$, and $\mathbf{C}_{\text{noise}}$ denotes the noise covariance matrix. One way to model the noise is through measurement of the ambient before the experiment recording. In the paper, the noise covariance matrix $\mathbf{C}_{\text{noise}}$ takes the form of a diagonal matrix with its elements estimated from the variance of the ambient measured at the sensor.

In this chapter, the Bayesian inversion problem is concerned with the estimation of the unknown model parameter $\mathbf{m}$ which is defined as the tunnel position, through maximization of the posterior PDF defined in Equation (3-11). In our formulation, a non-informative, or conservative, prior PDF [42] is used in the Bayesian inference. The chosen prior PDF of the unknown tunnel position follows a uniform distribution defined over the spatial search grid space where the source is assumed to lie. Hence under the assumption that the model $\mathbf{m}$ take values one, the posterior density function can be written as follows,

$$\pi_{\text{posterior}}(\mathbf{m}) \propto exp\left\{-\frac{1}{2}\left(u_{\mathbf{m}}(x,z,t)-u_{\text{obs}}(x,z,t)\right)^{T}\mathbf{C}_{\text{noise}}^{-1}\left(u_{\mathbf{m}}(x,z,t)-u_{\text{obs}}(x,z,t)\right)\right\}.$$

Equation (3-15)

3.1.2.4 Physical Model II & 2D Elastic Full Wave-form Bayesian Inversion

Contrary to the case of physical model I, the full information content in the seismic signal is used in the optimization of the inversion process. Under physical model II, all types of the elastic waves are involved in the optimization. Hence we shall model the seismic inverse problem using the 3D elastic wave equation. The technique used for the forward modeling is the FDTD [35] where the ground subsurface model is a horizontally stratified model wherein each soil layer has its own values of density, compressional wave speed values, and shear wave speed values. The Bayesian inversion methodology to estimate the unknown source location then follows from Section 3.1.2.3.2.

3.1.3 Experimental Model

The tunnel that we are interested to detect and locate is a heritage tunnel which has depth varying between 3 *m* to 9 *m*. Figure 3-1 displays the topological information of the tunnel site. A geophysical survey is conducted at the site to determine the compression wave speed profile near the tunnel. The compressional wave profile displays in Figure 3-2 shows that the compressional wave travels faster with increased soil depth. We will be using the soil layering and properties predicted from this velocity profile for the signal processing calculations.

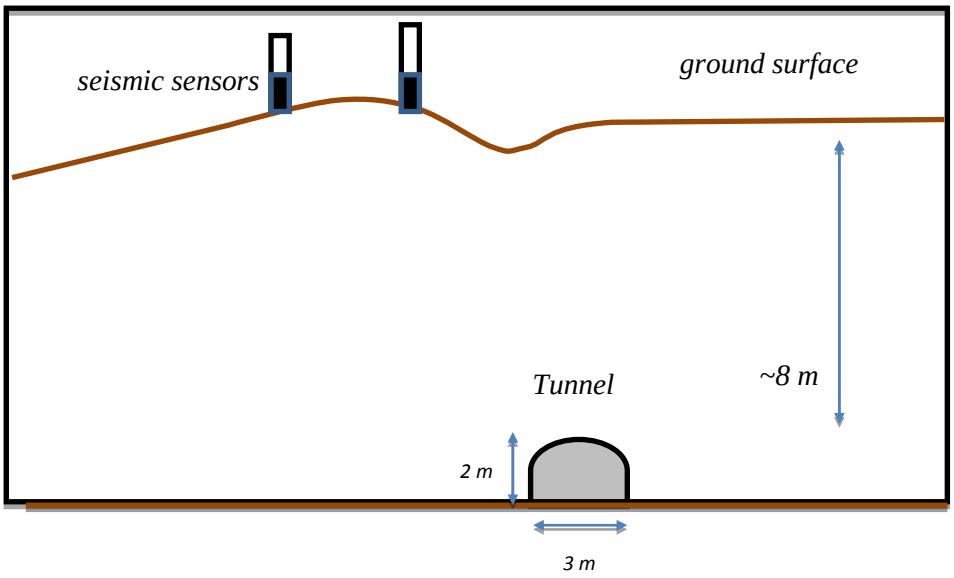

Figure 3-1 Estimated topographical information of tunnel trial site

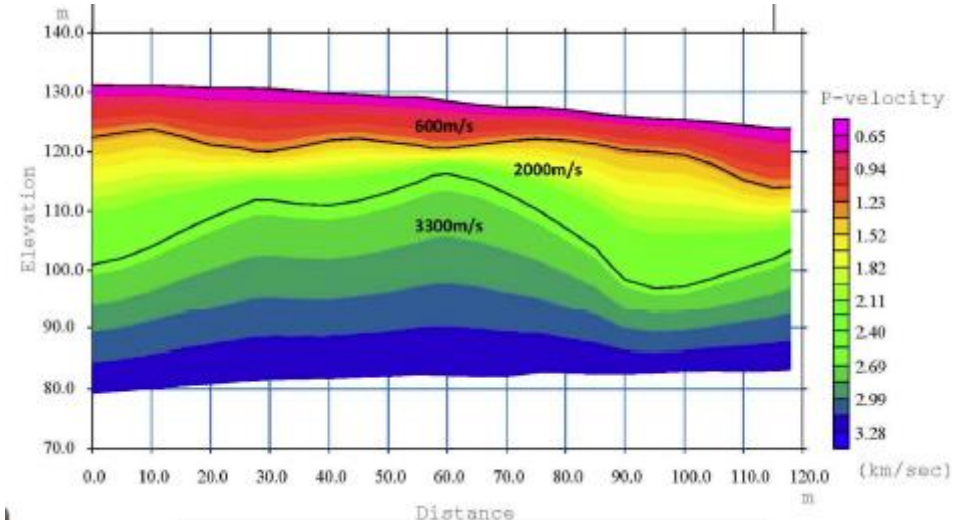

Figure 3-2 Compressional wave speed profile near tunnel

The seismic source is provided by a weight drop. A cylinder with a hemispherical end cap weighing 18 *kg* is designed to drop from a 1 *m* height to generate the seismic impact forcing on the ground surface. The support structure functions as a guide to ensure that the weight will not tumble when it lands on the ground surface.

In addition, soft rubber pads are added on the metal plate at the base of the support structure so as to ensure that the weight will generate one main broadband seismic impulse function (see Figure 3-3) with minimum spurious re-bounce signals. The seismic sensors used for the experiment are the geophones (see Figure 3-4) which measures particle velocity. The geophones provide measurement in frequency range from 4.5 *Hz* to 100 *Hz.* In the experiment, two vertical component *GS11D* geophones are deployed. The geophones are connected to the Brüel & Kjær 32-bit, 4-channel digital recorder to digitize the measured seismic signals.

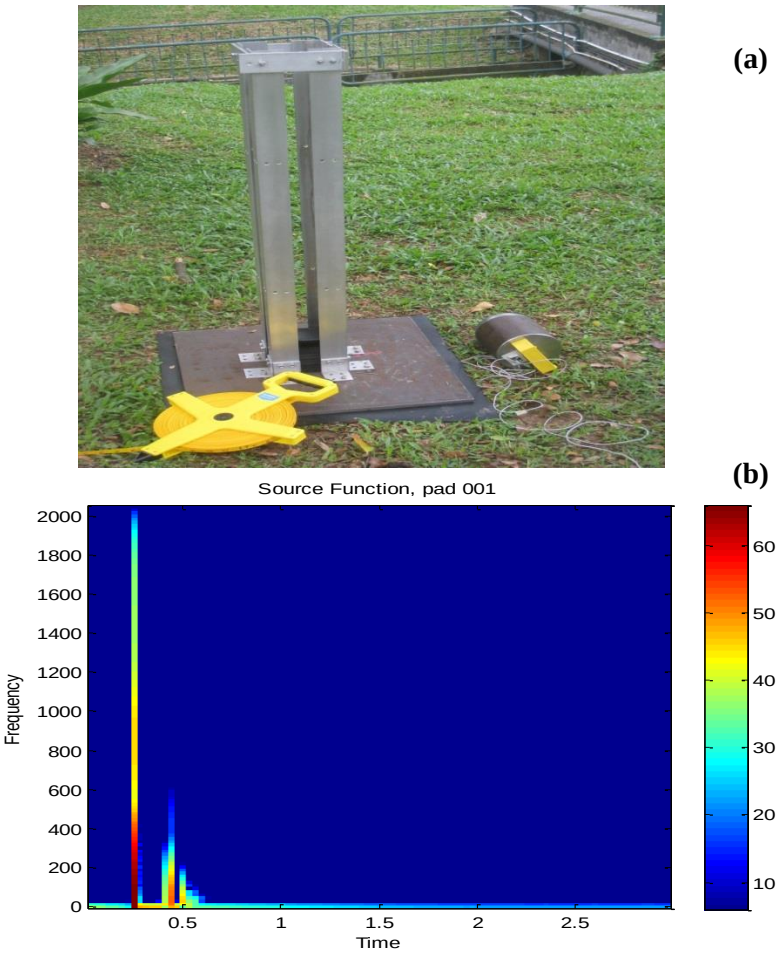

Figure 3-3 (a) Seismic source, weight drop, (b) Spectrogram of the measured source function from weight drop. The signal is measured by an accelerometer mounted on the 18kg weight drop.

(a) (b)

Figure 3-4 Seismic sensors and the acquisition system.
(a) Vertical GS11D geophones, (b) Bruźl & Kjaer digital recorder

3.2 Results And Analysis

The ground at the experiment site is uneven and the soil layering is inhomogeneous. In our paper, we make some simplification and assume that the ground comprises of horizontally stratified layers. Figure 3-5 describes the soil layering structure and the 2D search space to solve the tunnel localization problem to determine the tunnel range and depth.

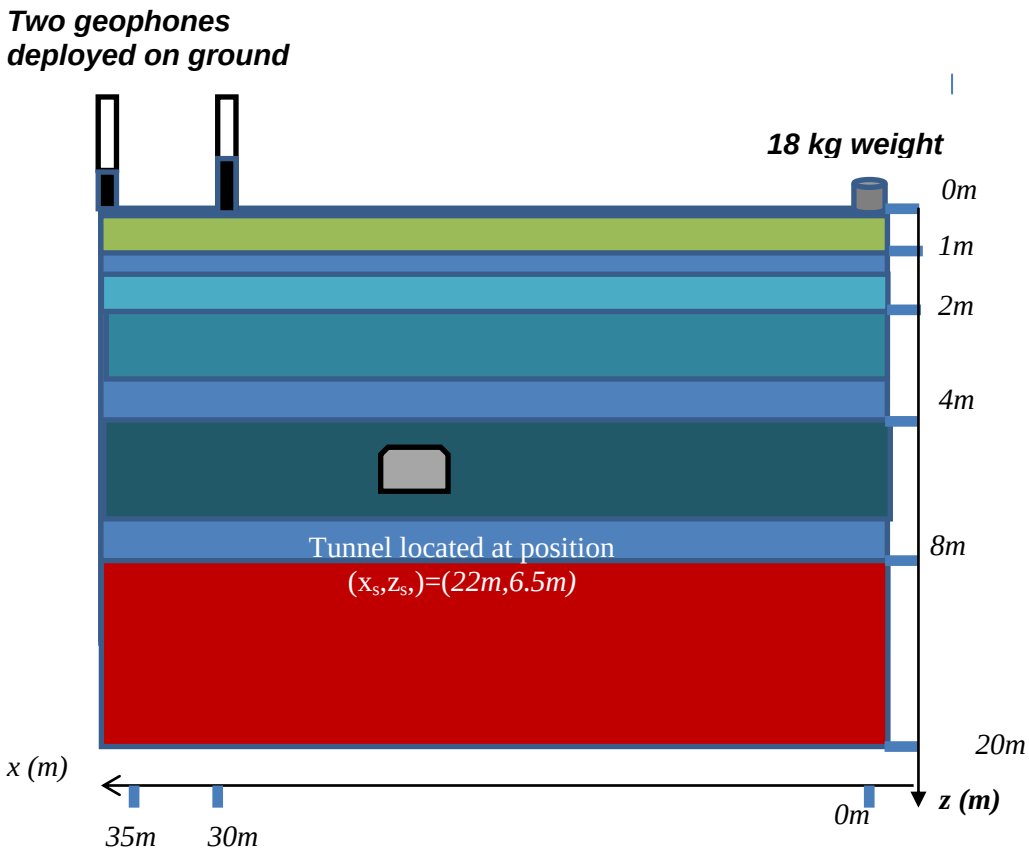

Figure 3-5 Configuration of the experiment test plan

In the analysis of the field data, two soil models are introduced as follow. The first soil model is a *3-layer* soil model with a constant P-wave speed for each layer (see Table 3-1).

Soil layer profile (d denotes the depth in m)	P wave speed v_p (m/s)
Layer 1: $0 < d \leq 10$	600
Layer 2: $10 < d \leq 20$	2000
Layer 3: $20 < d \leq 100$	3300

Table 3-1 Soil Model I: P wave speed profile for a 3-layer soil model

The second soil model defines a horizontally stratified 5-layer soil structure and P, S wave speeds and soil density values for each layer are described in Table 3-2.

Soil layer profile (d denotes the depth in m)	P wave speed v_p (m/s)	S wave speed v_s (m/s)	Density ρ (g/cm^3)
Layer 1: $0 < d \leq 1$	600	100	1.4
Layer 2: $1 < d \leq 2$	800	150	1.4
Layer 3: $2 < d \leq 4$	1500	300	1.5
Layer 3: $4 < d \leq 8$	2000	400	1.6
Layer 5: $8 < d \leq 100$	3000	600	1.6

Table 3-2 Soil model II: P, S wave speed and density profile for a 5-layer soil model

3.2.1 Comparison of the Signal Models & Signal Analysis Algorithms

We shall compare the results for the four cases of the signal models & signal analysis algorithms outlined in Section II when implemented on the field data.

3.2.1.1 Physical Model I & Delay-and-Sum Beamformer

First we examine the result obtained with physical model I of acoustic ray tracing signal model and the signal analysis algorithm of sum-delay beamformer. For this example, we applied the *3-layer* soil model I. The output from the sum-delay beamformer is a 2D power image function of location parameter *x, z.* The location of the tunnel is derived by seeking for the position where a peak in the 2D beamformer output occurs. The processing result is presented in Figure 3-6. The simplified physical model of acoustic approximation & ray tracing leads to a low-resolution beamformer output that provides a coarse estimation of the location of the tunnel.

One can roughly deduce from Figure 3-6 possibly that the tunnel lies within in the region defined by $[x,z] \in [20\,m,25\,m]x[5\,m,10\,m]$. However the beamformer image also contains multiple spurious peak locations. Henceforth the result does not provide clear distinctive indication of the presence of only one underground source.

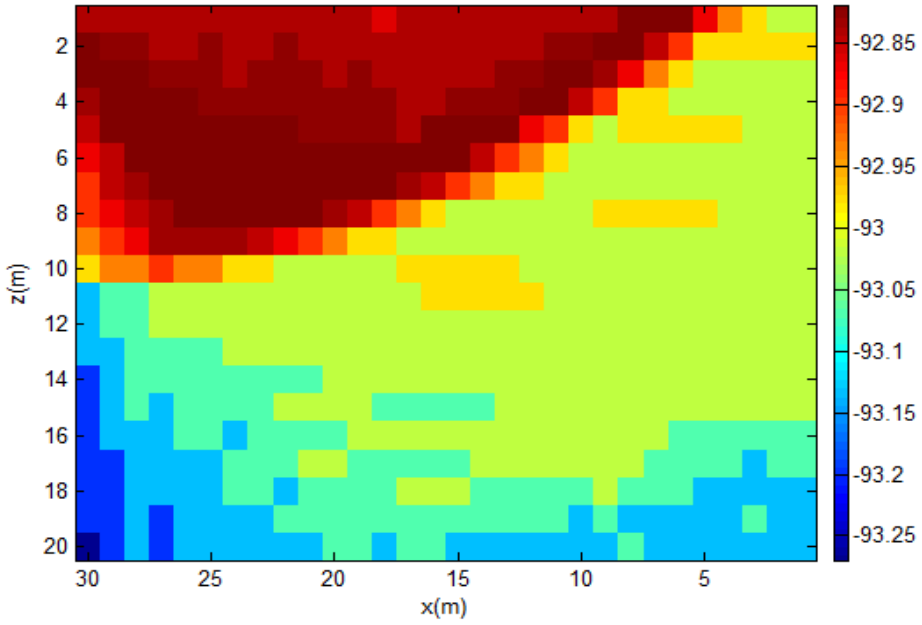

Figure 3-6 (Acoustic physical model I & Sum-and-Delay beamformer)
The figure displays the Sum-and-Delay beamforming power computed over the grid space $[x,z] \in [0\,m,30\,m]x[0\,m,20\,m]$. The source location is estimated from the location where a peak in the beamforming power output occurs.

3.2.1.2 Physical Model II & Frequency-Wavenumber (F-K) Beamformer

Before processing the F-K beamformer, the measured seismic signal is first filtered into a narrow spectral band of 25 *Hz* to 45 *Hz.* Here the *3-layer* soil model I is also used to describe the ground structure where it is assumed that dispersive R wave propagates in the top layer. In the processing of the F-K beamformer, the wave speed of the first soil layer is allowed to vary over a range of values of *300 m/s, 400 m/s, 500 m/s* and *600 m/*s respectively. Figures 3-7 to 3-10 displays four F-K

beamformer outputs corresponding to wave speed values of *300 m/s, 400 m/s, 500 m/s* and *600 m/*s respectively. Here the F-K beamformer output corresponding to wave speed *300 m/s* gives a better resolution of the location of the tunnel as compared to the other wave speed values. And comparing against the sum-delay beamformer (Figure 3-11) shows a slight improvement where the signal-to-noise ratio is slightly enhanced by 0.5 *dB*, though as before the beamforming result does not provide clear distinctive indication of the presence of only one underground source.

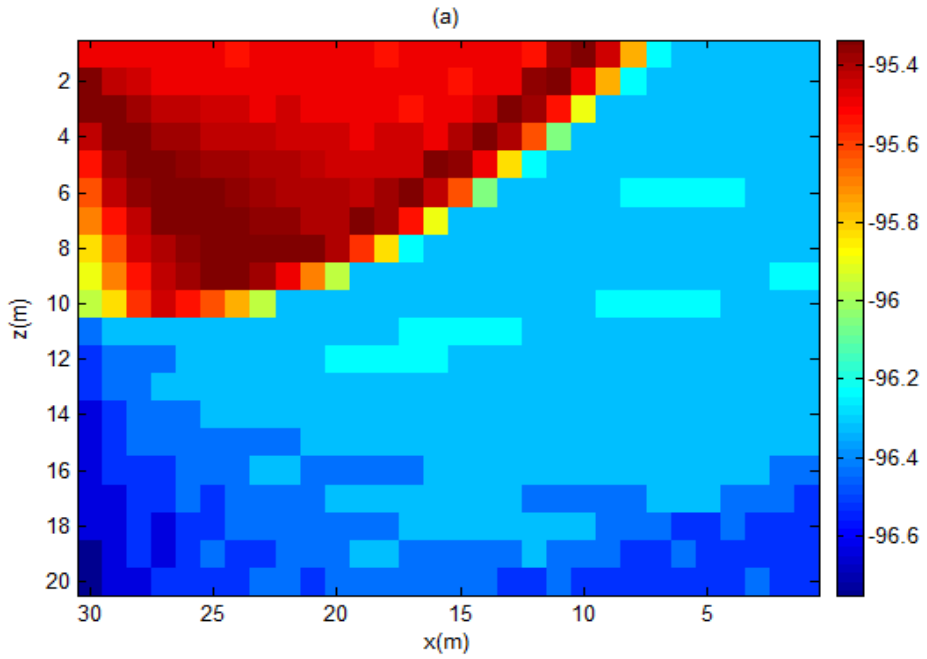

Figure 3-7. Elastic physical model II & F-K beamformer (25Hz to 45Hz), wave speed = 300 m/s

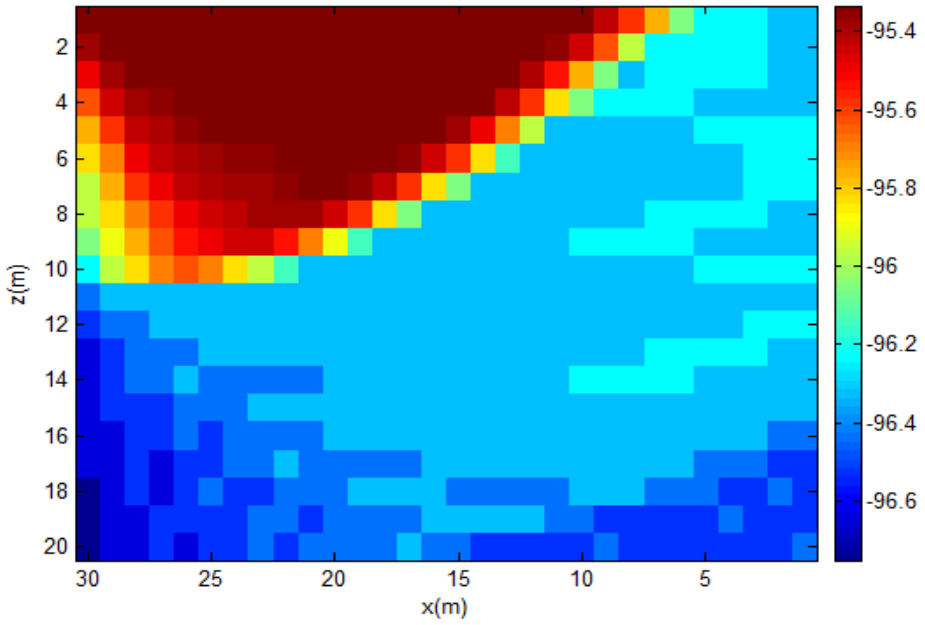

Figure 3-8 Elastics physical model II & F-K beamformer (25Hz to 45Hz), wave speed = 400 m/s

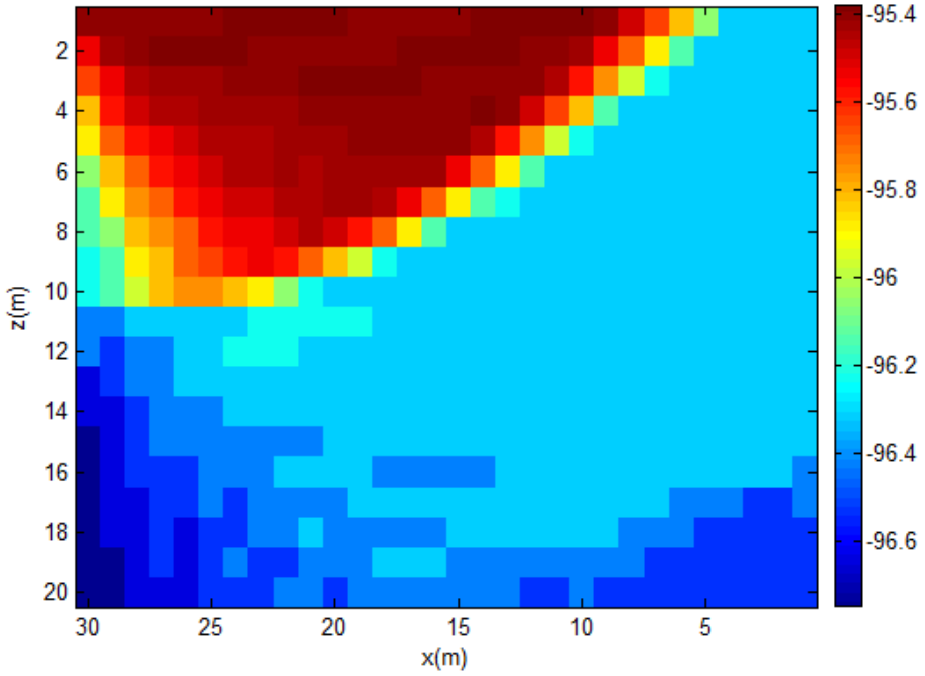

Figure 3-9 Elastic physical model II & F-K beamformer (25Hz to 45Hz) & wave speed = 500 m/s

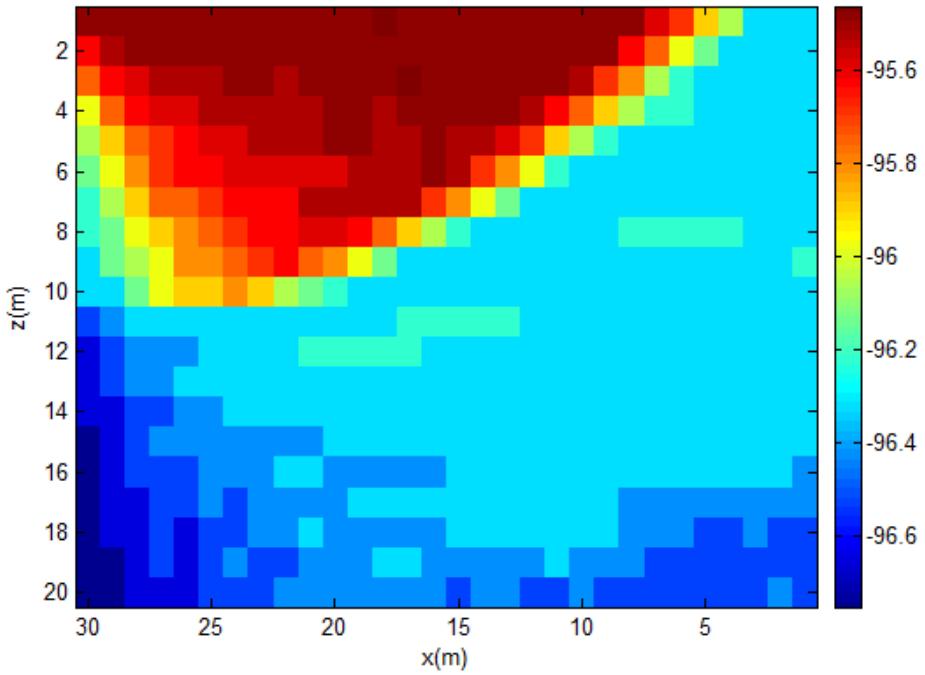

Figure 3-10 Elastic physical model II & F-K beamformer (25Hz to 45Hz), wave speed = 600 m/s

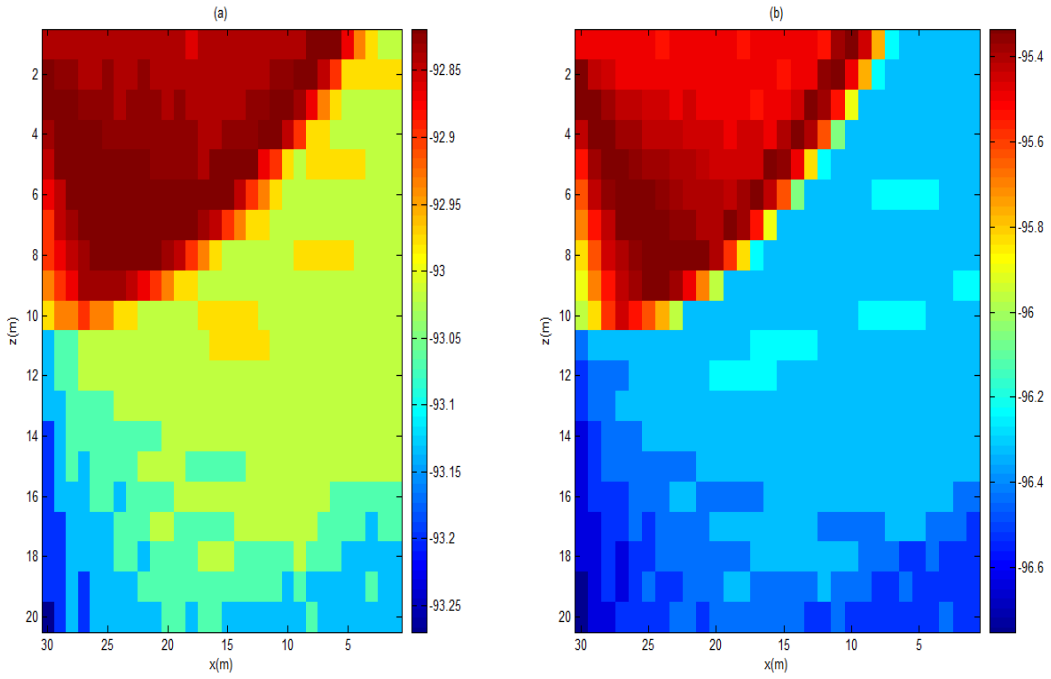

Figure 3-11 (a) Acoustic physical model I & Sum-and-Delay beamformer. (b) Elastic physical model II & F-K beamformer (spectral bin 25Hz to 45Hz), wave speed = 300 m/s

3.2.1.3 Physical Model I & Bayesian Inversion

In this analysis, the forward model is described by physical model I, an acoustic approximation of the elastic wave equation. The soil layer structure used in this example is the *5-layer* soil model II. The source location is obtained by computing the posterior PDF given by Equation (3-12) over the full grid and then finding the position in the grid space where maximum value of the posterior PDF occurs. In the example, the noise covariance matrix is assumed to take a diagonal form where the variances are computed from the ambient seismic recording. The grid search is carried out in discrete steps of 1 *m* resolution hence the total number of forward model computations is $20 \times 25 = 500$ times. The results of inversion are shown in Figure 3-12. The posterior PDF values generated for the entire grid space have a very small dynamic range (optimal value of the posterior PDF is value one), indicating that all positions are equally likely.

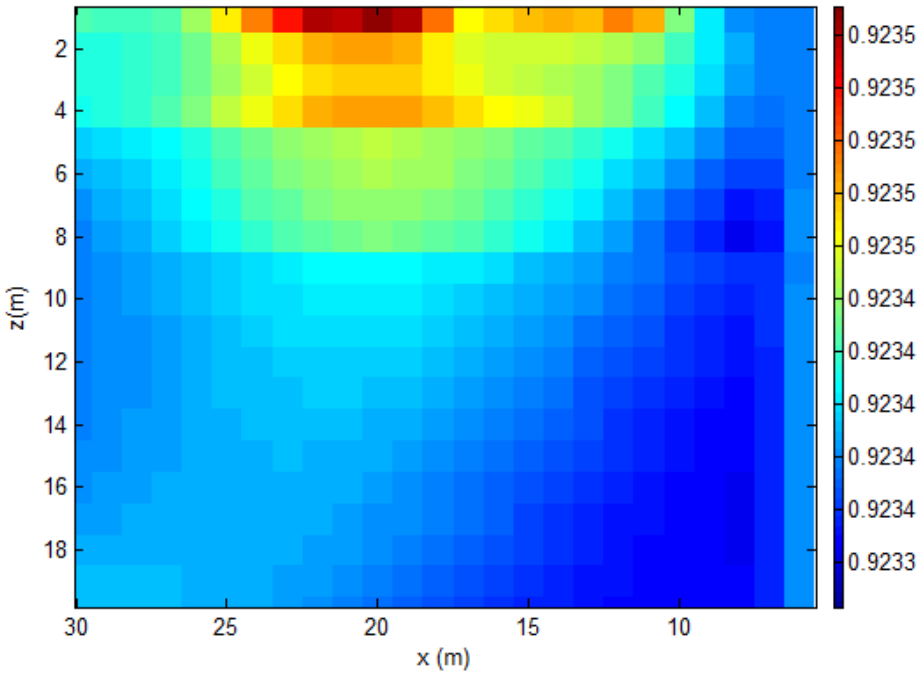

Figure 3-12. (Acoustic physical model I & Bayesian inversion method) The figure displays the posterior PDF values computed over the grid space $[x, z] \in [0\ m, 30\ m] \mathrm{x} [0\ m, 20\ m]$. *The source location is estimated from the location where a peak in the posterior PDF output occurs.*

3.2.1.4 Physical Model II & Bayesian Inversion

In this analysis, the forward model is described by physical model II, FDTD 3D elastic wave model. The ground subsurface elastic model is known and described in Table 3-2 which contains the elastic parameters (P, S wave speeds and density) of a *5-layer* soil model. Applying Equation (3-12), the posterior PDF over the full search grid is computed and the results of inversion are shown in Figure 3-13. The location of the tunnel is estimated at the position $(x, z) = (22\ m, 9\ m)$ deduced from the peak position of the posterior PDF image displayed in Figure 3-13.

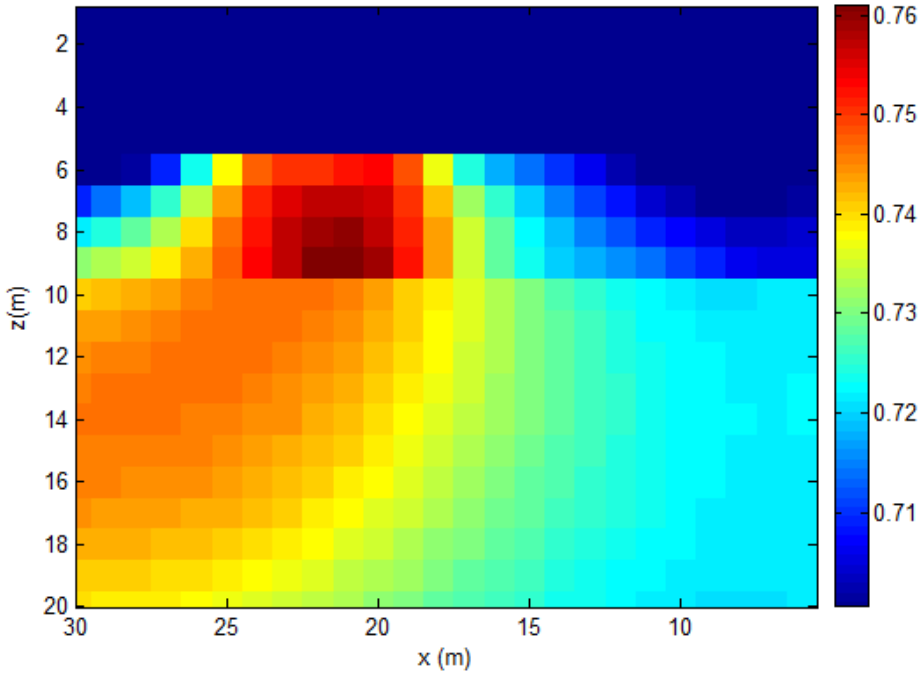

Figure 3-13 (Elastic physical model II & Bayesian inversion method) The figure displays the posterior PDF values computed over the grid space $[x, z] \in [0\ m, 30\ m] x [0\ m, 20\ m]$. *The source location is estimated from the location where a peak in the posterior PDF output occurs.*

3.3 Discussions

In Section III, we evaluated the four cases of the two physical models with beamforming or Bayesian inversion algorithms.

The beamforming algorithms are less affected by the choice of either physical model I or II as the results of both cases do not differ significantly. Both beamformers can only provide a coarse resolution of the location of the tunnel.

The Bayesian inversion algorithm implemented is more sensitive to requirement to choose an accurate physical model to describe the received signal. By choosing a simplified acoustic ray tracing forward model, the results from the inversion algorithm lead to non-conclusive estimate of the location of the tunnel source with the

posterior PDF values at the grid space having all equally likely values. The best localization result is provided by the choice of physical model II as the forward model incorporated in the Bayesian inversion framework. Physical model II which solves the 3D FDTD elastic wave equation is at the advantage that the forward model completely models all the elastic wave components received. However this is obtained at the expense of increased computational load to implement the FDTD elastic wave model as compared to the implementing the simplified acoustic ray tracing physical model.

The dynamic range of the F-K beamformer is slightly larger (*0.*5 dB) as compared to the sum-delay beamformer, as the algorithm models dispersive R wave. This result indicates that radiation of R wave constitutes a significant source for estimating the location of the tunnel. Similarly in the paper [7] on detection of underground buried mines using seismic waves, R wave is used for the detection task. The dominance of R wave also explains the poor performance of the Bayesian inversion method applied with the acoustic ray tracing physical model I, since the inversion algorithm requires a well-defined forward model to estimate the seismic observational data for the inversion process. The use of an appropriately chosen physical model II and the Bayesian inversion method afforded a significant improvement in the tunnel location estimate. The use of full waveform Bayesian inversion[35] is an emerging area. Future work can include extending the inversion to include the ground subsurface elastic parameters. An important issue will be the optimization strategy to implement a multi-dimensional parameter search for the Bayesian inversion. One possible approach is to apply the statistical MCMC search strategy [45, 46].

3.4 Conclusions

In this chapter, the concept of using physical models to describe the received signal, and then devising beamforming or inversion algorithms for each physical model in order to solve the underground seismic source localization problem is implemented. Two physical models, the simplified acoustic ray tracing model and the FDTD 3D full elastic wave model, and two different beamformers (sum-day beamformer and F-K beamformer) and the inversion algorithm for source localization are proposed. Four cases of physical model-signal analysis algorithms are implemented and evaluated on field data. Our results show that the FDTD 3D elastic wave model with the Bayesian inversion algorithm produce the best localization results. The Bayesian inversion result with the acoustic ray tracing model is unable to provide any estimate of the location with all posterior PDF values calculated over the grid space having equally likely values. Both beamformers provide fairly similar coarse resolution of the location of the tunnel. We thus obtained the conclusion that the use of Bayesian inversion for localization is most advantageous for source localization when the forward model is required to completely describe all the elastic wave components as is the case of the FDTD 3D elastic model.

BIBLOGRAPHY

1. R. Miller, C. B. Park, J. Ivanov, D. W. Steeples, N. Ryden, R. F. Ballard, J. L. Llopis, T. S. Anderson, M. L. Moran, S. A. Ketcham, “Tunnel Detection Using Seismic Methods,” *in Proc. American Geophysical Union Meeting, Baltimore MD, 2007. NS21A-07.*

2. A. C. Gurbuz, J. H. McClellan, W. R. Scott, G. D. Larson, “Seismic tunnel imaging and detection,” *IEEE International Conference on Image Processing, 3229-3232, 2006.*
3. Y. Ashida, “Seismic imaging ahead of a tunnel face with three component geophones,” *International Journal of Rock Mechanics & Mining Sciences, **38(6)**, 823-831, 2001.*
4. S. L. Walters, R. D. Miller, Jianghai Xia, “Near surface tunnel detection using diffracted P-waves: a feasibility study,” *Society of Exploration Geophysics (SEG) Annual Meeting, San Antonio, Texas 2007. SEG-2007-1128.*
5. S. Sloan, S. Peterie, J. Ivanov, R. Miller, and J, McKenna, “void detection using near-surface seismic methods,” *Advances in Near-surface Seismology and Ground-penetrating Radar: 201-218, 2010.*
6. M. Alam, V. Cevher, J. H. McClellan, G. D. Larson and W. R. Scott, Jr., “Optimal maneuvering of seismic sensors for localization of subsurface targets,” *IEEE Tans. on Geoscience and Remote Sensing, **45(5)**, 1247-1256, May 2007.*
7. W. R. Scott, Jr., J. S. Martin and G. D. Larson, “Experimental model for a seismic landmine detection system,” *IEEE Trans. Geosci. Remote Sens., **39**, 1155-1104, 2001.*
8. A. Behhoodian, W. R. Scott, Jr., and J. H. McCellan, “Signal processing of elastic surface waves for localizing buried land mines,” *Proceedings of the 33rd Assilomar Conference on Signals, Systems, and Computers, Pacific Grove, CA, **2(2)**, 827-830, 1999.*
9. Z. Motyka, “Near-surface 3D visualization of underground structures by means of seismic holography,” *Proc. SPIE 4072, Fourth International Conference on*

*Vibration Measurements by Laser Techniques: Advances and Applications, **553**, 2000.*

10. V. Cerveny, “Seismic Ray Theory,” *(Cambridge University Press, New York, 2005), Chap. 3 & 4.*
11. W. W. Symes, “The seismic reflection inverse problems,” *Inverse Problems **25**, 1-39, 2009.*
12. A. J. Berkhout, “Seismic migration: Imaging of acoustic energy by wave-field extrapolation A. Theoretical aspects,” *(Elsevier Science Publishing Company Inc. New York, 1984), Chap. 5-7.*
13. M. Leggett, N. R. Goulty, J. E. Kragh, “Study of traveltime and amplitude time-lapse tomography using physical model data,” *Geophys. Prosp., **41(5),** 559-620, 1993.*
14. R. G. Pratt, N.R. Goulty, “Combining wave-equation imaging with traveltime tomography to form high-resolution images from crosshole data,” *Geophysics, **56(2)**, 208-224, 1991.*
15. R. G. Pratt, M.H. Worthington, “The application of diffraction tomography to cross-hole seismic data,” *Geophysics, **53(10)**, 1284-1294.*
16. R. G. Pratt, M. H. Worthington, “Inversion theory applied to multisource cross-hole tomography, Part I: Acoustic wave equation method,” *Geophysical Prospecting, **38**, 287-310, 1990.*
17. R. G. Pratt, “Seismic waveform inversion in the frequency domain, Part I: Theory and verification in a physical scale model,” *Geophysical Journal International, **64**, 888-901, 1999.*

18. G. J. Hicks, R. G. Pratt, “Reflection waveform inversion using local descent methods: Estimating attenuation and velocity over a gas-sand deposit,” *Geophysics, **66**, 598-612, 2001.*
19. R. G. Pratt, “Inversion theory applied to multisource cross-hole tomography, Part II: Elastic wave equation method,” *Geophysical Prospecting, **38**, 311-329, 1990.*
20. P. Mora, “Nonlinear two-dimensional elastic inversion of multi-offset seismic data,” *Geophysics **52,** 1211-1228, 1987.*
21. P. Mora, “Elastic wavefield inversion of reflection and transmission data,” *Geophysics, **53**, 750-759, 1989.*
22. E. Crase, A. Pica, M. Noble, J. McDonald, A. Tarantola, “Robust elastic nonlinear waveform inversion: Application to real data,” *Geophysics, **55**, 527-538, 1990.*
23. E. Crase, C. Wideman, M. Noble, A. Tarantola, “Nonlinear elastic inversion of land seismic reflection data,” *Journal of Geophysical Research, **97**, 4685-4705, 1992.*
24. O. Gauthier, J. Virieux, A. Tarantola, “Two-dimensional non-linear inversion of seismic waveforms: Numerical results,” *Geophysics **51,** 1387-140, 1986.*
25. R. Brossier, S. Operto, J. Virieux, “Seismic imaging of complex onshore structure by 2D elastic frequency-domain full waveform inversion,” *Geophysics, **74(6)**, 105-118, 2009.*
26. C. Gelis, J. Virieux, G. Grandjean, “Two-dimensional elastic full waveform inversion using Born and Rytov formulations in the frequency domain,” *Geophys. J. Int. **168**, 605-633, 2007.*
27. Y. Choi, C. Shin, “Frequency-domain elastic full waveform inversion using the new pseudo-Hessian matrix: Experience of elastic Marmousi 2 synthetic data,” *Bulletin of the Seismological Society of America, **98**, 2402-2415, 2008.*

28. J. Kaipo, E. Somersalo, “Statistical and computational inverse problems,” *(Springer-Verlag, New York, 2004), pages 1-246.*

29. D. S. Sivia, J. Skilling, “Data analysis, a Bayesian tutorial,” *(Oxford science publication, 2nd edition, Oxford, 2006), pages 1-246.*

30. F. Qin, Y. Luo, K.B. Olsen, W. Cai, G.T. Schuster, “Finite difference solution of the eikonal equation along expanding wavefronts,” *Geophysics **57**, 478-487, 1992.*

31. J. Vidale, “Finite-difference calculation of travel times,” *Bulletin of the Seismological Society of America, **78(6)**, 2062-2076, 1998.*

32. M. A. Perez, J. C. Bancroft, “Traveltime computation through isotropic media via the eikonal equation,” *CREWES Research Report, Vol. **12**, 181-200, 2000.*

33. K. Aki, P. G. Richards, “Quantitative Seismology, Second Edition,” *(University Science Books, Sausalito, California, 2002), Chap. 2.*

34. P. M. Sheary, “Introduction to Seismology, Second Edition,” *(Cambridge University Press, New York, 2009), Chap. 3.*

35. P. M. Manning, G. F. Margrave, “Elastic wave finite difference modeling as a practical exploration tool,” *CREWES Research Report, Vol. **10**, 18-1 to 18-16, 1998.*

36. R. Graves, “Simulating seismic waves propagation in 3D elastic media using staggered grid finite differences,” *J. Acoust. Soc. Am. **100**, 3061-3069, 1996.*

37. S. Rost, C. Thomas, “Array seismolology: Methods and Applications,” *Review of Geophysics, Vol. **40(3)**, 2-1 to 2-27, 2002.*

38. J. Virieux, S. Operto, “An overview of full-waveform inversion in exploration geophysics,” *Geophysics, **74(6)**, 1-26, 2009.*

39. N. Bleistein, J. K. Cohen, J. W. Stockwell, Jr., “Mathematics of multidimensional seismic imaging, migration and inversion,” *(Springer-Verlag, New York, 2001), Chap. 1, 2 and 3.*

40. A. Malinverno, “A bayesian criterion for simplicity in inverse problem parameterization,” *Geophys. J. Int.* ***140****, 267-285, 2000.*

41. T. J. Ulrych, M. D. Sacchi, A. Woodbury, “A Bayes tour of inversion: a tutorial,” *Geophysics* ***66****, 55-69, 2001.*

42. J. A. Scales, L. Tenorio, “Prior information and uncertainty in inverse problems,” *Geophysics* ***66****, 389-397, 2001.*

43. A. J. W. Duijndam, “Bayesian estimation in seismic inversion: Part I: Principles,” *Geophysical Prospecting* ***36,*** *878-898, 1988.*

44. A. J. W. Duijndam, “Bayesian estimation in seismic inversion: Part II: Uncertainty analysis,” *Geophysical Prospecting* ***36****, 899-918, 1988.*

45. M. K. Sen, P. L. Stoffa, “Bayesian inference, Gibbs’ sampler and uncertainty estimation in geophysical inversion,” *Geophysical Prospecting,* ***44****, 315-350, 1996.*

46. J. Martin, L. C. Wilcox, C. Burstedde, O. Ghattas, “A stochastic newton MCMC method for large-scale statistical inverse problems with application to seismic inversion,” *SIAM J. Sci. Comput.,* ***34(3)****, 1460-1487, 2012.*

CHAPTER 4

JOINT SEISMIC INVERSION & LOCALIZATION COMPARING SIMULATED ANNEALING AND METROPLOLIS HASTING

The results presented in chapter 3 have shown that the full waveform Bayesian inversion, where full-wave 3D elastic wave equation modelling is performed provides the best resolution and accuracy for the localization task. In that formulation, the only unknown model parameter to be estimated from the seismic array measurement is the (x, z) location of the tunnel. The elastic ground parameters are assumed known from a separate geophysical measurement.

In this chapter, we present methodologies where the inversion problem is expanded to a joint inversion problem to solve for both the elastic ground parameters and the source location. Two optimization algorithms, namely the Simulated Annealing method and the Metropolis Hasting Monte Carlo method, are applied for solving the joint inversion problem. Both methodologies fall under the class of global optimization methods to provide point estimates by searching for the model parameters maximizing the posterior probability density function of the unknown model parameters. In addition, the Metropolis Hasting Monte Carlo method can also provide a complete solution for the posterior probability density function of the unknown model parameter with information that includes the expectation and the variance for the model parameters. In this chapter, we evaluate both methodologies

on simulated data and compare the results of the joint inversion, while Chapter 5 will focus on the evaluation of real field data.

4.1 Methodology

The seismic inverse problem can be stated as follows: a system comprises of a seismic source generates seismic wave-fields as output. From the output, i.e. observational data made by seismic sensors, and a forward model relating the observational data and seismic source, knowledge about the seismic system can be inferred. The Bayesian approach formulates the inverse problem in terms of statistical inference, incorporating uncertainties in the seismic measurement, the forward model and prior information on the parameters. The solution of the inverse problem is the posterior joint probability density of the parameters, which encode the degree of confidence in their estimate. The information summarized from the posterior distribution includes the maximum posterior solution (MAP), the posterior expectation and the posterior covariance.

The subsection 4.1.1 presents the parameterization of the physical model of the elastic earth adopted in the seismic inverse problem studied in this thesis. A reduced parameterization scheme of the ground elastic model is proposed in order to alleviate the ill-posedness when solving for the inversion of a high dimension parameter space. Subsection 4.1.2 outlines the Bayesian inversion framework, with discussions on the numerical implementation of the forward model, the formulation of the posterior joint probability density of the parameters (the parameters include elastic parameters describing the ground medium, and the source location vector),

and implementation of two numerical optimization algorithms (Simulated Annealing and Monte Carlo Metropolis Hasting) for solving the inversion algorithm.

4.1.1 Physical Model

The physical model refers to models of the ground in which the elastic seismic waves propagate. In the following subsections, we will describe the parameterization used to describe this elastic ground medium.

4.1.1.1 Parameterization of Elastic Ground Model

The ground is assumed as a horizontal stratified medium where P and S waves propagate. The seismic wave equation is described by the Navier Equation (Equation 2-5) and the elastic parameters include the P- and S- wave speeds and the soil density.

In the thesis, we assume a five-layer horizontally stratified elastic ground medium described in Figure 4-1 and Table 4-1. Each soil layer is parameterized with P- and S-wave speeds and soil density values described by a vector $\mathbf{m}_G(z)$ as follows,

$$\mathbf{m}_G(z) = \left\{ v_p(z_k), v_s(z_k), \rho(z_k), k = 1,...,5 \right\}$$

and $\mathbf{m}_G(z) \in \Re^N$, N=15.

Fgure 4-1 Description of the five layer soil model used in the study.

Soil layer : z_k (*d* denotes depth in m)	P wave speed v_p (*m/s*)	S wave speed v_s (*m/s*)	Density ρ (*g/cm³*)
$z_1: 0 < d \le 1$	$v_p(z_1)$	$v_s(z_1)$	$\rho(z_1)$
$z_2: 1 < d \le 2$	$v_p(z_2)$	$v_s(z_2)$	$\rho(z_2)$
$z_3: 2 < d \le 4$	$v_p(z_3)$	$v_s(z_3)$	$\rho(z_3)$
$z_4: 4 < d \le 8$	$v_p(z_4)$	$v_s(z_4)$	$\rho(z_4)$
$z_5: 8 < d \le 100$	$v_p(z_5)$	$v_s(z_5)$	$\rho(z_5)$

Table 4-1 Parameterization of the five-layer soil model

4.1.1.2 Reduced Modelling of Ground Elastic Model

Markov Chain Monte Carlo (MCMC) methods, such as the Metropolis Hasting algorithm applied for solving the optimization of Bayesian inversion, works well in low dimension of the parameter space [1]. Henceforth it is crucial that some form of dimension reduction be applied to the parameter space. The challenge has been in the development of appropriate reduced models that are faithful over the full high-dimensional parameter space, see Ref [1].

The elastic ground model parameters are the P- and S-wave speeds and soil densities defined for each homogeneous soil layer. This thesis adopted a five-layer soil model which leads to 15x1 dimension space. Our approach for dimension reduction is to apply the physical relationships between elastic wave speeds and soil density so as to solve only for the soil density values of the five soil layers.

First, we consider the empirical relation between density $\rho(z)$ and the P-wave speed $v_p(z)$ of Gardner et al. [2], defined as follows,

$$\rho(z) = 0.31\left[v_p(z)\right]^{0.25}. \qquad \text{Equation (4-1)}$$

The ratio of the P-wave to S-wave speed is dependent on the soil properties (porosity, water saturation, crack intensity and clay content). Table 4-2 tabulates the measurements for P-wave speed (v_p), S-wave speed (v_s) and the ratio v_p/v_s for different soil types [3]. We shall apply Table 4-2 for calculations of the S wave speeds from the P wave speeds.

We can now defined the reduced elastic parameter $\mathbf{m}_R(z)$ as follows,

$$\mathbf{m}_R(z) = \{\boldsymbol{\rho}, (x_s, z_s)\}, \qquad \text{Equation (4-2)}$$

and apply Equation (4-1) and Table (4-2) to compute the P and S wave speeds.

Soil & Rock Type	$v_s(m/s)$	$v_s(m/s)$	v_p / v_s
Hard	6000 - 4300	4000 - 2700	1.45 -1.5
Very Stiff	4200 - 3000	2700 - 1500	1.5 - 2
Stiff	3000 - 2000	1500 - 700	2 - 3
Moderate	2000 - 1500	700 - 400	3 – 4
Loose and soft	1500 - 600	400 - 100	4 – 6

Table 4-2 Values of v_p / v_s for different soil types [3]

4.1.2 The Joint Bayesian Inversion and Localization Problem

The joint Bayesian inversion and localization problem is to infer from the seismic measurements both information about the physical ground model, and information about presence of the tunnel such as its location.

The joint seismic inversion and localization problem is formulated as follow. To determine from the seismic observational data measured by an array of seismic sensors on the ground surface an unknown parameter vector, $\mathbf{m(x)} = \{\rho(\mathbf{x}), (x_s, z_s)\}$, $\mathbf{m(x)} \in \Re^N$ where $\rho(\mathbf{x})$, (x_s, z_s) denote the soil density values and the source

location vector respectively. The forward model $\mathrm{g}(\mathbf{m})$ to map the parameters $\mathbf{m}$ to the data measurement $\mathbf{d}_{obs}$ is given as follows,

$$\mathbf{d}_{obs} = \mathrm{g}(\mathbf{m}) + \mathbf{n} \qquad \text{Equation (4-3)}$$

where $\mathbf{n}$ is the error term modelling the random ambient noise and the system errors. The forward modelling operator g solves the Navier wave equation.

The solution of the Bayesian inversion methodology is the posterior joint probability density of the parameters. Applying Bayes Theorem, the posterior joint probability density of the parameters, $\pi_{\text{posterior}}(\mathbf{m})$ can be written as follows, (see Chapter 2)

$$\pi_{\text{posterior}}(\mathbf{m}) = \pi(\mathbf{m}|\mathbf{d}_{\text{obs}}) \propto \pi_{\text{prior}}(\mathbf{m})\pi(\mathbf{d}_{\text{obs}}|\mathbf{m}) \qquad \text{Equation (4-4)}$$

where $\pi_{\text{prior}}(\mathbf{m})$ is the prior joint probability density function of the parameters, and $\pi(\mathbf{d}_{\text{obs}}|\mathbf{m})$ is the likelihood function.

4.1.2.1 Forward Model

The forward model $\mathrm{g}(\mathbf{m})$ solves the Navier wave equation defined by Equation (2-6) to model the elastic waves propagating from the tunnel location to the seismic sensors on the ground surface. We solve the $2\mathrm{D}$ Navier wave equation on the spatial domain $\Omega = [0, L_x] \times [0, L_z]$, where $x \in [0, L_x]$ represents the range on the ground, and $z \in [0, L_z]$ represents the depth beneath the surface. The ground is assumed as a horizontal stratified medium comprising of multiple horizontal homogeneous layers where each layer is parameterized by a P- and S-wave speed

and soil density. The source is modelled with forcing input to the Navier wave equation using a Ricker[3] wavelet with a mean spectral energy density at 0.5 Hz, and a spatial delta function.

The time dependent Navier wave equation is solved using the FDTD method [4,5] where the partial differential operators in the elastic wave equations are expressed via 2nd order finite differential expansion in space and time respectively. In this thesis, we applied the 2D FDTD numerical algorithm from the CREWES numerical software [4]. The initial and boundary conditions for the FDTD solver are defined as follows: The elastic ground medium is in equilibrium at time t = 0, i.e., stress and displacement are set to zero everywhere in the medium. The internal interfaces within the elastic ground medium are represented in terms of the changes of elastic wave speeds and density in a horizontal stratified medium assumed in this thesis. Explicit boundary conditions are imposed on the four edges of the finite-sized vertical grid where the FDTD calculations are performed. Different boundary conditions can be defined dependent on the problem to investigate. In the FDTD calculations performed in this thesis, the boundary conditions on the edges are defined as followed; a free surface at z=0, a mirror surface at offset x=0, a transparent boundary at the right side, and a rigid bottom. The free surface boundary condition at z=0 simulates a real seismic experiment under flat topography and allow R-waves to be simulated. The mirror surface at offset x=0 act as if there is a continued geological model anti-symmetric about the zero x axis. The bottom is modelled as a rigid boundary and therefore a strong reflector. In our case where these reflections are

[3]Ricker wavelets are zero-phase wavelets with a central peak and two smaller side-lobes. A Ricker wavelet is uniquely defined in terms of its peak frequency given as $r(t) = \left(1 - 2\pi^2 f^2 t^2\right)\exp\left(-\pi^2 f^2 t^2\right)$. Ricker wavelet is commonly used by geophysicists to generate synthetic seismograms.

not wanted, we introduce a large value for the depth of the final ground layer. For the FDTD calculations, the ground subsurface is divided into uniform mesh where the spatial rate in *x*- and *z*-directions is defined in order of 1 *m*.

We shall be applying the described forward model as the 'truth', i.e., to generate the simulated measurement plus added noise (Section 4.1.4). The same forward model is also the one used in the inversion.

4.1.2.2 Prior Selection for Location Vector and Soil Density Vector

The prior distribution for the soil density vector $\boldsymbol{\rho}$ is assumed as an increasing sequence of step functions, where the bounds for the step function values ρ_i are selected based on the prior knowledge of the soil layering structure of ground of similar type [16]. For example, the top layer comprises mostly of water saturated soft sand, while the other deeper soil layers are assumed to be composed either of dry sand or clay.

The prior pdf for the soil densities is defined as follows,

$$\pi_{prior}(\boldsymbol{\rho}) = \begin{cases} 1 & a_i \le \rho_i \le b_i, \text{for } i = 1,2,3,4 \\ 0 & \text{otherwise} \end{cases} \qquad \text{Equation (4-5)}$$

where the bounds satisfy the following inequality relationships, $a_{i+1} \ge a_i$ & $b_{i+1} \ge b_i$.

The density value of the bottom soil layer is assumed as constant, $\rho_5 = 2g/cm^3$.

The chosen prior PDF of the location vector follows a uniform distribution defined over the spatial search grid space where the source is assumed to lie.

4.1.2.3 Likelihood Function

The likelihood function $\pi(\mathbf{d}_{\text{obs}} | \mathbf{m})$ defines the probability that a set of parameters reproducing the measured data $\mathbf{d}_{\text{obs}}$. Apply Equation (4-3) and using an additive

Gaussian noise model with probability distribution of zero mean and covariance matrix $\mathbf{C}_{\text{noise}}$, the likelihood function is written as follows,

$$\pi(\mathbf{d}_{\text{obs}}|\mathbf{m}) = \exp\left\{-\frac{1}{2}(\mathbf{d}_{\mathbf{m}} - \mathbf{d}_{\text{obs}})^T \mathbf{C}_{\text{noise}}^{-1}(\mathbf{d}_{\mathbf{m}} - \mathbf{d}_{\text{obs}})\right\} \quad \text{Equation (4-6)}$$

where $\mathbf{d}_{\mathbf{m}} = g(\mathbf{m})$ satisfies the forward model described in Section 4.1.2.1.

One way to model the noise is through measurement of the ambient signal before the experiment recording. Here the noise covariance matrix takes the form of a diagonal matrix with its elements estimated from the variance of the ambient measured at the sensor.

4.1.2.4 Posterior Joint Density Function of Parameters

The prior distribution for model parameter $\mathbf{m}$, which is the soil density vector $\boldsymbol{\rho}$, is an increasing sequence of step functions each of which follows a uniform distribution. Hence under the assumption that the model $\mathbf{m}$ take $\pi_{prior}(\mathbf{m})$ values one, the posterior density function can be written as follows,

$$\pi_{\text{posterior}}(\mathbf{m}) \propto \exp\left\{-\frac{1}{2}\left(\mathbf{d}_{\mathbf{m}} - \mathbf{d}_{\text{obs}}\right)^T \mathbf{C}_{\text{noise}}^{-1}\left(\mathbf{d}_{\mathbf{m}} - \mathbf{d}_{\text{obs}}\right)\right\} \text{Equation (4-7)}$$

Under the same assumption that the prior is one, the maximum posterior solution (MAP) is defined as follows,

$$\mathbf{m}^* = \arg\max_{\mathbf{m}}\left(\exp\left\{-\frac{1}{2}\left(\mathbf{d}_{\mathbf{m}} - \mathbf{d}_{\text{obs}}\right)^T \mathbf{C}_{\text{noise}}^{-1}\left(\mathbf{d}_{\mathbf{m}} - \mathbf{d}_{\text{obs}}\right)\right\}\right) \text{Equation (4-8)}$$

Equation (4-8) can be rewritten into another form such that it minimizes the negative log-posterior density function, i.e.

$$\mathbf{m}^{*} = \arg\min_{\mathbf{m}_R}\left(\frac{1}{2}\left(\mathbf{d}_{\mathbf{m}} - \mathbf{d}_{\text{obs}}\right)^{T}\mathbf{C}_{\text{noise}}^{-1}\left(\mathbf{d}_{\mathbf{m}} - \mathbf{d}_{\text{obs}}\right)\right) \qquad \text{Equation (4-9)}$$

where we can define the optimization cost function as follows,

$$\mathrm{F}\left(\mathbf{m}\right) = \frac{1}{2}\left(\mathbf{d}_{\mathbf{m}} - \mathbf{d}_{\text{obs}}\right)^{T}\mathbf{C}_{\text{noise}}^{-1}\left(\mathbf{d}_{\mathbf{m}} - \mathbf{d}_{\text{obs}}\right) \qquad \text{Equation (4-10)}$$

Equation (4-9) is identical to weight least squares expression (2-14) used in the deterministic inversion algorithm where the quantity in bracket of Equation (4-9) is minimized as a function of parameters $\mathbf{m}$, subject to the constraint that observational data $\mathbf{d}_{\mathbf{m}}$ satisfies the forward model described in Section 4.1.2.1.

The other posterior information summarized from the posterior distribution includes the posterior expectation (conditional mean) and the posterior covariance described as follows,

$$\mathbf{m}_{CM} = \mathrm{E}\left\{\mathbf{m} \mid \mathbf{d}_{obs}\right\} = \int \mathbf{m}\pi\left(\mathbf{m} \mid \mathbf{d}_{\text{obs}}\left(x,z,t\right)\right)d\mathbf{m} \qquad \text{Equation (4-11)}$$

$$\begin{aligned}\mathbf{C}_{\mathbf{m}} &= \mathrm{E}\left\{\left(\mathbf{m}-\mathbf{m}_{CM}\right)\left(\mathbf{m}-\mathbf{m}_{CM}\right)^{T}\right\} \\ &= \int\left(\mathbf{m}-\mathbf{m}_{CM}\right)\left(\mathbf{m}-\mathbf{m}_{CM}\right)^{T}\pi\left(\mathbf{m} \mid \mathbf{d}_{\text{obs}}\left(x,z,t\right)\right)d\mathbf{m}\end{aligned} \qquad \text{Equation (4-12)}$$

The posterior expectation and covariance can be calculated from the model samples $\left\{\mathbf{m}_i : i = 1,...N\right\}$ generated from the algorithm as follows,

$$\tilde{\mathbf{m}}_{CM} = \frac{1}{N}\sum_{i=1}^{N}\mathbf{m}_i, \qquad \text{Equation (4-13)}$$

$$\tilde{\mathbf{C}}_{\mathbf{m}} \approx \frac{1}{N}\sum_{i=1}^{N}\left(\mathbf{m}_i - \tilde{\mathbf{m}}_{CM}\right)\left(\mathbf{m}_i - \tilde{\mathbf{m}}_{CM}\right)^{T}. \qquad \text{Equation (4-14)}$$

4.1.3 Optimization Algorithms

In this section, we present two optimization algorithms for solving the posterior joint probability density function for the parameters.

The first algorithm is the Simulated Annealing method, which solves Equation (4-9) to determine the point estimate of the parameters. The second algorithm is the Monte Carlo Metropolis Hasting method that is able to provide a complete solution of the posterior distribution that includes the MAP point estimate, and posterior expectation and covariance of the parameters.

These two optimization methods are designed to search for global optimum among the many local optima and have been applied to the seismic inverse problems [6-9]. Local optimization algorithms seek the nearest local optimum because of the standard strategy where the algorithms generate trial point based on current estimates, evaluating function at proposed location and then accepting the new value if it improves solution. To avoid being trapped into local optima, the global optimization algorithms such as the Simulated Annealing and Metropolis Hasting algorithms have developed specific schemes in the search strategy to find other optima, i.e., also allowing selection of new points that do not improve solution. The details of the search strategies for these two algorithms are described in the next two subsections.

4.1.3.1 Simulated Annealing

Simulated annealing is a probabilistic approach proposed by Kirkpatrick, Gelett and Vecchi [10] and Cerny [11] for finding the global minimum of a cost function that may possess several local minima. It originates from a physical process whereby a

solid is slowly cooled so that when eventually its structure is “frozen”; this happens at a minimum energy configuration. The cooling process is controlled by the temperature such that the molecules are allowed to move freely at high temperatures and restricting their motion at low temperatures.

The steps to implement the simulated annealing are described as follow [12].

- Propose an update $\mathbf{m}^{(j+1)}$ of the unknown parameter and evaluate the optimization function $\mathrm{F}(\mathbf{m}^{(j+1)})$
- Accept updates that improve solution
- Accept some updates that don’t improve solution. Acceptance probability depends on “temperature” parameter and is defined as follow, $\exp\left[-\frac{1}{T(t)}\left(\mathrm{F}(\mathbf{m}^{(j+1)}) - \mathrm{F}(\mathbf{m}^{(j)})\right)\right]$
- As T goes to zero, the values simulated from this distribution becomes More concentrated around a narrow neighbor-hood of F.

In this study, we apply the Matlab function *SIMULANNEALBND* for the simulated annealing calculations.

4.1.3.2 MCMC Metropolis Hasting Algorithm

The Metropolis Hasting algorithm [13-15] is an MCMC method. At each step, a new sample is generated by proposing a candidate and then accepting or rejecting based on the associated Hastings ratio.

We apply the Metropolis Hasting Algorithm to generate acceptable solutions to the problem as follows,

- At each step, vary one component of the parameter vector $\mathbf{m}$ generated from prior distributions, see Section 4.1.2.2.
- Compute $\mathbf{d}_{\mathbf{m}}$ using the forward model described in Section 4.1.2.1.
- Compute the acceptance probability $P_{acc} = \frac{\pi_{posterior}\left(\mathbf{m}^{(pro)}\right)}{\pi_{posterior}\left(\mathbf{m}^{(cur)}\right)}$, $\mathbf{m}^{(pro)}$ is the proposed variable, and $\mathbf{m}^{(cur)}$ is the current variable value. The parameters are changed at each step by random selection from a uniform probability density function.
- Accept the changes to $\mathbf{m}^{(pro)}$ if $\min\{P_{acc},1\} > \text{rand}$;

4.1.4 Simulation Parameters

We apply the forward model described in Section 4.1.2.1 to generate a simulation set of measurements as follows: The seismic source is modeled with a forcing input to the elastic wave equation using a Ricker wavelet. The true location of the source is given by $(x_s, z_s) = (1,10)\,m$. Figure 4-2 describes the physical model where the soil density values are given as $\boldsymbol{\rho} = |1.53,1.75,1.8,1.85,2|^T$. The P- and S-wave speeds are computed by applying Equation (4-1) and Table (4-2). Applying the above described parameters to the forward mode, the "clean" seismic data is generated at positions $(x, z) = \{(20,1),\ (25,1),\ (30,1),\ (35,1),\ (40,1),\ (45,1)m\}$. The simulation set of measurements $\mathbf{d}_{obs}$ is generated by adding a Gaussian noise vector. The noise variance is 0.005, while the variance of the clean signal is *5*.

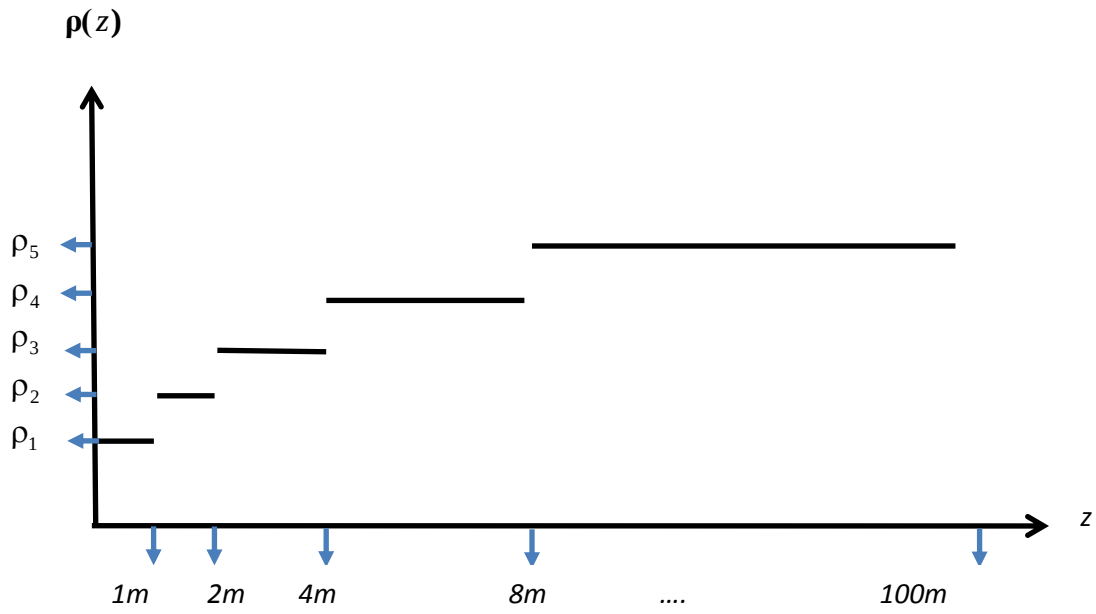

Figure 4-2 Prior model selection of soil density vector $\boldsymbol{\rho}$ *described as an increasing sequence of step functions relative to depth*

Next, Table 4-3 displays the bounds for the density values needed to define the priors for the soil density vector, Section 4.1.2.2.

Density values for each layer	Lower bound a_i (g/cm^3)	Upper bound b_i (g/cm^3)
ρ_1	1.5	1.6
ρ_2	1.7	1.9
ρ_3	1.7	1.9
ρ_4	1.7	1.9

Table 4-3 Prior bounds for the soil density parameter of the topmost four soil layers

4.2 Results And Analysis

In this section, the Simulated Annealing inversion method is compared with the MCMC Metropolis Hasting inversion method in solving the tunnel detection problem in which the data consists of synthetic traces generated from the steps described in Section 4.1.4.

The analysis of the solution of the posterior distribution derived from the MCMC Metropolis Hasting method is first discussed in Section 4.2.1. This is followed by the discussion of the results from Simulated Annealing algorithm in Section 4.2.2. Finally we conclude with a discussion of the results from these two methods in Section 4.2.3.

4.2.1 Results of Monte Carlo Metropolis Hasting Algorithm

Figure 4-3 plots the course of the posterior joint probability density values (Equation 4-7) of the proposed model $\mathbf{m}^{(pro)}$ which are accepted by the Metropolis Hasting algorithm for each realization. From Equation (4-7), the optimal value of the posterior joint density of the parameters is one, and this occurs when the parameters matches the true values. Figure 4-3 shows that the accepted posterior joint density values fluctuate over a range between 0.5 and 0.9 over the 5000 iteration runs. The average value of the accepted posterior joint density values is $\mu_{\pi_{\mathbf{m}}} = 0.71$ with standard deviation $\sigma_{\pi_{\mathbf{m}}} = 0.09$.

Figure 4-5 and 4-6 displays the histogram plots for the samples of two of the parameters, namely depth and range, generated by Monte Carlo Metropolis Hasting. Recall that the true location of the source is given by $(x_s, z_s) = (1, 10)\text{m}$. Figure 4-5 shows that the most of the Monte Carlo Metropolis Hasting range samples falls in the

bar at 1 m which coincides with the source range x_s = 1 m. Whereas Figure 4-6 shows that there is no clear specific bar where a majority of the Monte Carlo Metropolis Hasting depth samples lie. From Figure 4-6, we observe a peak at bar 10 m (this coincides agrees with the source depth z_s = 10 m), and another broader peak across bars 12 m to 20 m.

We can compute the posterior mean and variance to get a quantification of the uncertainty of the solution. This is done by applying Equation (4-13) and (4-14) on all the parameter samples accepted by Monte Carlo Metropolis Hasting algorithm. In our calculations, we also include estimation of the mean and variance from different subsets of the parameter samples generated from the Monte Carlo Metropolis Hasting algorithm. The first subset is formed from the parameter samples which are accepted by the Metropolis Hasting algorithm with high confidence, i.e., high posterior density values. We form this set from the random samples with posterior joint density values larger than $\left(\mu_{\pi_{\mathbf{m}}} + \sigma_{\pi_{\mathbf{m}}}\right) = 0.87$ where $\mu_{\pi_{\mathbf{m}}}$ denotes the mean of the posterior density values for all 5000 random samples, and $\sigma_{\pi_{\mathbf{m}}}$ denotes the standard deviation or spread of the posterior density values. There are 684 samples accepted by the Monte Carlo Metropolis Hasting with posterior joint density larger than $\left(\mu_{\pi_{\mathbf{m}}} + \sigma_{\pi_{\mathbf{m}}}\right)$. Also, we compute the mean and variance from subset of parameter samples accepted by Monte Carlo Metropolis Hasting with the posterior joint density values less than $\left(\mu_{\pi_{\mathbf{m}}} + \sigma_{\pi_{\mathbf{m}}}\right)$. The results of the calculations are displayed in Table 4-5. The MAP estimate is also presented in the same table.

From Table 4-5, we observe large deviations from the true values for the means of range and depth computed from all the Metropolis Hasting accepted random

samples. There is a significant improvement in the results for the means computed from the parameter samples with high posterior joint density values. The MAP results perform the best, where the MAP estimate of depth deviates less than 10 % from the true value, and the MAP range estimate agrees with the true value.

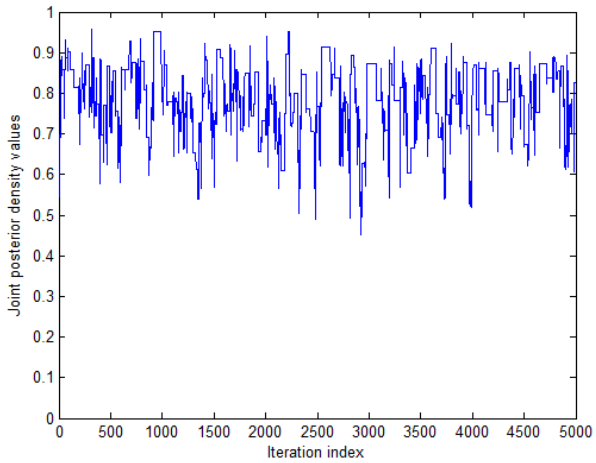

Figure 4-3 Joint posterior density function values of the proposed model accepted by the Metropolis Hasting algorithm

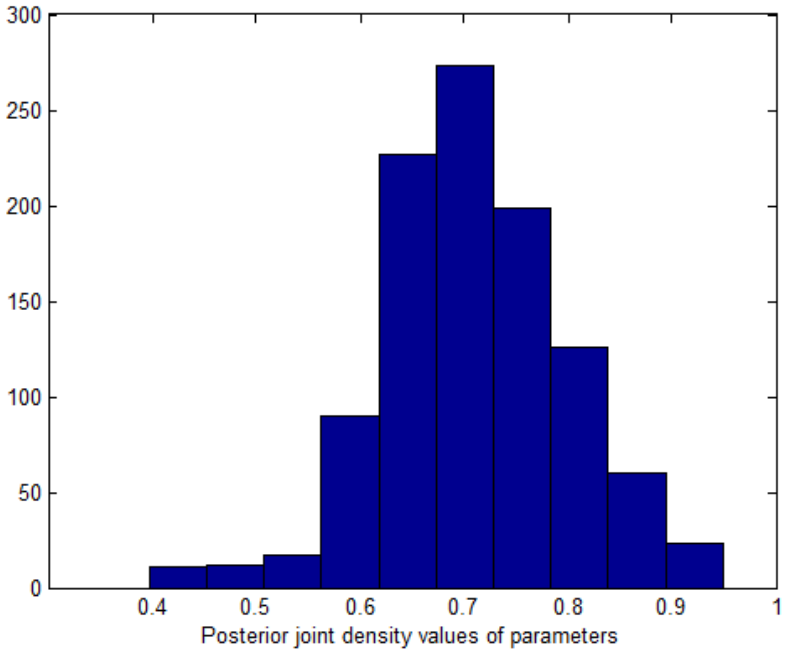

Figure 4-4 Histogram plot of the joint posterior density values accepted by the Metropolis Hasting algorithm

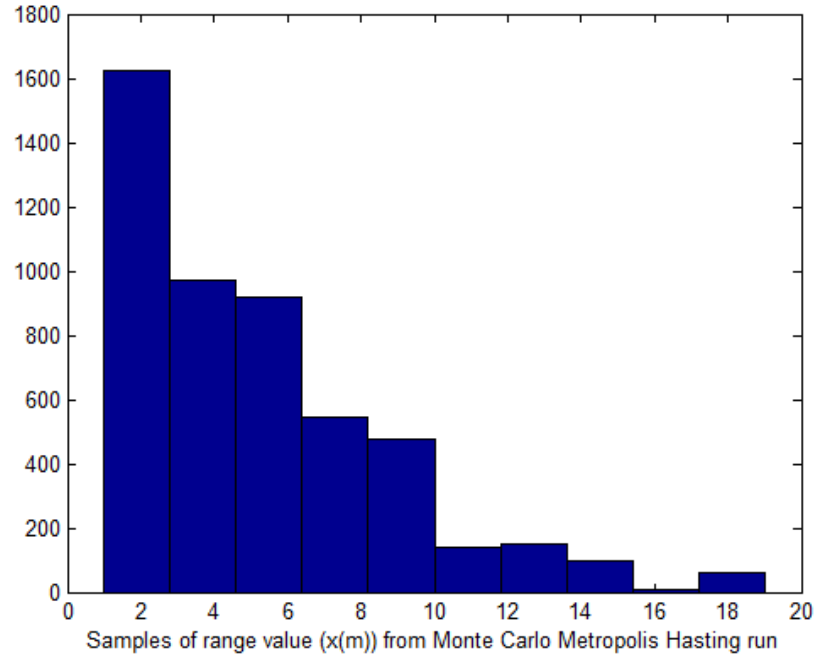

Figure 4-5 Histogram plot of the samples of range (x) parameter accepted by the Metropolis Hasting algorithm

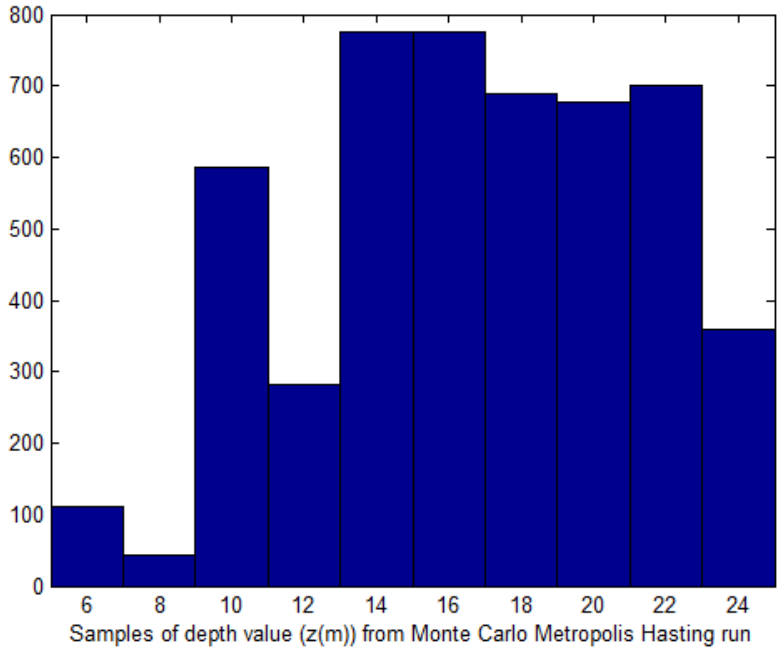

Figure 4-6 Histogram plot of the samples of depth (z) parameter accepted by the Metropolis Hasting algorithm

	True values (m)	All parameter samples accepted by MC Metropolis Hasting		Subset of parameter samples with posterior values> $\left(\mu_{\pi_m} + \sigma_{\pi_m} = 0.87\right)$		Subset of parameter samples with posterior values< $\left(\mu_{\pi_m} + \sigma_{\pi_m} = 0.87\right)$		MAP estimate
		mean	variance	mean	variance	Mean	variance	
x (range)	1	5.09	3.79	1.77	1.10	5.61	3.8	1
z (depth)	10	17.07	4.54	13.74	2.42	17.60	4.58	11

Table 4-5 Posterior means, variances and MAP calculated from the parameter, x (range) and z (depth), accepted by the Metropolis Hasting algorithm

Table 4-6 displays the means, standard deviations and the MAP estimates computed for the soil density parameter vector. It can be observed from the values displayed in Table 4-6 that the Metropolis Hasting inversion is able to provide fairly good estimates for the soil densities.

Soil density at *i-th* layer (ρ_i)	True values (g/cm^3)	Mean estimates	Standard deviation estimates	MAP estimates
ρ_1	1.53	1.55	0.0281	1.53
ρ_2	1.75	1.75	0.0397	1.76
ρ_3	1.80	1.80	0.0459	1.78
ρ_4	1.85	1.85	0.0368	1.85

Table 4-6 Means, standard deviations, and MAP estimates of soil density values generated using Metropolis Hasting Monte Carlo algorithm.

Figures 4-8 to 4-11 display the histogram plots of the soil density vector samples generated by the Metropolis Hasting algorithm. The histogram graph of the parameter samples can be interpreted as displaying the approximated PDF of the parameter. Observe only the approximated PDF for soil density of layer number 3 (see Figure 4-10) matches a Gaussian distribution. The approximated PDF for soil density of soil layer 2,4, (Figure 4-9,4-11) are better described by lognormal distributions.

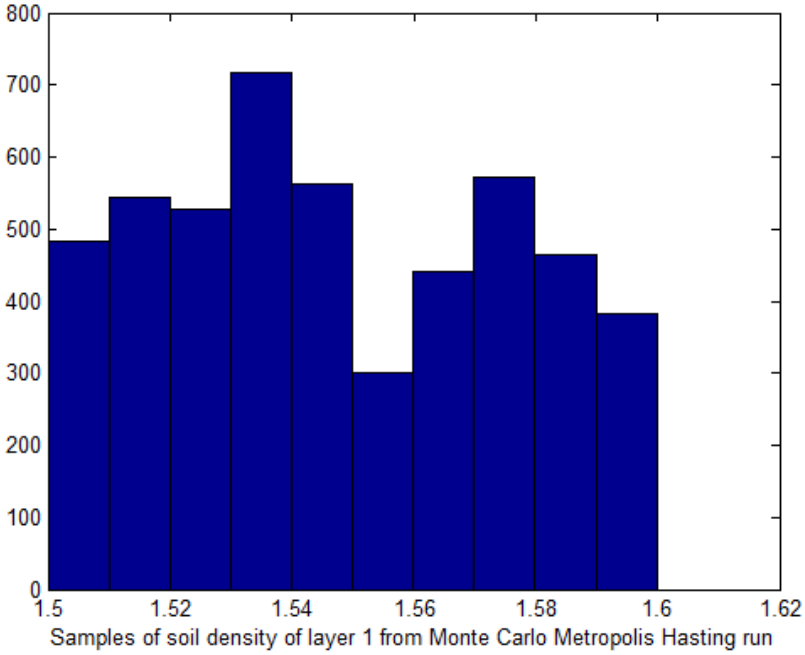

Figure 4-8. Histogram display of samples of soil density layer #1 accepted by Monte Carlo Metropolis Hasting. Actual density value of soil layer #1 = 1.53g/cm^3

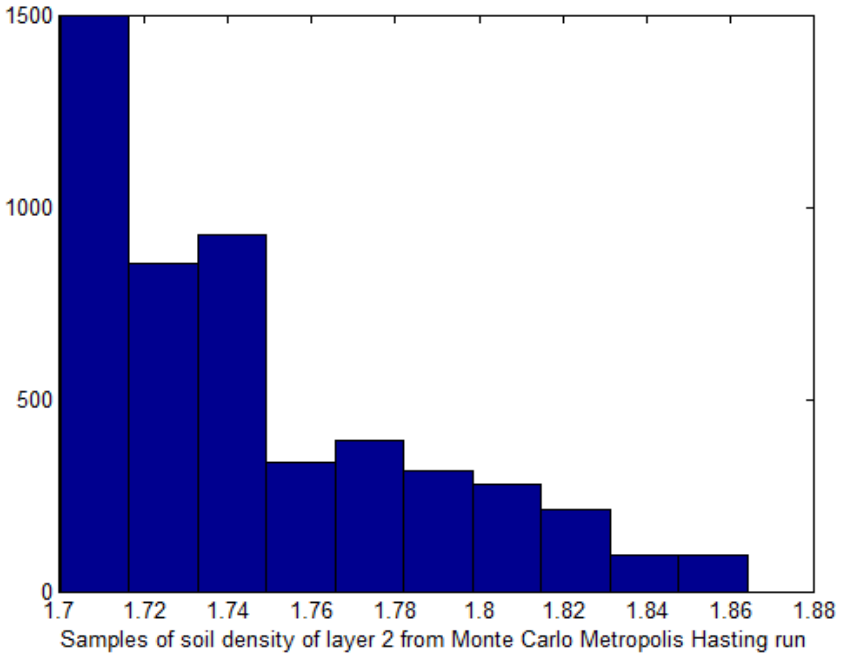

Figure 4-9. Histogram display of samples of soil density layer #2 accepted by Monte Carlo Metropolis Hasting. Actual density value of soil layer #2 = 1.75g/cm^3

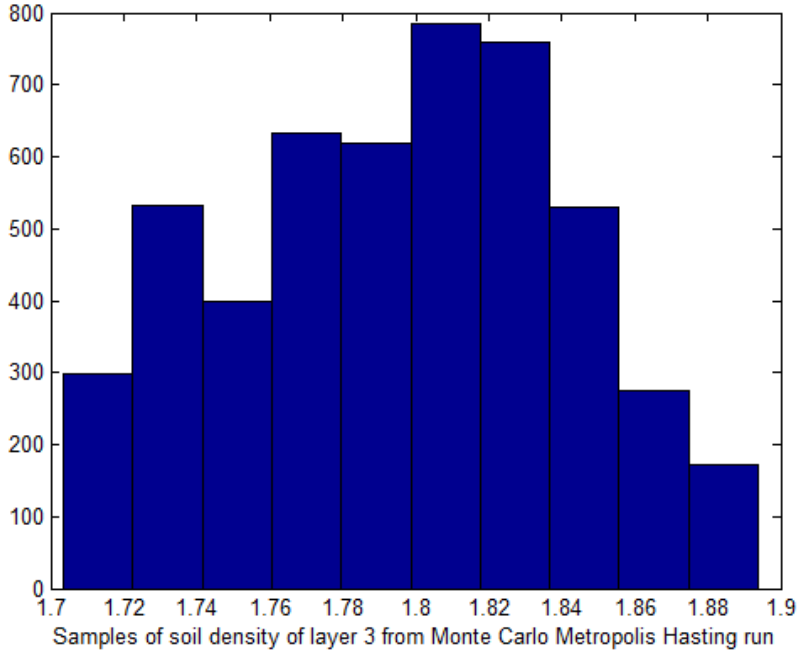

Figure 4-10. Histogram display of samples of soil density layer #3 accepted by Monte Carlo Metropolis Hasting. Actual density value of soil layer #3 = 1.8g/cm^3

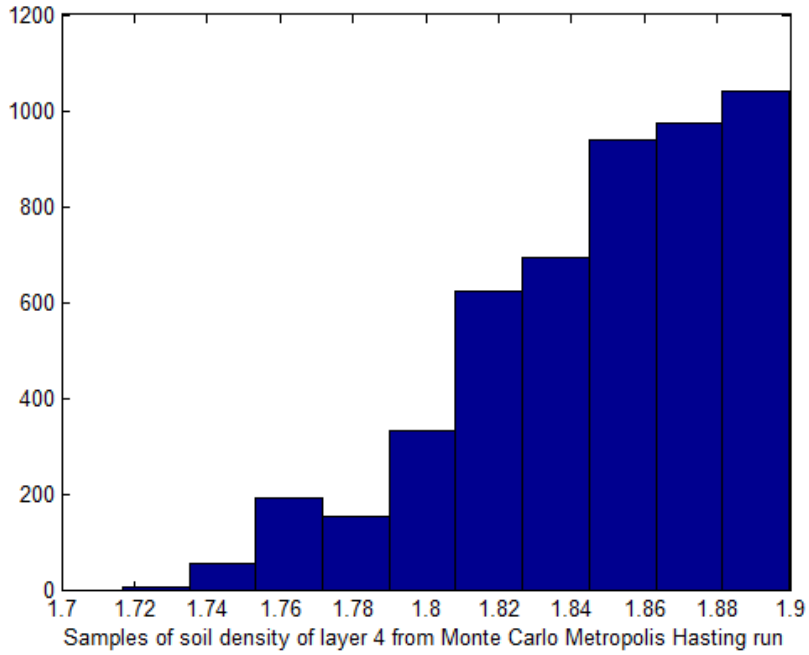

Figure 4-11 Histogram display of samples of soil density layer #4 accepted by Monte Carlo Metropolis Hasting. Actual density value of soil layer #4 = 1.85g/cm^3

4.2.2 Results of Simulated Annealing Algorithm

In this Section, we present the point estimate of the parameters computed with the Simulated Annealing algorithm. The Matlab function *SIMULANNEALBND* used for the calculations allows one to apply the lower and upper bounds on the search space for the parameter. Similar to the implementation of the Metropolis Hasting algorithm, for the depth and range parameter, the bounds are derived from the spatial domain $\Omega = (x, z) = [0, 20]\text{m} \times [0, 25]\text{m}$ where the source is expected to be located. The bounds for the soil density values follow from Table 4-3. Simulated Annealing requires a good starting point, i.e., a good initial guess for the unknown parameters to ensure convergence. The MAP estimate calculated from 50 MCMC runs of the Metropolis Hasting algorithm is chosen as the initial input of the

parameters for the Simulated Annealing algorithm. For this simulation, 1000 iterations for the Simulated Annealing function are executed.

Table 4-7 displays the point estimates of the parameters from Simulated Annealing algorithm. The result of the source depth and range from Simulated Annealing algorithm performs better as compared against the means calculated by Metropolis Hasting Monte Carlo method (Table 4-5), and gives comparable performance relative to the MAP estimate. For the soil density estimates, the Simulated Annealing algorithm is only able to perform well for the top two soil layers, while the results for the bottom two layers are better for the Metropolis Hasting algorithm.

	True values	Initial Guess from MAP estimate calculated from 50 MCMC runs of the Metropolis Hasting algorithm i	Estimates from Simulated Annealing
x_s (m)	1	6	1.64
z_s (m)	10	10	11.10
ρ_1 (g/cm^3)	1.53	1.52	1.53
ρ_2 (g/cm^3)	1.75	1.74	1.75
ρ_3 (g/cm^3)	1.80	1.74	1.86
ρ_4 (g/cm^3)	1.85	1.80	1.86

Table 4-7 Results from the Simulated Annealing algorithm

4.3 Discussions

In this chapter, the concept of jointly solving for the elastic ground parameters and the source location is implemented. We implemented two global optimization algorithms, namely the Monte Carlo Metropolis Hasting algorithm and the Simulated Annealing algorithm, for the inversion. The chapter introduced a ground physical model for reduction of the parameter space to reduce the ill-posedness for solving a large dimension inversion problem. In addition, we also introduced an additional constraint on the prior model for the soil layer density parameter that it be modelled as an increasing sequence of step functions relative to depth.

The results of the inversion of the soil density values show that both the global optimization method, i.e., Monte Carlo Metropolis Hasting algorithm and Simulated Annealing, are able to provide fairly good estimates which agree with the investigations in the literatures that focus only on geo-inversion of the elastic medium [6,7,8]. The results of Monte Carlo Metropolis Hasting inversion to solve the source localization problem,i.e., invert for source depth and source range, display large fluctuations in the range and depth samples generated, though the point MAP estimates derived from 5000 runs of the Metropolis Hasting method are relatively close to the true values.

The results of the Simulated Annealing using an initial guess as the MAP estimate calculated from a small number of runs of the Monte Carlo Metropolis Hasting algorithm (in the simulation, we use 50 runs), is able to improve the accuracy of the range and depth estimate of the source. Simulated Annealing also produce good estimates of the soil density for the topmost layer and the second soil layer,

though there is a slight deviation of the soil density of the deeper soil layer from the true values.

The two global optimization methods, Monte Carlo Metropolis Hasting and Simulated Annealing, investigated in this chapter are successful on a global level in the estimation of the geo-parameters. The results of the investigation further show that the combination of Simulated Annealing and Monte Carlo Metropolis Hasting is able to refine and improve the source localization results.

4.4 Conclusions

We have investigated the use of two global, stochastic inversion method, Simulated Annealing and Monte Carlo Metropolis Hasting method, to solve the seismic inversion problem. The seismic inversion is formulated into a reduced framework such that we only need to invert for the soil density values from the seismic observations, and apply the empirical models to estimate the P- and S-wave speeds from the inverted soil density values. The inversion also modelled the soil density values of the horizontal stratified elastic ground as an increasing sequence of step functions so as to improve the efficiency of the search during the inversion process.

The result of the investigation was that the Simulated Annealing using an initial guess as the MAP estimate calculated from a small number of runs of the Monte Carlo Metropolis Hasting algorithm is able to improve the accuracy of the range and depth estimate of the source.

BIBLOGRAPHY

1. C. Lierberman, K. Wilcox, O. Ghattas, “Parameter and state model reduction for large scale statistical inverse problems,” *SIAM J. Sci. Comput., **32**, 2523-2543, 2010.*
2. G. H. F. Gardner, L. W. Gardner, A. R. Gregory, “Formation velocity and density – the diagnostic basics for stratigraphic traps,” *Geophysics, **93**, 770-780, 1974.*
3. K. Ali, “Soil parameters which can be determined with seismic velocities,” *Jeofizik, **16**, 17-29, 2012.*
4. P. M. Manning, G. F. Margrave, “Elastic wave finite difference modeling as a practical exploration tool,” *CREWES Research Report, Vol. **10**, 18-1 to 18-16, 1998.*
5. R. Graves, “Simulating seismic waves propagation in 3D elastic media using staggered grid finite differences,” *J. Acoust. Soc. Am. **100**, 3061-3069, 1996.*
6. K. Mosegaard, P. D. Vestergaard, “A simulated annealing approach to seismic model optimization with sparse prior information,” *Geophys. Prospect., **39**, 599-611, 1991.*
7. E. Landa, W. Beydoun, A. Tarantola, “Reference velocity model estimation from prestack waveforms: Coherency optimization by simulated annealing,” *Geophysics, **54**, 984-990, 1989.*
8. Z. Koren, K. Mosegaard, E. Landa, P. Thore, A. Tarantola, “Monte Carlo estimation and resolution of seismic background velocities,” *J. Geophys. Res., **96**, 20289-20299, 1991.*
9. P. W. Cary, C. H. Chapman, “Automatic 1-D waveform inversion of marine seismic refraction data,” *Geophys. J. R. Astron. Soc., **93**, 527-546, 1988.*

10. S. Kirkpatrick, C. D. Gelett, M. P. Vecchi, “Optimization by simulated annealing,” *Science, **220**, 621-630, 1983.*
11. V. Cerny, “A thermodynamic approach to the travelling salesman problem: An efficient simulation,” *J. Optim. Theory Appl., **45**, 41-51, 1985.*
12. B. Dimitris, J. Tsitsiklis, “Simulated Annealing,” *Statistical Science, **8(1)**, 10-15, 1983.*
13. N. Metropolis, A. W. Rosenbluth, M. N. Rosenbluth, A.H. Teller and E. Teller, “Equations of State Calculations by Fast Computing Machines,” *Journal of Chemical Physics, **21**, 1087-1092, 1953.*
14. W. K. Hastings, “Monte Carlo Sampling Methods Using Markov Chains and Their Applications,” *Biometrika, **57**, 97-109, 1970,*
15. S. Chib, E. Greenberg, “Understanding the Metropolis-Hastings Algorithm,” *The American Statistician, **49(4)**, 327-335, 1995.*
16. M. D. Braja, “Principles of soil dynamics,” *PWS-Kent Publishing Company, 1993.*

CHAPTER 5

SEISMIC INVERSION APPLIED TO UNDERGROUND TUNNEL LOCALIZATION PROBLEM

5.1 Introduction

The goal of seismic inverse problem is to provide information about the ground subsurface from seismic measurements [7-9]. This involves estimation of subsurface material properties such as elastic wave velocities, density, etc, from surface [2-4, 6] and down-hole [1, 5] measurements of seismic data.

In the literatures, there are two main approaches to solving the seismic inversion problem.

The first approach solves the linear seismic inverse problem by assuming a smooth background model with perturbations for the subsurface. It is then assumed dominance presence of only single scattered wave-field. Tarantola [10] casts the inverse problem as a local optimization problem, the aim of which is least squares minimization of the misfit between the recorded and modelled data. The least squares solution is then computed by searching for the perturbation model parameter along the gradient of the misfit function. Each step of the iterative algorithm consists of a forward propagation of the actual sources in the current model, and a forward propagation (backward in time) of the data residuals. The correlation at each point of the space of these two fields yields the corrections of the

elastic models. This approach is similar to methods of migration of data. Several other studies include the extended ray theory approach [11,12] where the forward problem is solved by a combination of the Born approximation and ray theoretical methods. The perturbed seismogram is defined in terms of perturbations of P- and S-wave impedances and density and the inversion method is based on generalized least squares.

The second approach is the full waveform inversion (FWI) where full wave equation modelling is performed in the seismic inversion processing. All types of waves are involved in the optimization which includes multi-scattered waves (multiples). A good overview of the full-waveform inversion in exploration geophysics can be found by a paper written by Virieux & Operto [13]. Local optimization such as least squares does not prevent convergence of the misfit function to local minima for FWI contributed by the following factors. Such as the presence of noise, or large parameterization of the model space leading to a high underdetermined inversion problem, or inaccurate forward modelling of the complex elastic field. All of these factors lead to a non-convex optimization function that the seismic inversion problem needs to solve. Several global optimization methods have been applied that include techniques such as simulated annealing [14], genetic algorithms [15-16] and Monte Carlo methods [17-18]. In Chapter 4 of this study, we compare two of these techniques, Simulated Annealing and Metropolis Hasting Monte Carlo method, for solving a joint seismic inversion and localization problem. The two algorithms are analysed using synthetic seismogram, and the results show that both methods perform comparably.

In this chapter, we expand the work developed in Chapter 4 to solve for both the elastic properties of the subsurface and location of an underground tunnel using observational seismic data recorded by an array of geophones on the ground surface. A seismic source ($18\ \mathrm{kg}$ weight) is used to generate seismic waves through the ground and recorded by an array of two geophones deployed on the ground surface. The ground elastic medium is modelled as a series of horizontal layers separated by straight interfaces. Each layer is characterised by a P-wave speed, S-wave speed and soil density value. We proposed a ground physical model relating the elastic wave speeds and the soil densities so that we need only estimate the soil densities and the tunnel location in the inversion. The soil densities for the horizontal layers are modelled using a prior of increasing sequence of step functions by applying the knowledge from geophysical surveys that the soil densities of the ground horizontal stratified layers increase with depths.

This chapter is organized as follows. In Section 5.2, we describe the seismic experiment setup for the underground tunnel localization problem. We refer to the readers to Chapter 4.1 for details on the methodologies for the Bayesian inversion scheme and the Metropolis Hasting and Simulated Annealing sampling methods. Section 5.3 presents the inversion results for the underground tunnel localization problem, and Section 5.4 presents the discussions and summarizes the chapter.

5.2 Experiment Setup

5.2.1 Experiment Layout

The tunnel that we are interested to detect and locate is a heritage tunnel which has depth varying between $3\ \mathrm{m}$ to $9\ \mathrm{m}$. Figure 5-1 displays the topological

information of the tunnel site and the measurement setup comprising of two geophones deployed on the ground surface

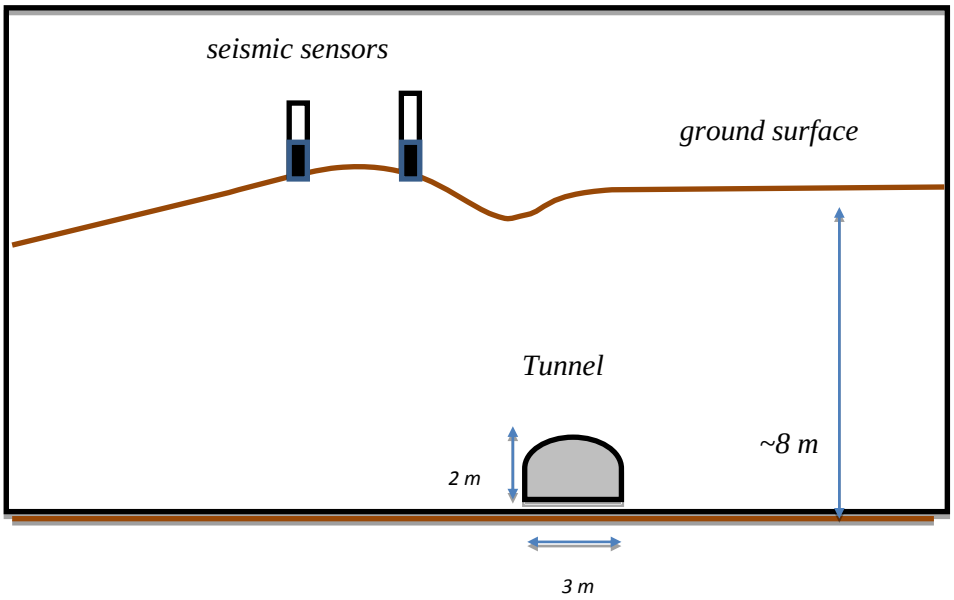

Figure 5-1 Estimated topographical information of tunnel trial site and the seismic measurement setup.

5.2.2 Seismic Source and Seismic Sensors

The seismic source is provided by a weight drop. A cylinder with a hemispherical end cap weighing 18 kg is designed to drop from a 1 m height to generate the seismic impact forcing on the ground surface. We refer the readers to Figure 3-3 for the display of the seismic signal time series and time-frequency plot generated by seismic source. The signal is impulsive and contains little spurious re-bounce signals. The seismic sensors used for the experiment are the geophones (see Figure 3-4) which measures particle velocity. The geophones provide measurement in frequency range from 4.5 Hz to 100 Hz. In the experiment, two vertical component

GS11D geophones are deployed. The geophones are connected to the Brüel & Kjær 32-bit, 4-channel digital recorder to digitize the measured seismic signals.

5.2.3 Geophysical Survey

A geophysical survey is conducted at the location site to determine the compressional wave speed profile near the tunnel. Figure 5-2 displays the location sites with the survey lines. Survey LINE-1 is closest to the tunnel and Figure 5-3 displays the configuration of the seismic array relative to the survey lines. Figure 5-4 shows a picture of the setup of the geophone array. Figure 5-5 displays a picture of the tunnel entrance walls which are made up of concrete.

Figure 5-6 displays the measured compressional P-wave profile measured at survey LINE-1 using the seismic refraction method [25]. The method measures the time it takes for a compressional sound wave generated by a sound source to travel down through the layers of the earth and back up to the geophones placed on the ground surface. From the time-distance information, the compressional P-wave speed variations and depths to individual layers are calculated and modelled. The P-wave profile measured along survey LINE-1 is used to set up the prior model parameters for the elastic parameters. As indicated in the prior model selection for the soil densities (see Section 4.1.1.1), the elastic compressional P-wave travels faster with increasing soil depth. Table 5-1 displays the bounds on the density values calculated from the P-wave speeds (refer to Equation (4-1)). The density value of the last layer is fixed, i.e. $\rho_5 = 2\ \text{g/cm}^3$.

Density values for each layer	Lower bound a_i (g/cm^3)	Upper bound b_i (g/cm^3)
ρ_1	1.5	1.6
ρ_2	1.7	1.9
ρ_3	1.7	1.9
ρ_4	1.7	1.9

Table 5-1 Bounds for soil densities for first four soil layers of the ground model

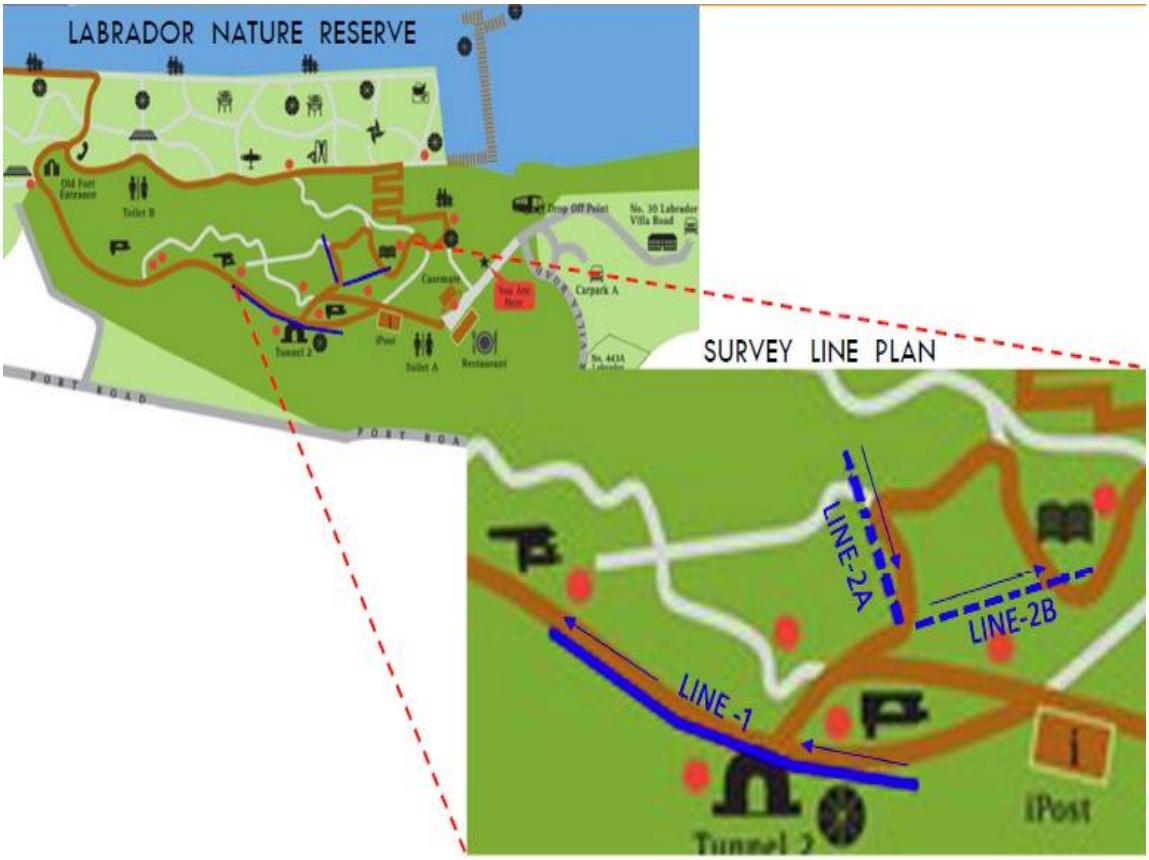

Figure 5-2 Location map of the tunnel and the survey lines.

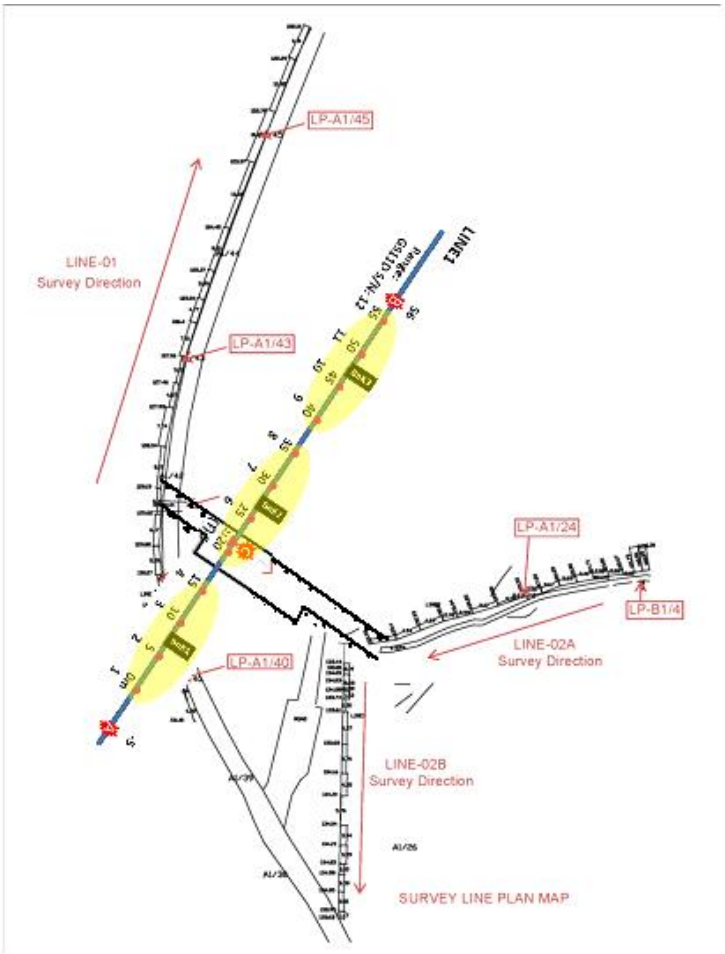

*Figure 5-3 Location map of the seismic array (**LINE1**) relative to the tunnel and the survey lines.*

Figure 5-4 Picture showing setup of survey LINE-1 for the geophysical measurement relative to the tunnel axis

Figure 5-5 Picture of tunnel entrance showing that tunnel is made up of concrete walls

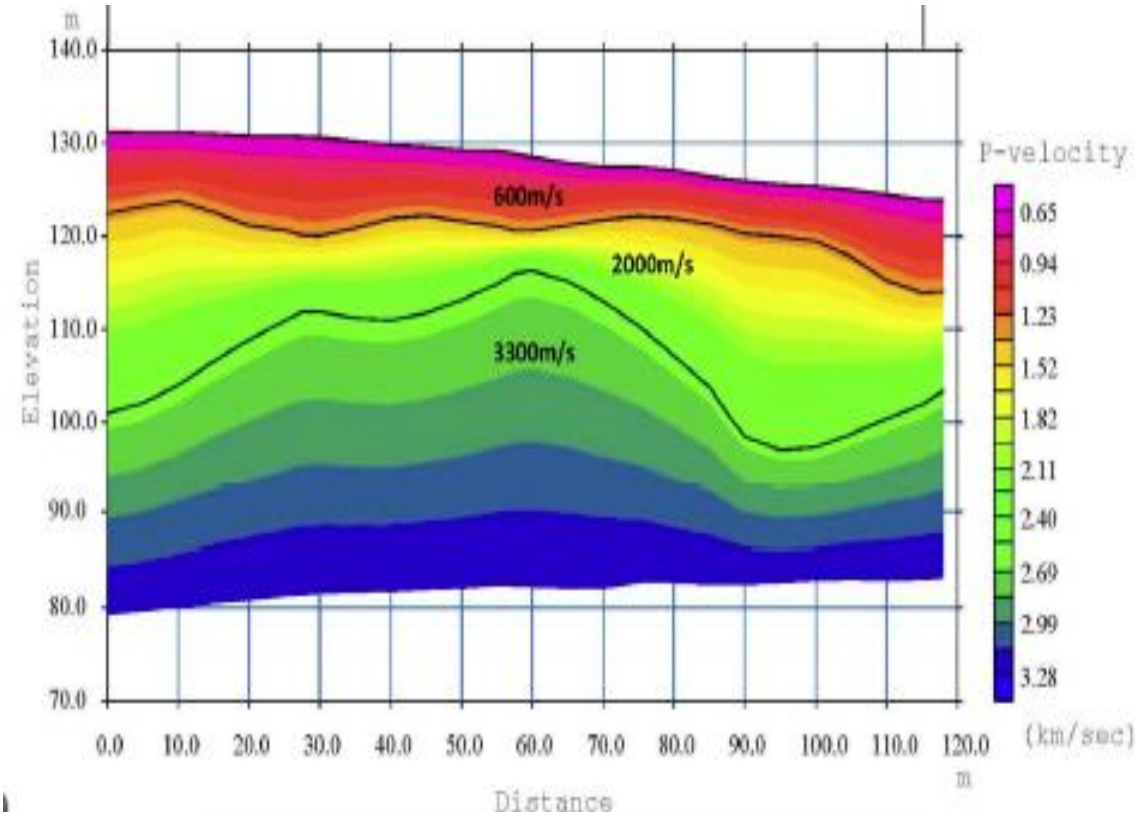

Figure 5-6 Compressional wave speed profile measured along LINE-1 located near tunnel measured using the seismic refraction method

5.2.4 Experiment Test Plan

Figure 5-7 describes the experiment layout. A seismic array comprising of two geophones that are spaced 5 m apart are deployed on the ground surface. The underground tunnel is located at $(x_s, z_s) = (22, 6.5)$ m. The seismic source is provided by a 18 kg weight deployed at $(x_s, z_s) = (0, 0)$ m. The seismic source provides a seismic wave that will propagate through the ground, interacting with the elastic ground medium, and the elastic waves are recorded by the seismic array.

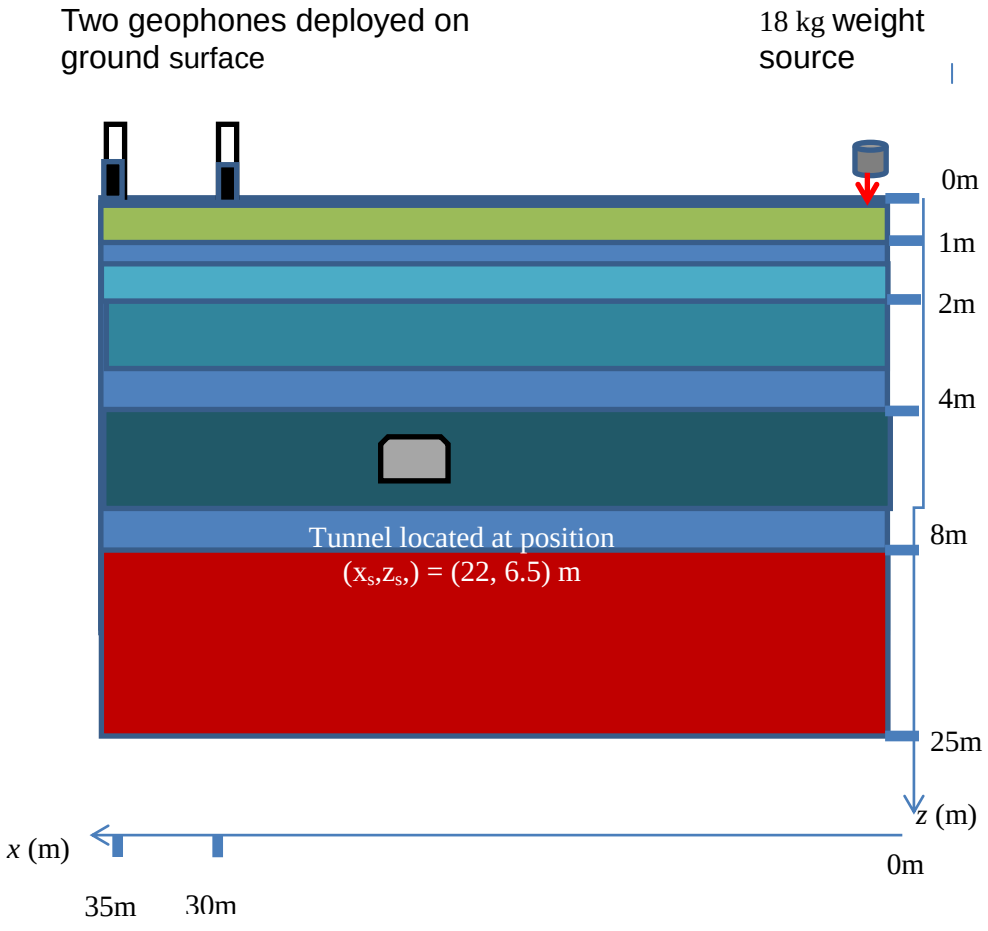

Figure 5-7 Configuration of the experiment test plan

5.3 Results And Analysis

The analysis of the solution of the posterior distribution derived from the MCMC Metropolis Hasting method is first presented in Section 5.3.1, and Section 5.3.2 presents the results from the Simulated Annealing method.

5.3.1 Results of Metropolis Hasting Algorithm

5.3.1.1 Marginal distribution of a posterior information of the source location parameter

Figures 5-8 and 5-9 display the histogram plots of the depth and range of the source produced by the above Metropolis Hasting algorithm. In the calculations, the chosen prior PDF of the location vector follows a uniform distribution defined over the spatial search grid space where the underground tunnel is assumed occur. The spatial search domain is defined as $\Omega = [0, L_x] \times [0, L_z] = [0,25]m \times [0,30]m$. $x \in [0, L_x]$ represents the range on the ground, and $z \in [0, L_z]$ represents the depth beneath the surface. Both the histograms for the depth and range parameters present multiple peaks indicating a multi-modal posterior PDF for each of these two location parameters estimated from the observed data. Table 5-2 presents the means & variances of the depth and range calculated from the Monte Carlo Metropolis Hasting samples. The MAP estimates for the depth and range are also computed and also presented in Table 5-2. The MAP estimates for the location vector occurs at $(x, z) = (20, 10)$ m which compares well against the true values. For the specific evaluation presented here, the MAP estimate occurs at iteration run 3508 and the MAP PDF value is 0.75. The means of depth and range estimated from the MCMC samples deviate significantly from the true value. The histogram plots

displayed in Figures 5-8 and 5-9, show deviation from a simple Gaussian distribution. Hence the mean value is inadequate for representing the results generated by the MCMC samples. We only consider the set of Monte Carlo Metropolis Hasting depth and range samples with posterior values greater than value $\beta = \mu + \sigma$ where μ, σ denote the mean and standard deviations of the posterior values, and re-calculate the mean values of depth and range from this smaller subset of MCMC samples. The new mean values of the range and depth yield values $(x, z) = (17.94, 9.37)\,\mathrm{m}$ which is more accurate. If we examine Figures 5-8, we will observe that the new mean value of the depth coincidence with the location of one of the peaks. Similarly the new mean value of the range also coincides with the location of one of the many peaks displayed in Figure 5-9.

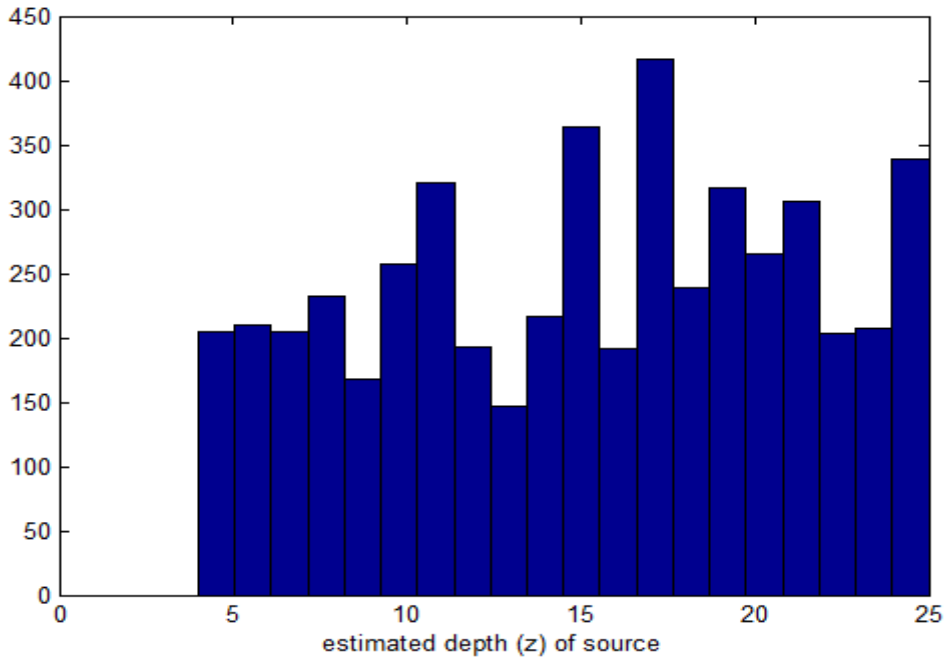

Figure 5-8 Histogram display for depth estimate (z). The horizontal axis plots depth of the source, and the vertical axis presents the number of MCMC samples that lie in the specific depth bin.

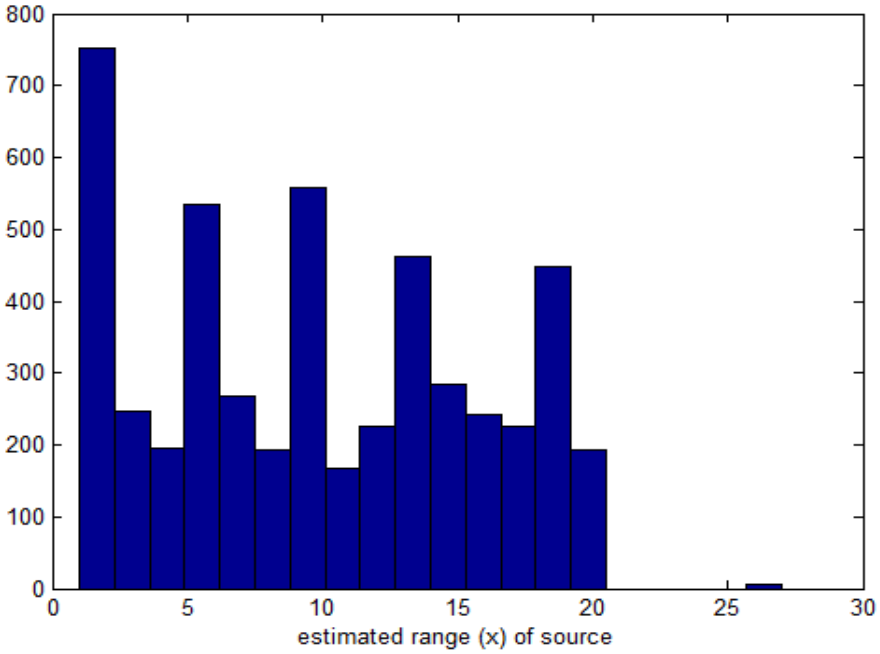

Figure 5-9 Histogram display for range estimate (x). The horizontal axis displays range of the source, and the vertical axis presents the number of MCMC samples that lie in the specific range bin.

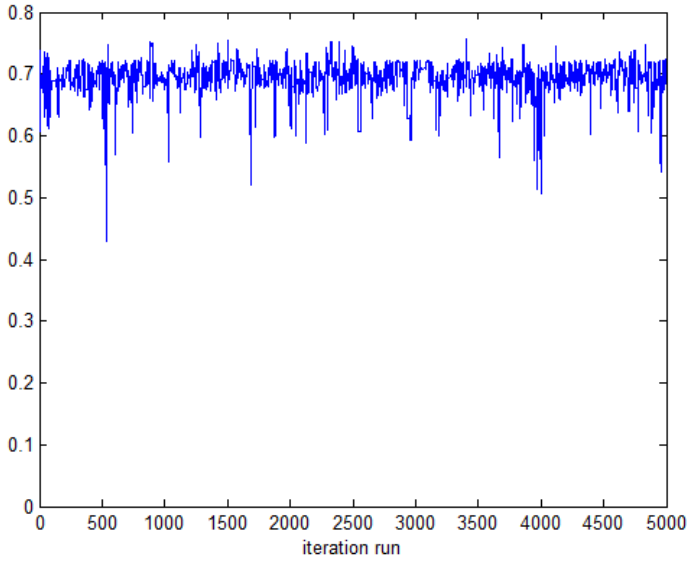

Figure 5-10 Posterior PDF values of the proposed model $\mathbf{m}_R$ which are accepted by the Metropolis algorithm.

	True values (m)	Mean estimates of MCMC samples accepted by Metropolis Hasting algorithm	Standard deviations of MCMC samples accepted by Metropolis Hasting algorithm	MAP estimate
x	22.5	9.87	5.94	20
z	6.5	15.11	5.69	10

Table 5-2 Means and standard deviations of the MCMC samples for model parameter x (range) and z (depth) accepted the Metropolis Hasting algorithm. Also displayed in table is the MAP estimate.

Source location vector	True values (m)	Mean estimates of MCMC samples accepted by Metropolis Hasting algorithm with posterior values $> \beta = \mu + \sigma = 0.7335$ where μ, σ denote the mean and standard deviations of the posterior values	Standard deviations of MCMC samples accepted by Metropolis Hasting algorithm with posterior values $> \beta = \mu + \sigma = 0.7335$ where μ, σ denote the mean and standard deviations of the posterior values
x	22.5	17.94	0.99
z	6.5	9.37	2.00

Table 5-3 Mean and standard deviation of the MCMC samples for model parameter x (range) and z (depth) accepted by Metropolis Hasting algorithm with posterior values $> \beta = \mu + \sigma = 0.7335$ where μ, σ denote the mean and standard deviations of the posterior values

We repeat the Metropolis Hasting algorithm for another MCMC run to check on the consistency and stability behaviour of the algorithm. The mean and standard

deviation results of the source location vector are presented in Table 5-4. A comparison of the results displayed with the previous MCMC run (refer to Table 5-3) show that the values generated from the two independent MCMC runs are fairly similar.

Source location vector	True values (m)	Mean estimates of MCMC samples accepted by Metropolis Hasting algorithm with posterior values $> \beta = \mu + \sigma = 0.7209$ where μ, σ denote the mean and standard deviations of the posterior values	Standard deviations of MCMC samples accepted by Metropolis Hasting algorithm with posterior values $> \beta = \mu + \sigma = 0.7209$ where μ, σ denote the mean and standard deviations of the posterior values
x	22.5	19.32	0.77
z	6.5	10.53	1.62

Table 5-4 Metropolis Hasting results for a different MCMC run.

5.3.1.2 Marginal distribution of a posterior information of the soil density vector

The prior model used to describe the soil density vector of the horizontally stratified soil layer contains more information than the non-informative uniform priors of the source location vector. The prior PDF for the soil density vector is described by Equation (4-5) and Table (5-1).

The histogram plots for the soil density MCMC samples are presented in Figures 5-11 to 5-14. The histogram plots displayed show that with the exception of the first soil layer, the histogram plots of the MCMC density samples for the deeper soil layers show small uncertainties in the estimation of the soil density value. The MAP estimates of the density vector are presented in Table 5-5 together with the corresponding mean estimates.

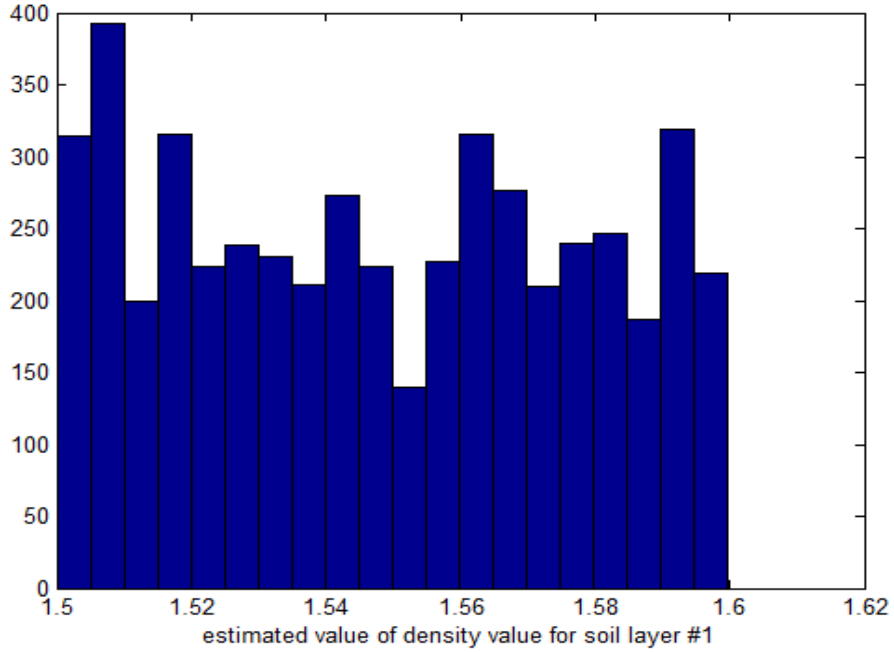

Figure 5-11 Histogram plot for the density value of soil layer # 1

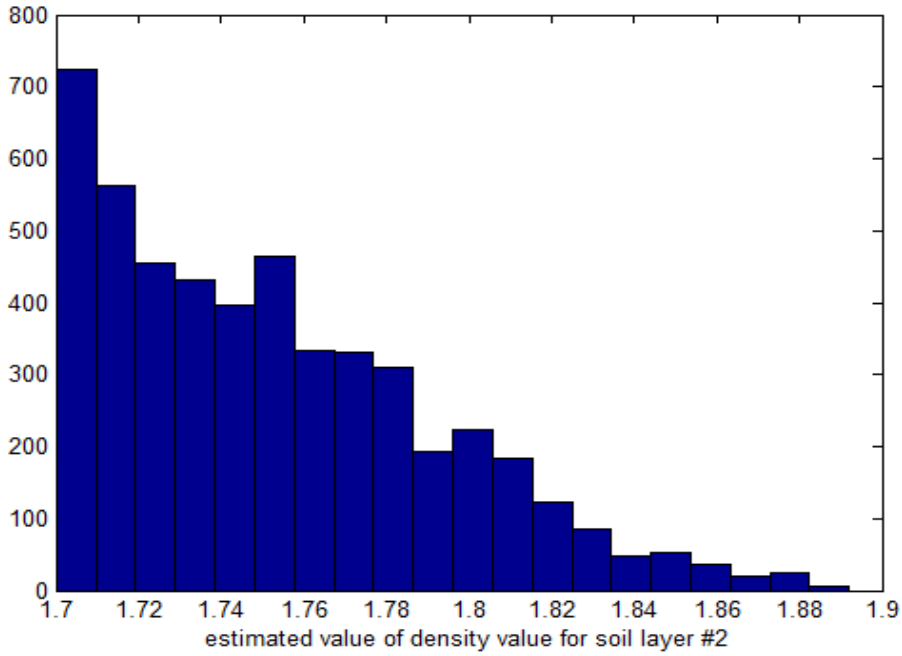

Figure 5-12 Histogram plot for the density value of soil layer # 2

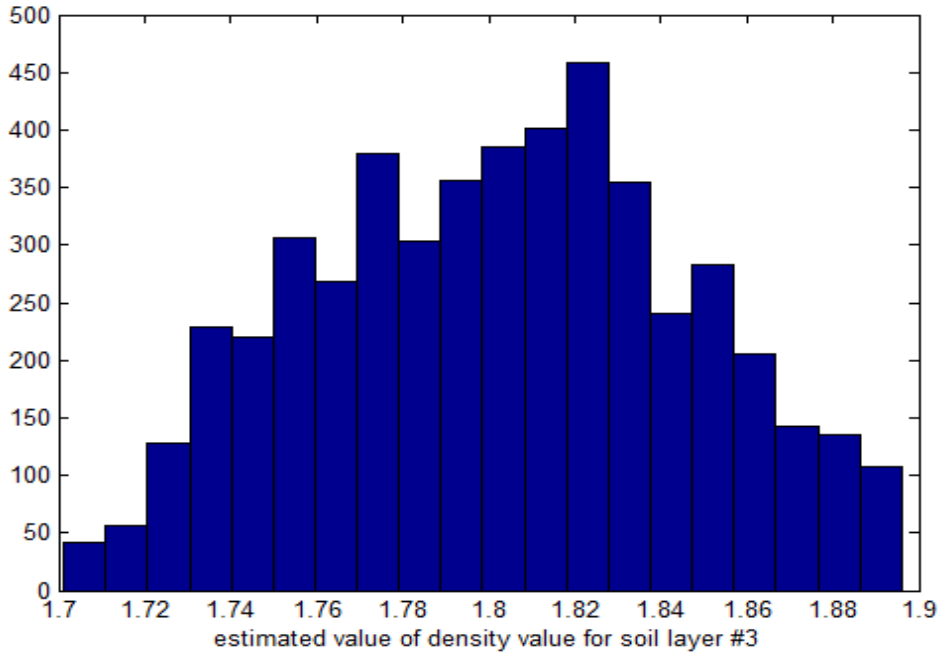

Figure 5-13 Histogram plot for the density value of soil layer # 3

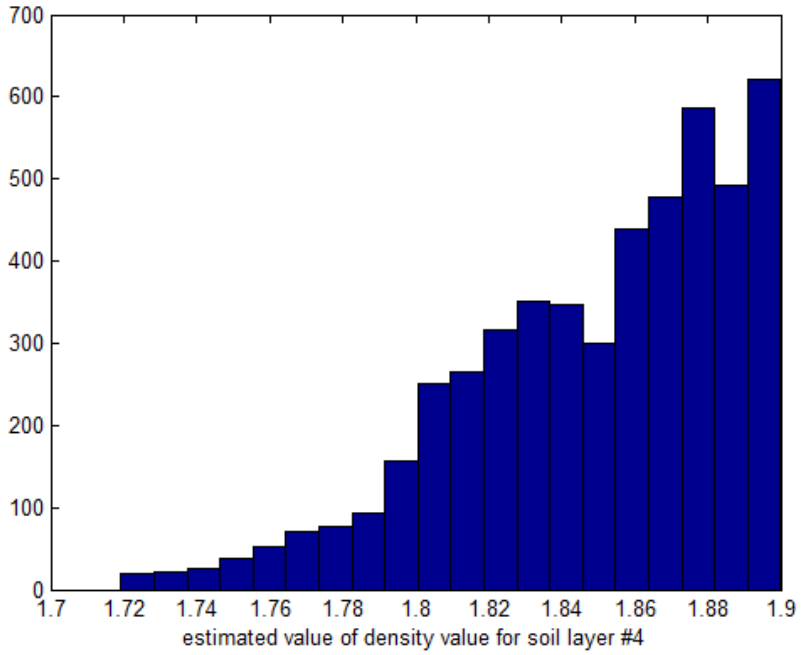

Figure 5-14 Histogram plot for the density value of soil layer # 4

Soil density (g/cm^3)	Mean estimates of MCMC samples accepted by Metropolis Hasting algorithm with posterior values > $\beta = \mu + \sigma = 0.7335$ where μ, σ denote the mean and standard deviations of the posterior values	Standard deviations of MCMC samples accepted by Metropolis Hasting algorithm with posterior values > $\beta = \mu + \sigma = 0.7335$ where μ, σ denote the mean and standard deviations of the posterior values	MAP estimate
ρ_1	1.54	0.029	1.58
ρ_2	1.76	0.039	1.72
ρ_3	1.81	0.045	1.83
ρ_4	1.85	0.042	1.89

Table 5-2 Means and standard deviations of the MCMC samples for model parameter x (range) and z (depth) accepted the Metropolis Hasting algorithm. Also displayed in table is the MAP estimate.

5.3.2 Results of Simulated Annealing Algorithm

We apply the MATLAB function simmulannealbnd.m to find the minimum $\mathbf{m}_R^*$ to the objective function specified by Equation (4-9). The matlab function defines a set of lower and upper bounds on $\mathbf{m}_R$, so that a solution is found in the range $\mathbf{l}_b \le \mathbf{m}_R \le \mathbf{u}_b$.

In the calculations, the lower and upper bounds for the soil density values are given by Table 5-1. The lower and upper bounds for the location vector (x, z) are obtained from the spatial domain $\Omega = [0, L_x] \times [0, L_z] = [0,25]m \times [0,30]m$ where the source is expected to be located. $x \in [0, L_x]$ represents the range on the ground, and $z \in [0, L_z]$ represents the depth beneath the surface.

The maximum number of iterations for the Simulated Annealing is fixed at 1000 runs. For efficient implementation that ensures good convergence, the Simulated Annealing requires a good starting point, i.e., a good initial guess for the unknown parameters. In our calculations, we obtain the initial guess from the MAP estimate derived from 50 MCMC runs of the Metropolis Hasting algorithm.

The results from the calculations of the Simulated Annealing algorithm are displayed in Table 5-5. The result of the source location vector from Simulated Annealing algorithm performs better as compared against the means calculated by Monte Carlo Metropolis Hasting method, and gives comparable performance to corresponding MAP estimate by the Metropolis Hasting method (see Table 5-2).

Source location vector *(x,z) (*m*)* Soil density vector ρ (g/cm^3)	Initial Guess from MAP estimate derived from 50 MCMC runs of Metropolis Hasting algorithm.	Estimates from Simulated Annealing
x	27	21.63
z	11	10.53
ρ_1	1.58	1.54
ρ_2	1.71	1.77
ρ_3	1.83	1.84
ρ_4	1.89	1.77

Table 5-5 Source location vector and soil density vector derived from the Simulated Annealing algorithm

5.3.3 Discussions

The histograms of the depth and range parameter computed from the Monte Carlo Metropolis Hasting samples both follow multi-modal distribution behaviour. Therefore single Gaussian distribution does not describe the data adequately. This is again verified in Table 5-2 where it is observed a large deviation of the mean values calculated from all the accepted MCMC samples from the location of the tunnel. The presence of the multiple peaks in Figure 5-8 and 5-9 indicates the possibilities of presence of more than one underground source. Thus the mean values of all the independent MCMC range and depth samples generated by the Metropolis Hasting sampling deviates largely from the true tunnel position. The MAP estimate calculated from the Metropolis Hasting samples however produces an estimate, $(x,z)=(20,10)\,\mathrm{m}$, that is not too far off from the position of the tunnel at $(x_s,z_s)=(22.5,6.5)\,\mathrm{m}$. This indicates possibility that the tunnel contributes the most amount of reflected seismic energy arriving at the geophones.

The combination of the Monte Carlo Metropolis Hasting algorithm with the Simulated annealing method leads to an estimated result, $(x,z)=(21.63,11.53)\,\mathrm{m}$, that is quite close to the Metropolis Hasting MAP estimate. The application of stochastic optimization method such as Simulated Annealing has been tried in geophysical applications [28-31] but the experience with the authors is that the method is very difficult to use. The main challenge is finding the annealing temperature schedule, and the optimum number of iterations to arrive at a good estimate. Our proposed method to use the Monte Carlo Metropolis Hasting algorithm to provide an initial guess for the algorithm, as well as incorporation of the prior

information for the model parameter greatly improve the efficiency of the simulated annealing method.

5.4 Conclusions

In this study, we applied the full 3D elastic wave Bayesian inversion for joint estimation of the soil layer densities and location of an underground tunnel using field seismic data recorded by an array of two seismic sensors on the ground surface. Two global optimization algorithms, Monte Carlo Metropolis Hasting and Simulated Annealing, are applied. The PDF curves of range and depth derived from plotting the histograms of Monte Carlo Metropolis Hasting generated samples displays multi-modal distribution behaviour, which made the mean estimate not a suitable parameter for processing the Monte Carlo samples. The MAP estimates derived from both the Monte Carlo Metropolis Hasting and Simulated Annealing methods however match well against the location of the underground tunnel. These results reflect that the point MAP estimate provides a more accurate representation for the location parameters exhibiting multi-modal distribution behaviour as observed in the field data.

BIBLOGRAPHY

1. R. G. Pratt, “Inversion theory applied to multisource cross-hole tomography, Part II: Elastic wave equation method,” *Geophysical Prospecting, **38**, 311-329, 1990.*
2. P. Mora, “Nonlinear two-dimensional elastic inversion of multi-offset seismic data,” *Geophysics **52,** 1211-1228, 1987.*

3. E. Crase, A. Pica, M. Noble, J. McDonald, A. Tarantola, “Robust elastic nonlinear waveform inversion: Application to real data,” *Geophysics, **55**, 527-538, 1990.*
4. E. Crase, C. Wideman, M. Noble, A. Tarantola, “Nonlinear elastic inversion of land seismic reflection data,” *Journal of Geophysical Research, **97**, 4685-4705, 1992.*
5. O. Gauthier, J. Virieux, A. Tarantola, “Two-dimensional non-linear inversion of seismic waveforms: Numerical results,” *Geophysics **51,** 1387-140, 1986.*
6. R. Brossier, S. Operto, J. Virieux, “Seismic imaging of complex onshore structure by 2D elastic frequency-domain full waveform inversion,” *Geophysics, **74(6)**, 105-118, 2009.*
7. C. Gelis, J. Virieux, G. Grandjean, “Two-dimensional elastic full waveform inversion using Born and Rytov formulations in the frequency domain,” *Geophys. J. Int. **168**, 605-633, 2007.*
8. Y. Choi, C. Shin, “Frequency-domain elastic full waveform inversion using the new pseudo-Hessian matrix: Experience of elastic Marmousi 2 synthetic data,” *Bulletin of the Seismological Society of America, **98**, 2402-2415, 2008.*
9. A. Tarantola, “Inversion of seismic reflection data in the acoustic approximation,” *Geophysics, **49**, 1259-1266, 1984.*
10. Z. Koren, K. Mosegaard, E. Landa, P. Thore, A. Tarantola, “Monte Carlo estimation and resolution analysis of seismic background velocities,” *Journal of Geophysical Resarch, **96**, 20289-20299, 1991.*
11. S. Jin, R. Madariaga, J. Virieux, G. Lambare, “Two-dimensional asymptotic iterative elastic inversion,” *Geophysical Journal International, **108**, 575-588.*

12. J. Virieux, S. Operto, “An overview of full-waveform inversion in exploration geophysics,” *Geophysics, **74(6)**, 1-26, 2009.*

13. K. Mosegaard, P. D. Vestergaard, “A simulated annealing approach to seismic model optimization with sparse prior information,” *Geophys. Prospect., **39**, 599-611, 1991.*

14. M. K. Sen, P. L. Stoffa, “Rapid sampling of model space using genetic algorithms: examples from seismic waveform inversion,” *Geophys. J. Int., **108**, 281-292, 1992.*

15. S. Jin, R. Madariaga, “Background velocity inversion by a genetic algorithm,” *Geophysical Research Letters, **20**, 93-96, 1993.*

16. S. Jin, R. Madariaga, “Nonlinear velocity inversion by a two-step Monte Carlo method,” *Geophysics, **59**, 577-590, 1994.*

17. K. Mosegaard, A. Tarantola, “Monte Carlo sampling of solutions to inverse problems,” *Journal of Geophysical Research, **100**, 12431-12447, 1995.*

18. M. Sambridge, K. Mosegaard, “Monte Carlo methods in geophysical inverse problems,” *Reviews of Geophysics, **40**, 1-29, 2002.*

19. P. M. Manning, G. F. Margrave, “Elastic wave finite difference modeling as a practical exploration tool,” *CREWES Research Report, Vol. **10**, 18-1 to 18-16, 1998.*

20. R. Graves, “Simulating seismic waves propagation in 3D elastic media using staggered grid finite differences,” *J. Acoust. Soc. Am. **100**, 3061-3069, 1996.*

21. N. Metropolis, A. W. Rosenbluth, M. N. Rosenbluth, A.H. Teller and E. Teller, “Equations of State Calculations by Fast Computing Machines,” *Journal of Chemical Physics, **21**, 1087-1092, 1953.*

22. W. K. Hastings, “Monte Carlo Sampling Methods Using Markov Chains and Their Applications,” *Biometrika, **57**, 97-109, 1970,*

23. S. Chib, E. Greenberg, “Understanding the Metropolis-Hastings Algorithm,” *The American Statistician, **49(4)**, 327-335, 1995.*

24. M. B. Dobrin, “Introduction to Geophysical Prospecting,” *McGraw-Hill Book Company, Inc., New York, Second Edition, 1960.*

25. S. Kirkpatrick, C. D. Gelett, M. P. Vecchi, “Optimization by simulated annealing,” *Science, **220**, 621-630, 1983.*

26. V. Cerny, “A thermodynamic approach to the travelling salesman problem: An efficient simylation,” *J. Optimization Theory Appl., **45**, 41-51, 1985.*

27. B. Dimitris, J. Tsitsiklis, “Simulated Annealing,” *Statistical Science, **8(1)**, 10-15, 1983.*

28. D. H. Rothman, “Nonlinear inversion, statistical mechanics and residual statics estimation,” *Geophysics **50**, 2797-2807, 1985.*

29. D.H. Rothman, “Automatic estimation of large residual static corrections,” *Geophysics **51**, 332-346, 1986.*

30. M.O. Jakobsen, K. Mosegaard, J. M. Pedersen, “Global model optimization in reflection seismology by simulated annealing,” *In: Model Optimization in Exploration Geophysics **2,** p. 361. Proceedings of the 5th International Mathematical Geophysics Seminar, Berlin, 1987,A. Vogel (ed.). Friedr. Vieweg & Son, Braunschweig, Wiesbaden.*

31. E. Landa, W. Beydoun, A. Tarantola, “Reference velocity model estimation from prestack waveforms: coherency optimization by simulated annealing,” *Geophysics **54**, 984-990, 1989.*

CHAPTER 6

CONCLUSIONS AND SUGGESTIONS FOR FUTURE RESEARCH

6.1 Conclusions

This study has mainly investigated the practical application of geophysics inversion to the localization problem of underground tunnel. The solution of geophysics inversion problem faces two problems, first is defining the appropriate forward model to describe the seismic data recorded, and second is solving the stability issue of the inversion when we want to estimate many parameters (such as seismic wave speeds and ground soil density values of the discretized ground medium) from seismic measurements recorded by an array of seismic sensors.

For the first problem, this PhD study investigated the linear acoustic ray tracing forward model and the nonlinear 3D elastic wave model. Two signal processing algorithms, namely the beamforming approach commonly used to solve the localization problem and the Bayesian inversion, are implemented to estimate the location (depth, range) of an underground tunnel. The Bayesian inversion method through the probability density function permits the incorporation of a priori information about the parameters, and also allow for incorporation of theoretical errors i.e. non-exact relationship between parameters and data. The results of the investigation are elaborated in Chapter 3.

The work in Chapter 3 assumes full knowledge of the ground material elastic parameters, hence leaving only the inversion process to estimate two parameters, depth and range, parameterizing the location of the tunnel. The second half of the thesis work focuses on the joint inversion of the material elastic parameters and the depth and range values of the tunnel location. This leads to the need to deal with the issues solving a large dimension parameter estimation problem with a finite data set. In Chapter 4, a reduced modelling scheme to reduce the dimension of the elastic parameter space is proposed so as to reduce the ill-posedness that arises from inferring many parameters from a few observations. Two different optimization algorithms, the Monte Carlo Metropolis Hasting and Simulated Annealing, are also investigated for sampling the reduced parameter space. Simulated Annealing has been tried in geophysical applications but the reported experience is that the method is very difficult to use. The main challenge is finding the annealing temperature schedule, and the optimum number of iterations to arrive at a good estimate. Similarly for Monte Carlo Metropolis Hasting algorithm, the challenge is finding the optimum number of iterations to get a good parameter estimate. Our proposed method to use a combination of the Monte Carlo Metropolis Hasting algorithm to first provide an initial guess for the algorithm, with incorporation of prior information of the soil layer structure to improve the sampling efficiency of the soil parameter vector greatly improve the efficiency of the simulated annealing method. This work has also be validated with field data recorded using an array of two geophones deployed on the ground surface to record the reflected and refracted seismic signals from an underground tunnel generated by a surface seismic source. The results of the analysis are presented in Chapter 5.

6.2 Suggestions of future works

One suggestion for future research and topics that have not been investigated in this project is incorporating more sophisticated wave phenomena of attenuation and anisotropy in the forward modelling and inversion. Another area of work will be looking into strategies to speed up the forward problem, such as devising more efficient numerical algorithms to solve the 3D seismic wave equation.